2019

Volt/var control with high solar PV penetration in distribution systems and its impact on the transmision grid

Ankit Singhal
Iowa State University

Volt/var control with high solar PV penetration in distribution systems and its impact on the transmission grid

by

Ankit Singhal

A dissertation submitted to the graduate faculty

in partial fulfillment of the requirements for the degree of

DOCTOR OF PHILOSOPHY

Major: Electrical Engineering (Electric Power and Energy Systems)

Program of Study Committee:
Venkataramana Ajjarapu, Major Professor
James D. McCalley
Umesh Vaidya
Zhaoyu Wang
Lizhi Wang

The student author, whose presentation of the scholarship herein was approved by the program of study committee, is solely responsible for the content of this dissertation. The Graduate College will ensure this dissertation is globally accessible and will not permit alterations after a degree is conferred.

Iowa State University

Ames, Iowa

2019

DEDICATION

I dedicate this thesis to India (Bharat), one of the oldest living civilizations whose ethos and values inspired me to complete this work.

TABLE OF CONTENTS

LIST OF TABLES

LIST OF FIGURES

ACKNOWLEDGEMENTS

I would like to take this opportunity to express my thanks to those who helped me with various aspects of conducting research and the writing of this thesis. First and foremost, Dr. Ajjarapu for his guidance, patience and support throughout this research and the writing of this thesis. His insights and words of encouragement have always inspired me. He is one of the most genuine researcher I have met. His mentoring with appropriate guidance and care not only helped me to sail through my academic journey; it made the process of PhD a learning and wholesome experience. I would also like to thank my committee members for their efforts and contributions to this work: Dr. James McCalley. Dr. Umesh Vaidya, Dr. Zhaoyu Wang and Dr. Lizhi Wang. I have always got encouragement and new perspectives while attending classes and discussing my research with all of my committee members.

This journey would not have been possible without the support of Pooja with whom I got married while working on this thesis. Her patience, emotional support and cheerful presence have always kept me in a stress free and joyful environment. I would like to express my gratitude to my father Mr. Mahendra Singhal, mother Mrs. Santosh Singhal, and siblings Anjali and Harshit who always support me in all my endeavor and decisions.

I also would like to acknowledge the contribution of my excellent research group members i.e. Amar, Alok, Pranav and Shiyang who helped me academically as well as personally throughout my journey. I sincerely thank to all of my roommates and friends in Ames, Iowa who listened to me, offered me advice and always wish best for me.

I also would like to acknowledge that my research work was supported in part by U.S. Department of Energys (DOE) Sunshot Initiative Program DE-0006341 that provided me several opportunities to attend conferences, present my work, conduct workshops interact with the power systems community at large.

ABSTRACT

With increasing distributed energy resources (DERs), both the distribution and transmission power systems are witnessing new challenges and opportunities. Voltage rise and voltage fluctuations are becoming major issues in the distribution network due to high solar PV penetration. Nevertheless, the volt/var control (VCC) capability of solar PV devices (inverter based DERs, in general) opens up various opportunities for both the distribution and transmission systems. In this work, we address the challenges in the distribution network and also explore the potential opportunities for the transmission system that can be provided by VCC capability of DERs in high PV penetration environment.

The first part of our work addresses the voltage challenges faced by the distribution system due to solar PV penetration by utilizing VVC capabilities of PV smart inverters. In this part, we focus on the slope sensitive local droop VVC recommended by the recent integration standards IEEE1547, rule21 and addresses their major challenges i.e. selection of appropriate parameters under changing conditions, issue of control being vulnerable to instability (or voltage oscillations) and bad set-point tracking performance i.e. high steady state error (SSE). This is achieved by proposing a local real-time adaptive VVC which has two major features i.e. a) it is able to ensure both low SSE and control stability simultaneously without compromising any of the objectives, and; b) it dynamically adapts its parameters to ensure good performance in a wide range of external disturbances such as sudden cloud cover, cloud intermittency and substation voltage change. Moreover, the adaptive control does not depend on the feeder topology information. The proposed control is implementation friendly as it fits well within the integration standard framework and depends only on the local bus information. The performance is compared with the existing

droop VVC methods under several scenarios on a large unbalanced 3-phase feeder (IEEE 123 bus test system) with detailed secondary side modeling.

The second part of our work focus on investigating the impact of DER VVC on the bulk transmission grid. We present a hypothesis that the multitudes of inverter-based DERs can be envisioned as geographically distributed reactive power (var) devices (mini-SVCs) that can offer enhanced var flexibility to a future grid as an ancillary service. To facilitate this vision, a systematic methodology is proposed to construct an aggregated var capability curve of a distribution system with DERs at the substation level, analogous to a conventional bulk generator. Since such capability curve will be contingent to the operating conditions and network constraints, an optimal power flow (OPF) based approach is proposed that takes curtailment flexibility, unbalanced nature of system and coupling with grid side voltage into account along with changing operating conditions. Further, the influence of several other factors such as revised integration standard 1547 on the capability curve is thoroughly investigated on an IEEE 37 bus distribution test system. In the last part of the work, we investigate the DERs' impact on the long-term voltage stability assessment on an integrated T-D system. Finally, a T-D cosimulation is employed to demonstrate how DER aggregated flexibility and var support can potentially enhance the transmission grid performance on an integrated T-D test system.

CHAPTER 1. OVERVIEW

1.1 Introduction

1.1.1 Motivation

The modern Power system is witnessing rapid changes in distribution side with high penetration of distributed energy resources (DERs). It is estimated that by 2020, 42% of the total capacity addition will be due to DER (3). It is interesting to note that the average projected growth rate for centralized power is 2.8 % while the same is 4.4% for distributed power in period 2012-2020. Among all, solar photovoltaic (PV) can be considered one of the most popular and fast-growing DER technology in the USA. It was the source of the highest new capacity addition (39%) in electricity generation in the USA in 2016 (4). Solar PV penetration is continuously rising and is expected to be tripled in the next 5 years in the USA (4). The fast solar PV growth can be assessed from the fact that, according to the SunShot initiative report, the United States alone is expected to have more than 300 GW of solar PV generation by 2030 (5). Especially, small buildings and residential rooftop solar constitute 65% of the total solar PV potential in USA (6). High solar penetration is being fueled because of continuous reduction in cost, environmental benefits and encouraging policies such as net metering, renewable target compliances. Figure 1.1 from a national lab report shows the continuous fall in solar PV costs for all three type of installations i.e. residential, commercial and utility-scale (1). Earlier, 20% PV penetration was considered as very high PV penetration, however, the conducive environment for DER growth is pushing the penetration to as high as 100%. A national report provides a case study of feeders in

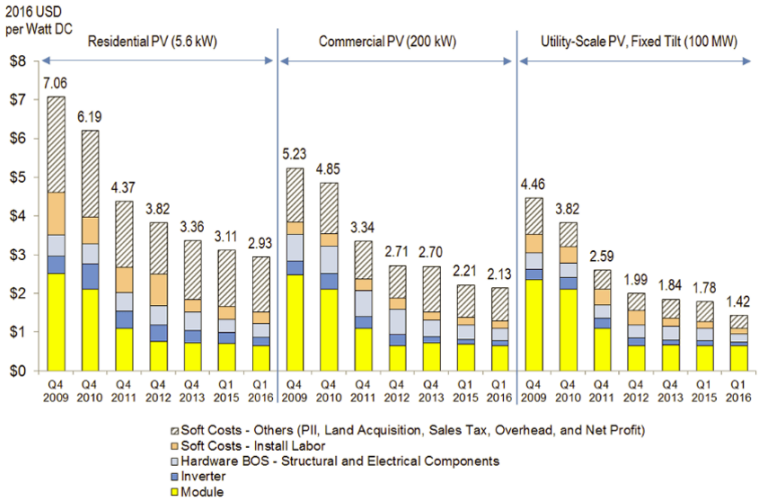

Figure 1.1 Solar PV cost trends in USA in last 7 years, NREL report (1)

different parts of US which have more than 80% solar PV penetration (7). Such fast advent of solar PV generation raises some concerns in the performance of traditional distribution system which is not designed to accommodate a large scale of generation. At the same time, DERs can also be exploited for the benefits of the distribution as well as transmission systems by controlling and coordinating them properly. In fact DERs are seen as alternative sources in a future grid to provide essential ancillary services such as ramping requirements, ensuring adequate inertia, and maintaining var reserves (8; 9). Those challenges as well as opportunities associated with DERs are discussed in the following sections.

1.1.2 Voltage Challenges with High Solar PV Penetration in Distribution System

The increasing solar PV penetration brings its own set of technical challenges such as voltage rise in distribution feeder and rapid voltage fluctuations due to cloud transients which could lead to the reduced power quality (10; 11; 12; 13; 14). These challenges can be attributed to two fundamental reasons. First, the conventional voltage regulatory schemes for distribution system have been designed assuming power will always flow in one direction

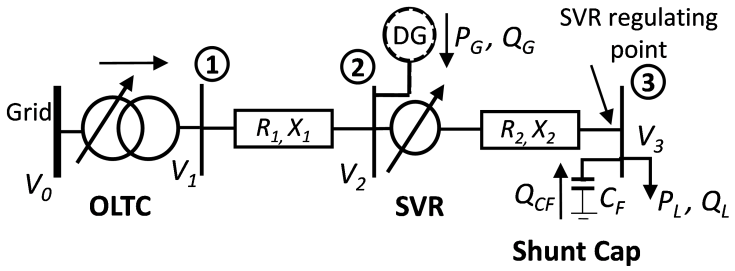

Figure 1.2 One line diagram of a typical distribution feeder with solar PV

i.e. from a substation to the loads. However, the introduction of solar PV (DER, in general) causes a reversal of power flow, resulting in voltage rise. Second, solar PV penetration introduces significant uncertainties and external disturbances such as cloud intermittency and sudden cloud cover, which potentially can cause various voltage related issues i.e. fast voltage fluctuations, power quality issues (voltage flicker), and sudden voltage rise and drops.

1.1.2.1 Voltage Violations

Voltage violations can be considered one of the biggest challenge with solar PV penetration. ANSI C84 standard in North America makes it compulsory for all power utilities to maintain customer voltage within the prescribed upper and lower limits (usually 0.95 and 1.05 pu) (15). Both over-voltage and under-voltage violations are possible with solar PV, though the over-voltage violation is more common due to voltage rise. It can be understood using a one-line diagram of a typical distribution feeder as shown in Figure 1.2. Voltages at DER connection point (node 2) can be approximated using DistFlow equations as (16).

$$V_2 = V_1 - (P_L - P_G)R_1 + (Q_L - Q_G - Q_{CF})X_1 \tag{1.1}$$

Where V_1 and V_2 are voltages at node 1 and 2 respectively. $P_L + jQ_L$ is the load connected and Q_{CF} is reactive power injected by the capacitor at node 3 respectively. DER is injecting power $P_G + jQ_G$ at node 2. It can be seen that if there is no DER i.e. $P_G = Q_G = 0$,

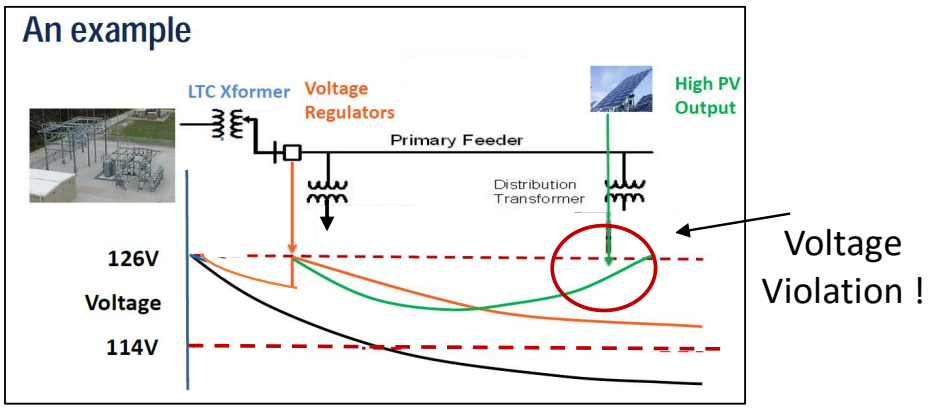

Figure 1.3 A conceptual representation of voltage rise caused by the solar PV integration

the voltage at node 2 is lower than the voltage at node 1. However, the non-zero DER generation leads to a relatively higher voltage at node 2. If DER generation is very high, it is possible for V_2 to exceed V_1 magnitude due to reverse power flow. It is illustrated as a conceptual diagram in Figure 1.3 (17). The black and green curves are voltage profiles without and with DER, respectively. DER causes non-decreasing voltage profile which can potentially cause the over-voltage violation. Maximum generation and the minimum load is the worst case scenario for voltage rise which can occur during the daytime in summers in the residential area.

Interestingly, along with voltage rise, solar PVs can also cause low voltage when it is connected between voltage regulators and its regulating point. It confuses the conventional voltage regulation technique (line drop compensation) and reduces the observed voltage drop which leads to under voltage. A detailed explanation and results are shown in (18). Moreover, a sudden drop in solar generation during high load period or fast ramping down solar generation can also cause low voltage violations.

1.1.2.2 Voltage Fluctuations

Another major challenge with solar PV integration is sudden changes in cloud pattern i.e. cloud intermittency and sudden cloud cover. Figure 1.4 shows the solar PV generation profile on a sunny day in winter at CSIRO's Energy Center at Newcastle (2). It can be seen that the actual PV profile does not always follow the ideal PV curve and can be highly intermittent in nature. Consequently, both intermittent cloud profile and sudden cloud cover can cause rapid voltage fluctuations in the customer voltage which can potentially lead to voltage flicker violations. These flicker may be irritating to customers and may also result in malfunctioning of appliances (11; 13; 14). A case study of Porterville distribution network in California shows the voltage flicker phenomena on arrival of sudden cloud cover (11). According to IEEE power quality standards, the voltage flicker is defined as the voltage fluctuations in loads which cause irritation to consumer eyes (19). This standard estimates the flicker severity based on the GE flicker curve as shown in Figure 1.5.

1.1.3 Volt/Var Control (VVC) in Distribution Systems

Volt/var control (VVC) is a fundamental operating requirement of all electric distribution systems. The prime purpose of VVC is to maintain an acceptable voltage profile at all points along the distribution feeder under all loading conditions. The acceptable voltage range is decided by different regulatory agencies at different places. In the USA, ANSI standards are followed by all the utilities. Conventionally 4 types of devices are used to control voltage and reactive power flow in distribution systems i.e. on load tap changer (OLTC), step voltage regulator (SVR), substation capacitor and feeder capacitor as shown in 1.2. They can be classified in two levels i.e. substation level (OLTC and substation capacitors) and feeder level (SVR and feeder capacitors). Grid voltage V_0 can be considered almost constant but due to losses in substation transformer, secondary voltage V_1 varies with the load. OLTC is a tap changer installed at substation transformer to regulate V_1 so that downstream voltage remains within the limit. A substation capacitor C_s is installed

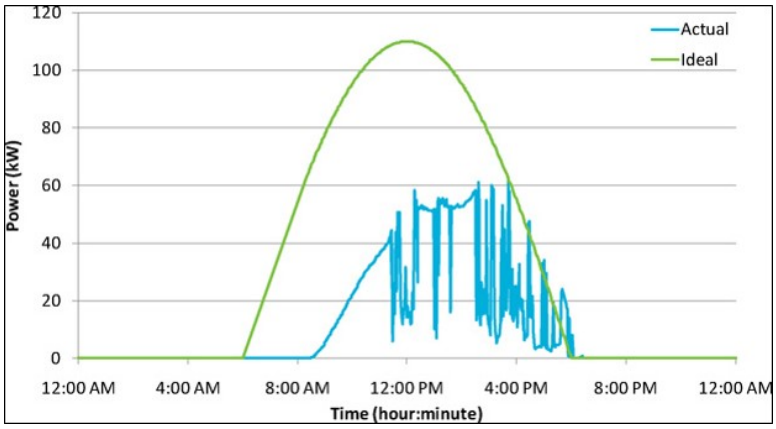

Figure 1.4 An ideal generation profile for solar PV, compared with a real profile from a cloudy day in winter (2)

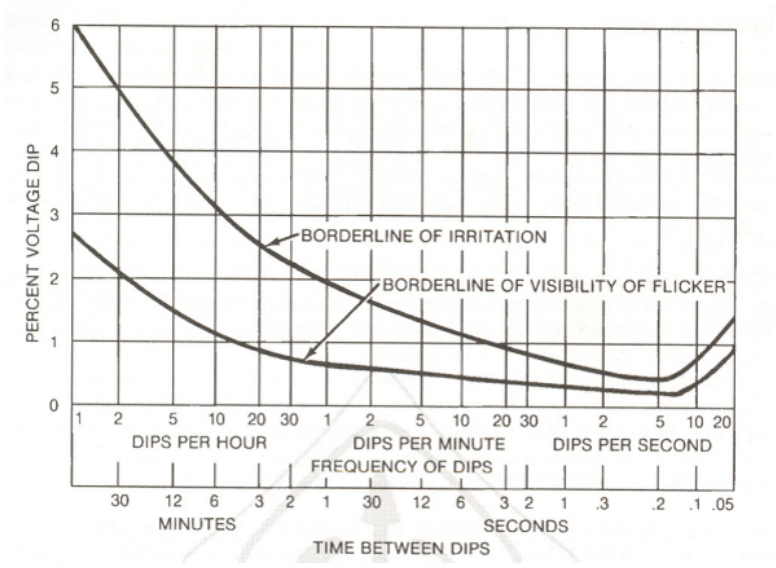

Figure 1.5 GE flicker curve from IEEE standard 141

at the substation to control the reactive power flow to maintain system power factor (PF). SVRs are tap changing transformers installed at different places on the feeder to boost the voltage at low voltage nodes. Mostly SVRs are used with line drop compensator (LDC) to regulate the voltage at other downstream nodes rather than its point of connection, SVR installed at node 2 is regulating the voltage at node 3. LDC simulates voltage drop between the two points ($V_2 - V_3$) using line impedance ($R_2 + jX_2$) and local current values. SVR changes the tap accordingly. Detailed explanations of the control methods can be found in (20). Feeder capacitor C_s is a fixed or switched capacitor installed at different places on the feeder to boost voltage. Generally, all the devices are locally controlled e.g. OLTC and SVR are controlled based on local bus voltages. Capacitors are controlled based either on time or local bus voltages.

However, these devices are not sufficient to mitigate voltage challenges associated with the solar PV due to their slow and discrete control. They can not handle the rapid variations caused by solar generation i.e. cloud transients (21; 22; 23). Fortunately, most of the inverter based DERs such as wind, solar PV, electric vehicle, synchronous generator based generation have inherent volt/var control capability which can be exploited to enhance voltage profile of the network. We will discuss them in detail, in the next section.

1.1.4 Solar PV Smart Inverters Volt/Var Control Capability

The grid-connected solar PV generation systems includes an inverter to convert input DC power to output grid-compatible AC power. Interestingly, the same inverter can also be utilized to regulate the voltage at the point of common coupling by injecting and absorbing the reactive power (var). These multi-functional PV inverters with volt/var capability are also commonly termed as 'smart inverters' and this mode is called as voltage control mode (VCM). Another DERs' common mode of operation is constant power factor (CPF) mode, in which, DERs are operated at unity or other constant power factor (usually lagging PF to compensate voltage rise). The inverters' capability of injecting or absorbing var is limited

by their rated capacity. Inverter must satisfy the following relation

$$\sqrt{P^2 + Q^2} \leq S \tag{1.2}$$

Where, P, Q and S are inverter real power output, var output and rated capacity, respectively. So, the maximum var magnitude which can be injected or absorbed by the inverter at any given time can be estimated as $Q_{max} = \sqrt{S^2 - P^2}$.

Due to their fast switching control actions at seconds time-scale and dynamic nature of control, the PV inverters have emerged as effective volt/var controllers to handle rapid variations in the modern distribution system by providing faster and continuous VVC capability in contrast to slower and discrete response of the traditional VVC devices.

1.2 Research Overview

1.2.1 Challenges, Need and Opportunities for Real-Time Local Volt/Var Control in Distribution Systems

The VVC capability of the PV inverter has been identified since some time. This concept was initially explored by few publications such as (24; 25) and since then, it has been popular in the literature. However, the utilities and the distribution system operators (DSOs) were reluctant to test this idea and they did not allow DERs to operate in voltage control mode, mainly because of lack of any DER integration standards and guidelines. DSOs prefer DER to operate in power factor control (PFC) mode only, to avoid unexpected issues. However, voltage control mode of DER is gaining a lot of recent attention among utilities due to upcoming integration standards. Although, the earlier version of IEEE integration standard 1547 did not allow DER in voltage control mode, in the recently revised version, a provision for utilizing DERs' VVC capability has been made compulsory (26). Moreover, the California and Hawaii utilities have come up with their own integration standard, Rule 21 and Rule 14 respectively (27). All these factors are facilitating the voltage control mode

operation of solar PV (28) and opening a new path to utilize DERs' full potential to enhance system performance.

Most of the PV inverter VVC methods can be categorized as an optimal power flow (OPF) based approaches which are solved using either centralized or distributed algorithms (see 2.1.3 for details). Though these methods can optimize the system-wide performance, their real-time implementability and economic viability are questionable due to requirement of communication infrastructure and large time to solve most OPFs. Additionally, their ability to respond to faster and sudden external disturbances is also limited such as cloud transients which are common occurrences in solar PV generation profile.

Need of an Adaptive Real-Time Local Control: Due to aforementioned reasons, there is a recent trend in utilities to explore real-time local control approaches which are also being recommended by current and upcoming integration standards such as IEEE1547 and Rule 21. Both these standards recommend the local droop control framework which has been explored in the latest literature, however, it has two major challenges associated (see 2.1.4.2 for details). The first issue is appropriate parameter selection. The droop control is highly sensitive to its control parameters which need to be changed dynamically to ensure a desirable control performance in all operating conditions and external disturbances. The second main issue is that the droop control is highly vulnerable to control stability, voltage flicker as well as significant deviation from the desired set-points. Due to the inherent design issues, the droop control always compromises between achieving control stability and achieving high set-point tracking accuracy. Without ensuring a stable good set-point tracking performance, a real-time control cannot guarantee to meet its objectives in all situations. The state of the art literature acknowledges this problem (see 2.1.4.2) but a comprehensive solution is not provided. In a real-world, in case of large systems, the problem becomes more complex due to thousands of inverter devices and continuously changing operating conditions and external disturbances such as a change in substation voltage, sudden cloud cover, cloud intermittency, sudden load changes, topology re-configuration

etc. If both the challenges of the droop control, namely, appropriate parameter selection and good set-point tracking performance, are addressed, high PV penetration presents an exciting opportunity to enhance distribution system performance by exploiting DERs to their fullest potential.

Overall, in this new environment of increasing renewables of intermittent nature, demand response and other pro-active functionalities, the unexpected external disturbances in distribution system will become more common; and thus, there is a need to develop a standard based adaptive local VVC framework that can ensure an effective set-point tracking without voltage issues and facilitate an easy plug-and-play implementation without reliance on much communication network.

1.2.2 Challenges and Opportunities for Transmission System in the New Environment of DERs

Reactive power (var) balance plays a vital role in maintaining transmission grid resiliency and, availability of sufficient var capability is often considered an indicator of voltage security (29; 30). The var related ancillary services have been mainly achieved by large synchronous generators and other strategically deployed var devices such as static synchronous compensator (STATCOM) and static var compensator (SVC). However, a growing footprint of distributed energy resources (DERs) is replacing fossil fuel based generation that may result in shortage of regional var availability (31; 32). It has initiated a discussion on utilizing DERs as alternative sources in the future grid, along with bulk generation plants, to provide essential ancillary services to the grid such as ramping requirements, ensuring adequate inertia, and maintaining var reserves (8; 9). In particular, the multitude of DER devices with volt/var control capability can be seen as the geographically distributed local var resources (*'mini- SVCs'*) by the transmission system operators (TSOs). The feasibility of this idea is based on following reasonings: 1) The inverter based DERs can inject/absorb var via fast local volt/var controls, thus can provide a significant amount of fast and

continuous capacitive/inductive var support, if aggregated; 2) Recently revised DER integration standards such as IEEE1547-2018 (26), California Rule 21, Hawaii Rule 14 (27) and Germany grid codes (32) have made it obligatory for DERs to provide var support for grid requirements; 3) The local and distributed nature of the var flexibility provided by DERs makes it a suitable contestant for var provision and; 4) The required infrastructure and protocol for DSO-TSO interaction has started gaining attention (33; 34; 35; 36)

Overall, in this new environment of DERs proliferation, TSOs can model the additional var resources flexibility provided by DERs into their planning and operational optimizations, in order to enhance grid performance i.e. voltage profile, load margin etc. However, a thorough assessment of DERs var flexibility is not readily available. There is a growing need to develop a systematic approach for DER capability or flexibility aggregation at the substation level so that it can be easily incorporated by TSO in their planning. At the same time, care must be taken to avoid any operational violations at the distribution system side by DERs utilization for the bulk grid. Further, another challenge in assessing the true impact of DERs on the grid is inability to solve an integrated transmission and unbalanced distribution system by the existing standard power flow solvers. In order to investigate the DERs' impact on the grid, a transmission-distribution (T-D) co-simulation environment is needed which can reliably solve the integrated T-D systems.

1.2.3 Research Objectives

There are two-fold objectives of our work:

1. To develop a fully local and real-time adaptive VVC with high PV penetration to mitigate over-voltage problem; to improve voltage set-point tracking and to ensure control stability under a changing operating conditions/external disturbances (such as cloud intermittency, changes in substation voltage) within the standard droop control framework.

2. To explore the potential of utilizing DERs volt/var control capability for the transmission grid benefits in following ways:

   (a) To develop an *aggregated var capability curve* of DERs that offer useful insight and enable TSO to utilize the available var flexibility from distribution systems.

   (b) To investigate the impact of DERs on long-term voltage stability margin of an integrated transmission-distribution system in a T-D cosimulation environment.

1.3 Research Contributions

1.3.1 Real-Time Adaptive Volt/Var Control in Distribution Systems

1. The proposed control achieves both control stability and high set-point tracking performance simultaneously by decoupling the two objectives without compromising either, thus eliminates one major challenge associated with droop control.

2. The proposed approach eliminates another major challenge of appropriate parameter selection by making the control parameters self-adaptive to changing operating conditions and external disturbances, in real-time, such as cloud cover, cloud intermittency, changes at substation voltage etc.

3. The proposed approach enables operators to utilize PV inverters beyond over-voltage mitigation, that is, for other volt/var related applications in distribution systems (e.g. CVR, loss minimization) as well as in transmission systems (e.g. aggregated var support) by virtue of a) real-time adaptive nature, b) tight voltage control with low SSE and, c) compatibility with the integration standards and utility practices (IEEE1547, Rule 21 (CA)).

1.3.2 Aggregation of DERs' Volt/Var Capability to Support the Grid

1. The proposed methodology provides an aggregated net *Q-capability* curve as function of aggregated DER *P-curtailment* resembling a virtual conventional generator capability curve. This enables TSO to model both P and Q flexibility as resources from distribution network into their planning, leading to a greater decision domain and improved optimality of commitment schedules as demonstrated in impact assessment via T-D cosimulation platform.

2. The proposed approach considers two main real-world aspects while aggregating capability unlike existing literature i.e. unbalanced three-phase distribution system and impact of transmission-distribution coupling.

3. In order to provide comprehensive insight, the influence of several factors on aggregated capability is investigated e.g. changing operating conditions, inverter oversize, grid side voltage, the revised integration standard 1547-2018 etc.

1.3.3 Impact Assessment of DERs on Long-Term Stability Margin of the Grid

1. The proposed long-term voltage stability assessment of an integrated T-D system reveals the possibility of distribution system being critical in causing long-term voltage collapse rather than the transmission system.

2. The DERs var support significantly improves the load margin of the system, given the support is from the substation which has critical distribution system connected.

3. The investigation demonstrates the significant error in load margin assessment if distribution systems are not modeled in detail; thus accentuates the need of using T-D cosimulation platform to estimate true load margin and assess accurate impact of DERs on the system.

1.4 Thesis Organization

The remainder of the thesis is organized as shown in Figure 1.6. Chapter 2 discusses a thorough literature review regarding various methods of smart inverter volt/var control in distribution systems, DERs' aggregation methodologies, T-D cosimulation techniques and platforms and DERs impact on the load margin.

Chapter 3 develops a real-time adaptive control strategy with high PV penetration. A theoretical analysis and convergence proof of the proposed control stability and steady state error is also provided. The proposed control is tested on an unbalanced three-phase distribution network with around 1500 nodes.

Chapter 4 and Chapter 5 focus on the potential impact of DERs volt/var control capability on the transmission grid. In specific, Chapter 4 hypothesizes that the DERs can be conceived as geographically distributed reactive power (var) devices (mini-SVCs). To facilitate this vision, a systematic methodology is proposed to construct an aggregated var capability curve of a distribution system with DERs at the substation level, analogous to a conventional bulk generator. Further, the influence of several other factors such as revised integration standard 1547 on the capability curve is thoroughly investigated on an IEEE 37 bus distribution test system.

Chapter 5 investigates the DERs' impact on long-term voltage stability assessment (VSA) of integrated transmission-distribution system using PV curve superimposition approach and reveals the possibility that the overall system loadability may be limited by the distribution system rather than the transmission system. Further, the analysis is verified on an IEEE 9 bus transmission system coupled with IEEE 37 bus distribution system via cosimulation with and without DER penetration.

Chapter 6 concludes the thesis along with discussion on future research.

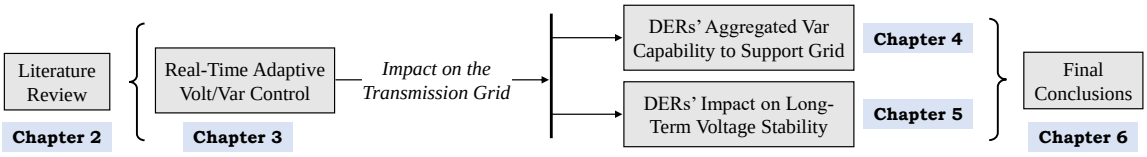

Figure 1.6 Organization of Thesis Chapters

CHAPTER 2. REVIEW OF LITERATURE

2.1 Volt/Var Control to Mitigate Voltage Challenges in Distribution System with High PV Penetration

2.1.1 Conventional Volt/Var Control Approaches

To mitigate voltage rise due to high solar PV penetration, few simple methods are suggested such as lowering primary substation voltage (37). But it might result in low voltages on some parts of the feeder. Some suggest to increase conductor diameter which lowers the line impedance but an overhaul of the existing infrastructure will not be economical (17; 10). Moreover, these methods are not adaptive to changing operating conditions (low solar output during peak load) and external disturbances such as cloud cover. Curtailment of solar power can also reduce voltage but it leads to underutilization of PV panel and non-economical to customers.

Nonetheless, VVC is an old problem in traditional distribution systems to keep voltages in the prescribed range in all loading conditions and it is being solved using tap and cap devices such as load tap changers (LTC), voltage regulators and switched capacitors as explained in 1.1.3. The major issue with these devices is that their control work in a discrete manner and on a slower time scale of few minutes; therefore, are not effective with high PV penetration where fast cloud transients are observed at seconds time-scale (21; 22; 23). Additionally, their settings are changed seasonally which make the control vulnerable to changes in operating conditions due to solar PV. In this new environment of increasing solar penetration, the nature of VVC is also changing and it necessitates the development

of control methods which can provide faster and continuous VVC capability. Fortunately, PV installations are equpped with the smart inverters which have the capability to provide VVC at much faster time-scale (seconds) and in non-discrete fashion.

2.1.2 Smart Inverter Constant PF Control Approaches

As discussed in the last chapter (see 1.2.1), DNOs prefer DER to operate in PFC mode to avoid problems. To comply with the preference, (38) proposes a PFC mode in which PFs are set at optimal value rather than 0.95 or unity which is generally set by DNO for all DERs. A linear optimization problem is formulated and constraints are framed such that all the voltage limits are obeyed. The objective function is set to minimize reactive power import from transmission grid to reduce the burden on the grid side. A more complex coordinated control strategy is presented in (39) which requires widespread and reliable communication network. A genetic algorithm is used to get optimal voltage level for each node in the network. Objective function minimizes losses and voltage fluctuations in the network. However, since these methods do not utilize the voltage control capability of DERs, they fail to exploit DERs' full potential to improve system performance. In fact, due to the revision in IEEE1547 integration standard and the recent utility practices (Rule 21), the path of operating DER in volt/var control (VVC) mode is now getting accepted which provides exciting opportunities in many applications of the 'smart grid'.

2.1.3 Volt/Var Control: OPF Based Centralized and Distributed Approaches

The PV inverter based VVC approaches can be classified in two layers i.e. optimization layer and set-point tracking layer. In the first layer, optimal set points for inverters are dispatched based on an optimal power flow (OPF) formulation. It is generally based on a centralized control as it requires system-wide information. The second layer essentially is a real-time local control which ensures that optimally dispatched set points are tracked accurately in real time operation in all operating conditions. Based on this classification,

we will review the PV inverter VVC methods in two broad categories: 1) OPF based centralized/distributed approaches and 2) local control approaches.

Most of the literature deals with the OPF based methods which are solved either in a centralized manner (40; 41; 21; 42) or using distributed algorithms (43; 44; 45; 22; 46; 47). There are several other distributed control methods proposed for PV inverter VVC which can be referred from the latest comprehensive survey papers (48) and (49). References (42) formulates PV inverter VVC as a radial OPF problem with conic convex relaxations. Inverter reactive power is taken as a decision variable and a balanced single phase circuit is considered for verification. The problem minimizes the line losses and energy consumption through conservative voltage reduction. Reference (21) formulates the same problem as multi-objective optimization using linearized DistFlow equations. The adaption law determines which of the two objective functions are being chosen i.e. voltage regulation or power losses based on the instantaneous voltage measurement. Similarly, (41) formulates the non-linear OPF and utilizes semi-definite programming (SDP) to obtain computationally feasible convex re-formulation. It provides PV inverter selection capability through sparsity-promoting regularization approach.

Since the fully centralized approaches are computationally intensive, another trend is to solve the same problems using distributed algorithms. Reference (44) cast the same problem as SDP and provides sufficient condition under which it can be solved using SDP relaxations. However, instead of solving it centrally, a distributed algorithm is used to solve the problem. It dispatches set points at a particular interval by minimizing system losses. Similarly, (47) proposes a distributed algorithmic framework based on the alternating direction method of multipliers (ADMM) to systematically decompose the main problem into sub-problems that can be solved in a de-centralized fashion. On the similar lines, (43) use a distributed second-order cone (D-SOCP) formulation and solves it using ADMM algorithm. (22) present a two-stage distributed architecture in which the second stage de-

centralized algorithm utilizes the consensus averaging of var resources to take var help from the neighboring nodes.

Challenges with OPF based Centralized/Distributed Methods:

- The extensive and high-quality communication infrastructure among the PV devices are required which is still not a reality for most distribution systems. It challenges the real-time implementation of these methods (50).
- Additionally, communication delays and the large time requirement for solving most OPFs limit their ability to respond to faster disturbances at seconds time scale such as cloud intermittency (51; 25; 50).
- Though distributed algorithms are relatively faster, most of these methods assume constant substation voltage and rely on full feeder topology information for control parameter selection which is usually not fully known to the utilities or not always reliable. It may lead to error in control parameter selection and control actions causing undesired control performance.
- Generally, in all centralized approaches, OPF is solved off-line and can be understood as a scheduling problem. Whereas, in real-life, a local-control layer is essential that ensure the real-time tracking of the dispatched optimal set-points. Moreover, in case of solar VVC, due to fast cloud transients and generation uncertainty, development of a fast and accurate real-time control becomes a critical need.

These issues make OPF based VVC methods 1) difficult to implement, and 2) vulnerable to fast external disturbances such as cloud transients, a sudden change in substation voltage and topology changes. To avoid these challenges, we focus on the local VVC approaches, in this work, which are usually faster, implementation friendly, and can respond to sudden external disturbances in distribution systems. A summary table of comparison between centralized/distributed and local approaches are shown in Table 2.1.

Table 2.1 Comparison of OPF based centralized/distributed and local control approaches

Attributes	Centralized Distributed	Local
Optimizing system performance	+	—
Coordination with transmission network	+	—
Economic viability	—	+
Implementation friendliness (integration standards compatible)	—	+
Ability to respond to sudden external disturbances/faster changes in real-time	—	+

2.1.4 Volt/Var Control: Real-Time Local Control Approaches

As discussed in the last section, a local control layer is crucial for PV inverter VVC in this new environment of fast cloud transients and other external disturbances. Recently local VVC are being focused more in the literature due to increasing utility needs as the local control methods are more practical and easy to implement. Among local approaches, droop VVC is the most popular local control framework among utilities and in the existing literature which will be the focus of this work. However, we will also review non-droop control approaches as described below.

2.1.4.1 Non-droop Local VVC Methods

Though we will be focusing on the standard droop VVC framework, in this work. Nonetheless, some of the attempts to develop non-droop local VVC methods are also worth noting (25; 50; 52; 22). For instance, a scaled var control proposed by (50) provides stability analysis of the control and demonstrates an improved local VVC performance. (52) proposes an integral local VVC with unlimited var resources, whereas in real-life var injection is limited by the inverter capacity. (25) proposes a simple approach based on impedance drop compensation. This approach is similar to line drop compensation method of conventional

LTCs. (22) presents an interesting two-stage architecture where the first stage deploys the fully local VVC similar to droop control. However, all these methods present challenges as described below.

Challenges with Non-Droop VVC Methods: Non-droop local VVC methods lead to the following challenges:

- Though these methods are local in terms of their control action, their parameter selection require centralized full topology information.
- They do not adapt their parameters to changing operating conditions and disturbances which may make them vulnerable to control instability or reduced control performance.
- Mostly all these methods take assumptions of linearized power flow and always constant substation voltage while designing the control. This may lead to error in voltage set-point tracking in real-time operations.
- Most importantly, they are not compatible with the IEEE1547 standard local droop VVC framework (26) which may jeopardize their real-time implementation. Whereas, our focus in this work is to develop a standard droop based adaptive control, in order to keep the control implementation friendly.

2.1.4.2 Droop VVC

The most popular among local approaches is the droop VVC framework. It was first proposed by (53) in an EPRI technical report and since then, due to its simple design and easy implementability, it now has been adopted by the IEEE1547 integration standard (26) and also being widely used by Rule 21 in California (28) and Rule 14 in Hawaii (27). The droop control is a piecewise linear volt/var control framework as shown in Figure2.1. The horizontal and vertical axes are local node voltage and inverter VAR injection respectively.

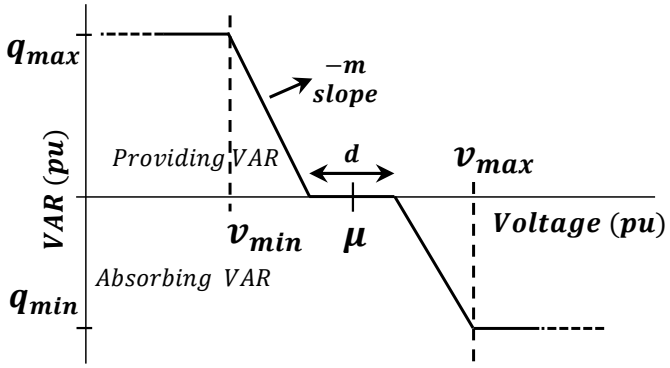

Figure 2.1 Conventional droop VVC framework recommended by IEEE 1547.8, Rule 21 (CA)

The positive and negative var denote the var supply and var absorption by the inverter respectively. In this control, the inverter senses the local voltage and then dispatches the corresponding var on the droop curve. $v_{min}, v_{max}, q_{min} q_{max}$ and m are the various control parameters which defines the behavior of the control. The droop VVC is purely local in nature and does not need feeder topology information or any other centralized data. Moreover, due to its compatibility with recent integration standards, it becomes easier for inverter manufacturer to build one standardized type of VVC in all smart inverters.

Challenges with droop VVC: In spite of being considered for the integration standards, the utilities are not confident in using the solar PV in voltage control mode due to associated risks. Local control is simple to implement based on the local bus information, however, ensuring the system-wide control stability and performance is a challenge in the local control design. The droop VVC has following two major challenges, which will be addressed in this work:

1. First major issue is of appropriate control parameter selection under different operating conditions and external disturbances. The standard droop control has various parameters which need to be chosen appropriately based on the feeder configuration and operating conditions such as load profile, solar penetration level, desired voltage set-point, cloud cover etc. Otherwise, it can lead to undesired control performance.

For instance, the droop VVC is highly sensitive to its droop (slope) parameter, and an improper slope selection can cause control instability or voltage oscillations (voltage flicker) as shown in (54; 55). It has been reported by several studies that the smart inverter settings need to be determined based on the various factors such as load condition, PV penetration, feeder configuration etc.; and a slight variation in the settings can yield significantly different responses (56; 57; 58; 59). Most literature on droop control (60; 61; 62) or other similar local control methods (63; 64) lack in analytical characterization and do not discuss the parameter selection and the control stability/-convergence issues. Moreover, the existing standards do not provide any guidelines on the parameter selection which makes it even more challenging to implement the conventional form of droop VVC.

2. Second major challenge with droop VVC is the compromise between achieving control stability and a good set-point tracking performance. This challenge is inherent to the droop VVC and the reason lies in the droop design itself. The droop VVC needs a smaller slope value to ensure control stability, however, the same slope may adversely affect the steady state performance of the control which leads to high steady state error (SSE) as indicated by (54). Further, the local droop VVC with high SSE becomes prone to voltage violations in external disturbances as confirmed by our findings in this work in the next chapter. Moreover, a tight voltage control with low SSE is not just required to prevent violations; rather tracking desired voltage set-points is an essential requirement, especially if the local control is being used to achieve a system-wide optimization objectives such as minimizing losses, energy consumption etc.

The delayed droop control, a variation of the conventional droop control, is proposed by (55), in which, a delayed block is added in front of the conventional droop VVC in order to reduce the effective slope of the control. It works well and improves the stability performance compared to the conventional droop under normal operating conditions; however, under

external disturbances, it is still vulnerable to instability and voltage violations due to lack of real-time parameter adaption and high SSE respectively, as detailed soon in the next chapter. Moreover, it does not discuss how to select parameters and dynamically adapt them to ensure a good tracking performance. Later, in our work, conventional and delayed VVC methods are compared with the proposed adaptive droop VVC.

In this work, to ensure both control stability and set-point tracking accuracy (low SSE), we propose a fully local and real-time adaptive VVC where control parameters are made self-adaptive to commonly occurring external disturbances such as cloud intermittency, cloud cover, changing load profile, and substation voltage changes without requiring centralized topology information.

2.2 Impact of DER Volt/Var Control Capability on the Grid

2.2.1 Aggregation of DERs Var Flexibility to Support the Grid

Much of the extant literature focuses on utilizing the var control potential of DERs to improve the distribution system performance. For instance (50; 55) demonstrate the benefit of local volt/var control in mitigating voltage challenges. Several optimization techniques are employed to minimize distribution system losses (44; 21), real power consumption (65) and var absorption (38) by the feeder etc. However, utilization of DERs' var potential for the benefit of the transmission grid has not been adequately explored.

Nonetheless, the proposition of utilizing DERs var control capability by TSO can be justified based on the following reasonings found in the literature:

1. The inverter based DERs can inject/absorb var via fast local volt/var controls (66; 55), thus can provide a significant amount of fast and continuous capacitive/inductive var support, if aggregated.

2. The proposition of DERs' var provision is gaining strength with recently revised DER integration standards such as IEEE1547-2018 (26), California Rule 21, Hawaii Rule 14

(27) and Germany grid codes (32) that have made it obligatory for DERs to provide var support for grid requirements

3. The local and distributed nature of the var flexibility provided by DERs makes it a suitable contestant for var provision. An assessment study for East Denmark identifies DERs var provision scheme technically and economically competitive to conventional dynamic var devices i.e. STATCOMs and SVCs (32)

4. The required infrastructure and protocol for DSO-TSO interaction has started gaining attention. Few studies have proposed and demonstrated the feasibility of information exchange loop between TSO and DSO (33; 34; 35; 36). Some TSOs in Europe such as SwissGrid have implemented a payment structure for voltage control where DSOs can participate in var provision based on the day-ahead reactive power plans sent out by TSO (33).

Thus, in this new environment of DERs, a consensus emerge from literature that motivates TSOs to consider DERs var flexibility in their optimization; although a thorough assessment of DERs var flexibility is not readily available. Previous works have aggregated the capability of asynchronous generators or DFIG for large wind farms (67; 68; 69) without considering distribution network constraints as they are not spread out throughout the network. Similarly, (70) has attempted to approximate the DER flexibility using geometric approach without physical network constraints. (34; 31; 71) introduce the optimization based approach with focus on the TSO-DSO interaction. (72) presents an innovative optimization based methodology to construct capability chart in form of single worst-case curve for wind generators (DFIG) for all loading condition. However, the voltage set-points of generators are manually set with local information and not optimally; and the methodology rely on the assumption of generators maximizing their own var contribution locally.

A systematic approach to aggregate widely spread DERs var capability with network constraints is not available in the literature. Based on this premise, the main goal of this

work is to adequately investigate the aggregation of var capabilities of multiple DER units in form of a net *P-Q capability curve* that can offer useful insight to TSO regarding the available var flexibility from distribution systems.

2.2.2 Impact of DER on Long-Term Voltage Stability Assessment of Integrated T-D System

Voltage collapse phenomenon of transmission system has always been a topic of interest for power system operators and researchers. Continuously increasing load demand is forcing grid to operate at closer to the loadability limit than ever. Several power grid blackouts in past have motivated various transmission voltage stability assessment (T-VSA) studies to accurately detect voltage collapse point and estimate load margin (73). Continuation power flow (CPF) is a widely accepted method to identify precise load margin by tracing accurate PV curves (74). However, in T-VSA studies, loads have always been modeled as an aggregated load. Whereas in real-life, the loads are spread throughout the distribution systems which are connected to load buses of transmission systems. Due to aggregation of loads rather than considering full distribution systems, the impacts of electrical distances of loads have been ignored in T-VSA studies which is a potential source of error in load margin estimation.

On the other hand, voltage collapse in distribution feeders also has been identified as a critical issue (75). A major blackout (June 1997) in the S/SE Brazilian system is attributed to voltage instability problem in one of the distribution networks which readily spread to the transmission grid (76). Moreover, distribution voltage stability assessment (D-VSA) has gained significant attention recently with the arrival of DERs on the feeders e.g. a continuation distribution power flow tool has been developed with DER integration (77). Several attempts have been made to assess how DER penetration improves load margin of distribution systems (78; 79; 80; 81; 82). However, in D-VSA, the substation bus has always been considered as a slack bus with an assumed constant voltage. Whereas in real-

life, this assumption doesn't hold true, and the substation voltage keeps changing based on the transmission power flow. This assumption might lead to significant errors in D-VSA results.

Thus, the T-VSA and D-VSA have been studied separately as independent systems neglecting their impact on each other so far. In reality, both transmission and distribution systems are coupled physically and affect each other. Especially, it is not possible to accurately capture DERs voltage supporting capability in T-VSA (83). Therefore, it is essential to consider an integrated transmission-distribution (TD) system and conduct TD-VSA studies for accurate estimation of load margin of the overall system.

In this work, we will investigate the impact of volt/var capability of DERs on the transmission system load margin.

2.2.3 Transmission-Distribution (T-D) Cosimulation

In order to investigate the true impact of DERs var support on transmission performance, T-D co-simulation is a more appropriate way rather than assuming aggregated load at substation as indicated by (83). The integrated system allows to include and observe the distribution system details as well as the changing substation voltage behavior which are not possible in traditional aggregated load modeling. A global power-flow (GPF) algorithm has been proposed by (84) to solve an integrated transmission-distribution system as a whole. A master-slave-splitting (MSS) method is developed to solve GPF iteratively until convergence. Several numerical results are presented to verify the convergence and accuracy of the proposed method. MSS is an interesting method to solve the integrated T-D system, however, it is not verified with the 3 phase unbalanced distribution systems with detailed modelings. (85) describes the integrated grid modeling system (IGMS), a power system modeling platform for integrated transmission-distribution analysis. It co-simulates the off-the-shelf open source distribution and transmission system solvers. A similar platform, bus.py is also developed by (86; 87) to enable communication between a distribution solver

(GridlabD) and a smart grid simulator using a python interface. Overall, the literature in co-simulation area is still in a nascent phase. Different co-simulation platforms are being developed based on different open source solvers and the application of interest.

In the proposed framework, we utilize a T-D co-simulation platform based on the established open-source power flow solvers (Pypower and GridlabD) to study and verify the true impact of DERs var support on the grid.

CHAPTER 3. REAL-TIME ADAPTIVE VOLT/VAR CONTROL WITH HIGH PV PENETRATION

3.1 Introduction

Volt/var control (VVC) of smart PV inverter is becoming one of the most popular solutions to address the voltage challenges associated with high PV penetration. This chapter focuses on the slope sensitive local droop VVC recommended by integration standard IEEE1547, rule21 and addresses their major challenges i.e. vulnerability to instability (or voltage oscillations), significant steady state error (SSE), and appropriate parameter selection under external disturbances. First, the sufficient condition for control stability and SSE convergence are derived followed by a small illustration and discussion to establish the problem. Based on the insights from the analysis and the discussion, a two-layer local and adaptive control framework is proposed. The adaptive VVC has two major features i.e. a) it is able to ensure both low SSE and control stability without compromising either and; b) it dynamically adapts its parameters to ensure good performance in a wide range of external disturbances such as sudden cloud cover, cloud intermittency, substation voltage change. Moreover, the adaptive control does not depend on the feeder topology information, thus also shown to be adaptive to the error in feeder topology information. The proposed control is implementation friendly as it fits well within the integration standard framework and depends only on local bus information. Towards the end, the performance is compared with the existing droop VVC methods (conventional droop and delayed droop) on an unbalanced 3-phase IEEE 123 test system with detailed secondary side modeling.

3.2 Droop Control Analysis: Inherent Challenges

Consider a general $N+1$ bus distribution system with one substation bus and N load buses with PV inverters. The power flow equations for the system can be written as

$$\begin{aligned} P^{inv} - P_d &= g_p(V, \delta) \\ Q^{inv} - Q_d &= g_q(V, \delta) \end{aligned} \tag{3.1}$$

Where $Q = [Q_2\ Q_3\ \dots\ Q_{N+1}]^T$ and $P^{inv} = [P_2\ P_3\ \dots\ P_{N+1}]^T$ are inverter reactive and real power injection vectors respectively at each bus. P_d and Q_d are similar vectors of real and reactive power loads at each bus. g_p and g_q are well-known power flow equations with voltage magnitude and angles as variables at all load buses (88).

The standard droop function $f_i(.)$ at i^{th} bus is shown in Figure2.1. It is a piecewise linear function with a dead-band d and slope m. Assuming the operating point is in non-saturation region, the inverter var dispatch at time t can be written as a function of previous voltage and other control parameters as

$$Q_{i,t+1} = f_i(V_{i,t}) = -m_i(V_{i,t} - \mu_i \pm d/2) \tag{3.2}$$

where, $Q_{i,t}$ and $V_{i,t}$ are the inverter var injection and the voltage magnitude respectively. Subscripts i and t denote i^{th} bus and time instant t. μ_i is the reference voltage and m_i is the slope of the curve. We consider the same slope for both the regions in the droop control for a given inverter as shown in Figure2.1. m can be maintained at desired value by changing control parameters as

$$m_i = q_{i,max}/(\mu_i - d/2 - v_{i,min}) = q_{i,min}/(\mu_i + d/2 - v_{i,max})$$

where $v_{i,min}$, $v_{i,max}$, $q_{i,min}$, $q_{i,max}$ are the four control set-points. It should be noted that in existing droop methods these parameters are either constant or un-controlled. Whereas, in this work, these parameters are dispatched based on the proposed adaptive control strategy. As detailed soon, dynamic control over these parameters leads to more reliable control performance compared to previous works.

3.2.1 Stability Analysis

As described in (54; 55), the local droop VVC can be modeled as feedback dynamical system ϕ with N states $[Q_{2,t}\ Q_{3,t}\ \dots\ Q_{N+1,t}]^T$ at discrete time t.

$$Q_{t+1} = \phi(Q_t) = f(h(Q_t)) \tag{3.3}$$

Where the vector $f(.) = [f_2\ f_3\ \dots\ f_{N+1}]$ contains local VVC functions which map the current voltage vector V_t to new inverter var injections vector Q_{t+1} i.e. $Q_{i,t+1} = f_i(V_{i,t})$. The new var vector Q_{t+1}, in turn, leads to the new voltage vector V_{t+1} according to power flow equations (1). The function h is an implicit function vector derived from (1) i.e. $h_i(Q_{i,t}) = V_{i,t}$. It is shown in (55) that the system ϕ is locally stable in the vicinity of an equilibrium point ($\bar{Q}$) if all eigenvalues of the matrix $\partial\phi/\partial Q$ have magnitude less than 1.

$$\left[\frac{\partial \phi}{\partial Q}\right]_{Q=\bar{Q}} = \left[\frac{\partial f}{\partial V}\right]\left[\frac{\partial V}{\partial Q}\right] \tag{3.4}$$

In the case of droop control, $\partial f/\partial V$ is a diagonal matrix with slope at each inverter as diagonal entries.

$$\left[\frac{\partial f}{\partial V}\right] = M = -diag(m_i) = -\begin{bmatrix} m_2 & \cdots & 0 \\ \vdots & \ddots & \vdots \\ 0 & \cdots & m_{N+1} \end{bmatrix} \tag{3.5}$$

Lets define $A = \partial V/\partial Q$ and $a_{ij} = \partial V_i/\partial Q_j$ which is a voltage sensitivity matrix with respect to var injection and can be extracted from the power flow Jacobian matrix from (1) as shown in (55).

$$[\Delta V] = [A]\,[\Delta Q] = \begin{bmatrix} a_{22} & \cdots & a_{2,N+1} \\ \vdots & \ddots & \vdots \\ a_{N+1,2} & \cdots & a_{N+1,N+1} \end{bmatrix}[\Delta Q] \tag{3.6}$$

Now, the sufficient condition for the control to be stable can be written as

$$\rho(MA) < 1 \tag{3.7}$$

Where ρ is spectral radius of a matrix which is defined as the largest absolute value of its eigenvalues. Condition (3.7) provides useful information for evaluating the stability of specific inverter slope settings. However, in order to obtain information for selecting the inverter slopes, we will derive another conservative sufficient condition for stability using spectral radius upper bound theorem (89).

Theorem 1: Let $\|.\|$ be any matrix norm on $\mathbb{R}^{n\times n}$ and let ρ be the spectral radius of a matrix, then for all $X \in \mathbb{R}^{n\times n}$:

$$\rho(X) \leq ||X|| \tag{3.8}$$

Proposition: If sum of each row of MA is less than 1, i.e.

$$m_i . \sum_{j=1}^{N} |a_{ij}| < 1 \quad \forall i, \tag{3.9}$$

Then the droop control will be stable i.e. $\rho(MA) < 1$

Proof: Using Theorem 1, if we apply $\|.\|_\infty$ on MA, then,

$\rho(MA) \leq \|MA\|_\infty = \max_{1\leq i\leq N} \sum_{j=1}^{N} |m_i.a_{ij}|$.

By condition 3.9, if $m_i . \sum_{j=1}^{N} |a_{ij}| < 1 \quad \forall i$, then the maximum of the sum of rows will also be less than one. Thus, the upper bound on spectral radius will always be less than one.

Remark 1: The condition (3.9) provides useful information to select slope for each inverter to ensure control stability, i.e. $m_i < m_i^c$, where m_i^c is critical slope given by $m_i^c = (\sum_j |a_{ij}|)^{-1}$. It should be noted that, usually, the entries of the sensitivity matrix A do not remain constant. Changes in operating conditions (cloud cover, load changes), as well as changes in feeder topology, lead to change in values of a_{ij} and m_i^c; thus can potentially cause instability if m_i are not updated dynamically. Intuitively, entries of A can also be seen as proportional to the reactance of the feeder lines (54) i.e. longer lines are more likely to have a higher magnitude of a_{ij} and lower value of the critical slope. Therefore, PV inverters on a rural network with long lines, especially towards the feeder end, will be more sensitive to instability and their slope selection should be more conservative. Therefore, non-adaptive

and homogeneous slope selection for all inverters makes system prone to control instability. Also, the uncontrolled changes in q_{min} and q_{max} with changes in solar generation leads to an undesired slope. For instance, in case of cloud cover, the generation drops and the q_{max} limit will be increased automatically leading to very high slope exactly when var support is not needed which creates stability/flicker issues. It is worth mentioning that the attempt to lower the effective slope by adding a delay block after droop in delayed droop (55) improves the stability compared to conventional droop i.e. $Q_{t+1} = f_i(V_{i,t}) + \tau.Q_t$, where τ is a delay coefficient. However, because of its non-adaptive nature and un-controlled parameters, it leads to issues under external disturbances and topology changes which will be illustrated through a comparison later in the section.

3.2.2 Steady State Error (SSE) Concerns

One of the major drawbacks of the droop control is a significant deviation from the set-point in steady state. To derive the analytical expression for SSE, lets assume the system is in equilibrium point $(\overline{Q}, \overline{V})$ at $t = 0$. Control equation (2) can be written in vector form at $t = 0$, as

$$[\overline{Q}] = [M][\overline{V} - \mu] \tag{3.10}$$

Now, consider an external disturbance perturb the equilibrium by causing sudden change in voltage, ΔV^d, at $t = 0$.

$$[Q_{t=1} - \overline{Q}] = [\Delta Q]_{t=1} = [M]\Delta V^d \tag{3.11}$$

Now (2) can be rewritten as following for $t > 0$

$$[\Delta Q]_{t+1} = [M][\Delta V]_t \tag{3.12}$$

Where $[\Delta Q]_{t+1} = [Q_{t+1} - Q_t]$ and $[\Delta V]_t = [V_t - V_{t-1}]$. Using (7) and (13), we can write

$$[\Delta V]_{t+1} = [A][M][\Delta V]_t \tag{3.13}$$

$$[\Delta V]_{t+1} = [A.M]^t[\Delta V]_{t=1} \tag{3.14}$$

Using (7), (12) and (15),

$$[V]_{t+1} = [V]_t + [A.M]^{t+1}\Delta V^d \tag{3.15}$$

$$[V]_{t+1} = [V]_{t=0} + \sum_{i}^{t+1}[A.M]^i\Delta V^d \tag{3.16}$$

In this case, the geometric progression series of matrices only converges if the condition (3.7) holds true (the stable case). Due to disturbance, initial voltage changes by ΔV^d i.e. $[V]_{t=0} = \overline{V} + \Delta V^d$. The new equilibrium voltage can be written as

$$\lim_{t\to\infty}[V]_{t+1} = \overline{V} + \Delta V^d + [I - A.M]^{-1}\Delta V^d \tag{3.17}$$

SSE vector can be written as

$$SSE = \lim_{t\to\infty}[V]_{t+1} - \mu \tag{3.18}$$

Equation (3.18) shows that, for a given disturbance, the only way to decrease SSE is to set higher values of slopes m_i which in turn might violate stability condition (3.9). In fact, in most cases, its a compromise between achieving acceptable low SSE and control stability in droop VVC. It can also be shown that the delayed droop (55) does not improve SSE compared to conventional control, though it improves the stability.

Remark 2: Note that it might be possible to maintain voltages within the ANSI range with high SSE, close to boundaries, for a given system conditions. But, any unexpected external disturbance can instantly push the voltages out of limits as illustrated later. Moreover, the tight voltage regulation capability with low SSE is not only desired just to maintain voltages within the ANSI range, rather it makes the system more flexible and provides enough room to the operator to perform other voltage-dependent applications such as CVR, loss minimization etc.; thus fully utilizing the PV inverters capability.

3.2.3 Illustration on a Small System

To corroborate the above analysis, we will illustrate the impact of external disturbances using a small modified IEEE 4 bus test system shown in Figure3.1. 600 kW load and 900 kW solar generation is added at node 3. A similar node 4 is added via a normally open switch to

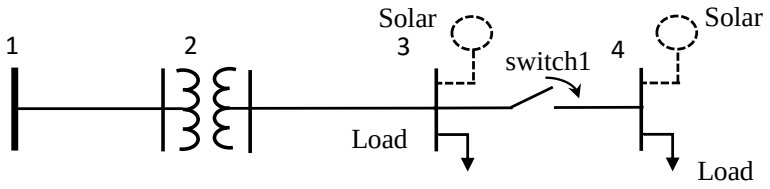

Figure 3.1 A small 4 bus example to demonstrate the impact of feeder reconfiguration and other external disturbances

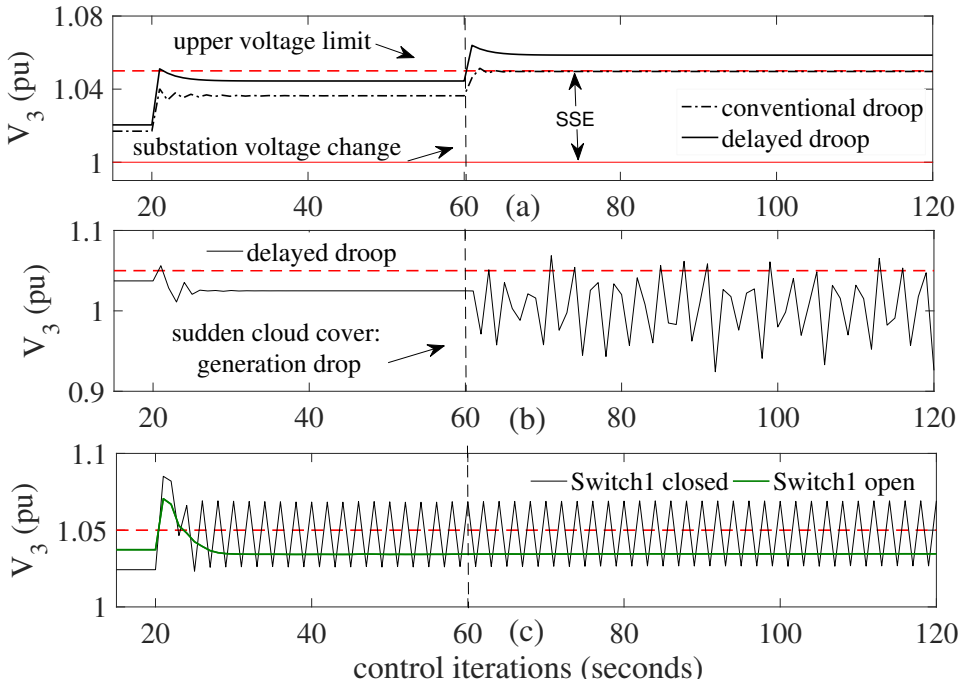

Figure 3.2 Impact of external disturbances on droop VVC under different slope settings: a) impact of change in substation voltage on conventional and delayed VVC at conservative slope settings; b) Impact of sudden cloud cover and; c) topology change on delayed droop VVC at non-conservative slope setting.

simulate the change in feeder topology. We will consider two types of initial slope settings to convey the main outcome of the analysis i.e. conservative ($m = 2$) and non-conservative ($m = 6$). Solar generation is applied at $t = 20$ to observe the impact of VVC with $\mu = 1$ at node 3 voltage profile. Figure3.2 (a) demonstrates how conservative settings cause high SSE (though, within the ANSI limit initially) for the droop controls (both conventional and droop) which leads to over-voltage violation due to a small change in substation voltage from 1.03-1.05 pu at $t = 60$. On the other hand, using non-conservative settings to reduce SSE makes the system prone to control instability or voltage flicker as shown in Figure3.2(b) and (c). Conventional droop is not shown as it is always unstable in this case. Figure3.2(b) shows that sudden drop in solar generation due to cloud cover at $t = 60$ increases q_{max} and makes the slope very high which causes voltage oscillations. Further, to simulate the impact of the topology change or error in topology information, switch1 is closed at $t = 60$. Delayed droop, as discussed before, is stable under normal conditions, however, change in feeder topology leads to voltage oscillations as shown in Figure3.2(c) at non-conservative settings. This example demonstrates it is difficult to achieve both low SSE and control stability under external disturbances with existing droop controllers. Moreover, this problem becomes more crucial in a large realistic system due to thousands of independent inverter devices, dynamic nature of generation and loads and higher possibility of inaccuracy in feeder topology information and in parameter selection.

Therefore, our intention is to develop a new droop based adaptive VVC strategy 1) to achieve both low SSE and low voltage oscillations (stability) simultaneously; 2) to make control parameters dynamically self-adaptive to external disturbances and inaccurate feeder information in real-time ; and 3) to keep VVC purely local and compatible to VVC framework recommended by recent utility and IEEE standards.

3.3 Adaptive Control Strategy

This section will introduce the proposed adaptive local VVC function $f_i^p(V_{i,t}, cp_i)$ which can be written as follows:

$$Q_{i,t+1} = f_i^p(V_{i,t}, cp_i) = \mathbb{P}[q_i^p - m_i^p(V_{i,t} - \mu_i)] \tag{3.19}$$

Where $cp_i = [m_i^p, q_i^p, q_{min,i}^p, q_{max,i}^p, v_{max,i}^p, v_{min,i}^p,]$ are control parameters. $\mathbb{P}$ is the saturation operator with $(q_{min,i}^p, q_{max,i}^p)$ as saturation var limit parameters applied at cut-off parameters $(v_{max,i}^p, v_{min,i}^p)$. q_i^p is an error adaptive parameter and its main function is to provide SSE correction. Desired adaptive slope m_i^p can be set as,

$$m_i^p = \frac{q_{min,i}^p - q_i^p}{\mu_i - v_{max,i}^p} = \frac{q_{max,i}^p - q_i^p}{\mu_i - v_{min,i}^p} \tag{3.20}$$

There are two unique features of this control. First, the functions of maintaining control stability and low SEE are decoupled. Two different parameters m^p and q^p are used to achieve control stability and low SSE respectively with different approaches so that none of the objectives are compromised. Second, all these parameters are dynamically adapted in real-time. Superscript p denotes the adaptive nature of the control parameters. To achieve this, a two-layer control framework is proposed as shown in Figure3.3. The inner layer is a fast VVC function $f_i^p(V_{i,t})$ to track the desired set-point μ_i according to (3.19). The outer layer dispatches the control parameters (cp_i) based on the proposed adaptive algorithm described later in the section. The outer layer works on a relatively slower time scale (t_o) to allow inner fast control to reach steady state before dispatching new control parameters, thus avoiding hunting and over-corrections. Control time-line is shown in Figure3.4. Control parameters are updated at every period T, control horizon of the outer loop control. Each iteration of the inner and outer loop control is denoted by t_{in} and t_o respectively. The adaptive algorithm consists of two strategies where q_i^p and m_i^p are dynamically adapted to take care of SSE and voltage instability/flicker respectively as described below.

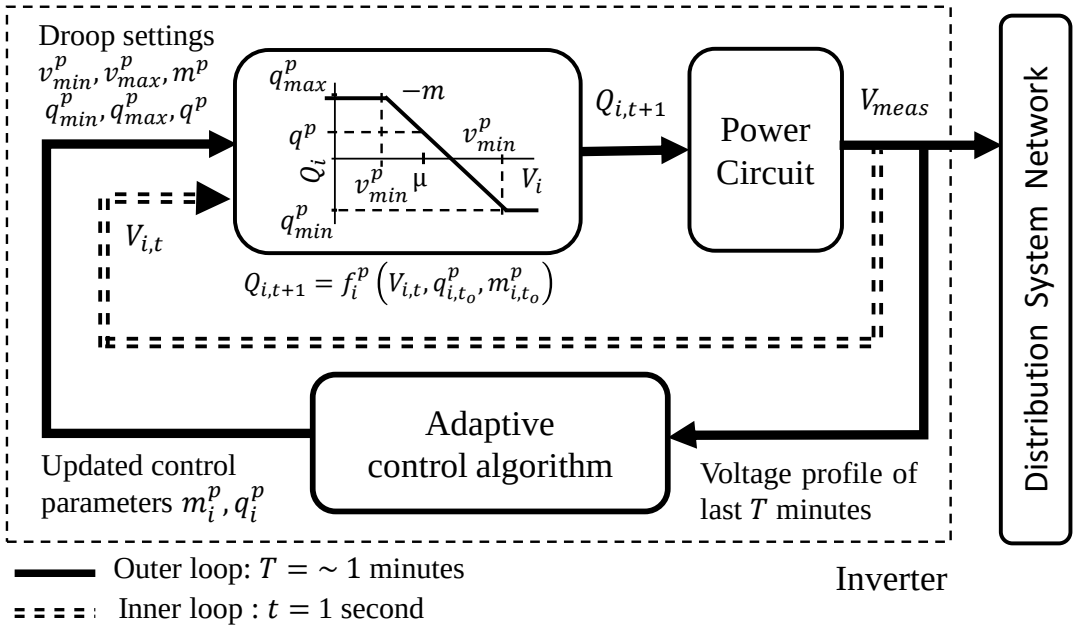

Figure 3.3 Two-layer framework of the proposed adaptive control approach

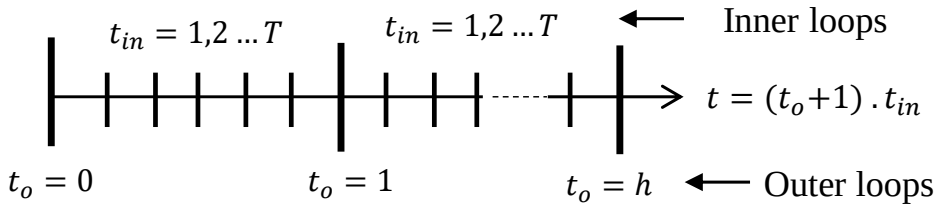

Figure 3.4 Time-line of adaptive inner and outer loop control

3.3.1 Error Adaptive Control: Strategy I

The aim of the strategy I is to minimize SSE by adapting the error adaptive parameter q_i^p. We will analyze how the proposed control (3.19) helps to mitigate the SSE and accordingly develop a mechanism to adapt q_i^p locally. Consider the system is at equilibrium point $(\overline{Q}, \overline{V})$ at $t = 0$ with $SSE = \overline{V} - \mu$. Now if the parameter q^p is changed at $t = 0$ by Δq^p, the new voltage deviation (SSE^{adp}) can readily be obtained by following the procedure provided in the Section II.B by replacing the conventional droop (3.2) with the adaptive control (3.19):

$$SSE^{adp} = \overline{V} - \mu + [I - AM]^{-1} A \Delta q^p \tag{3.21}$$

To achieve $SSE^{adp} = 0$, Δq^p required will be,

$$\Delta q^p_{req} = -(A^{-1} - M) SSE \tag{3.22}$$

Equation (3.22) provides the analytical expression of the required change in q^p parameter to achieve zero SSE in just one iteration. However, this solution requires the information of A matrix, SSE and slope (M) at all inverter buses which is not available to local bus controllers. Moreover, estimation of A is contingent to error in centralized feeder topology information and may not be reliable. Therefore, we propose a local version of the analytical solution (3.22) i.e. $\Delta q_i^p = -k_i^d . SSE_{avg,i}(t_o)$, where SSE_{avg} defined for each outer loop as

$$SSE_{avg,i}(t_0) = \sum_{t_{in}=1}^{T} (V_{t_0 t_{in},i} - \mu_i)/T \tag{3.23}$$

$SSE_{avg,i}$ denotes the average set-point deviation of voltage at i^{th} inverter bus. A tolerance band for $SSE_{avg,i}$ can be defined as $\mu_i \pm \epsilon_{sse}$, where ϵ_{sse} is tolerance for the deviation. In this strategy, the adaptive term $q_i^p(t_o)$ in (20) is updated at each outer loop interval t_o, based on the real-time estimation of $SSE_{avg,i}$ during the last time horizon T as

$$q_i^p(t_o) = q_i^p(t_o - 1) - k_i^d . SSE_{avg,i}(t_o) \tag{3.24}$$

It is important to note that SSE_{avg} is used as an algebraic value with sign. The sign of the error decides whether q_i^p needs to be moved positive or negative. If the voltage settles

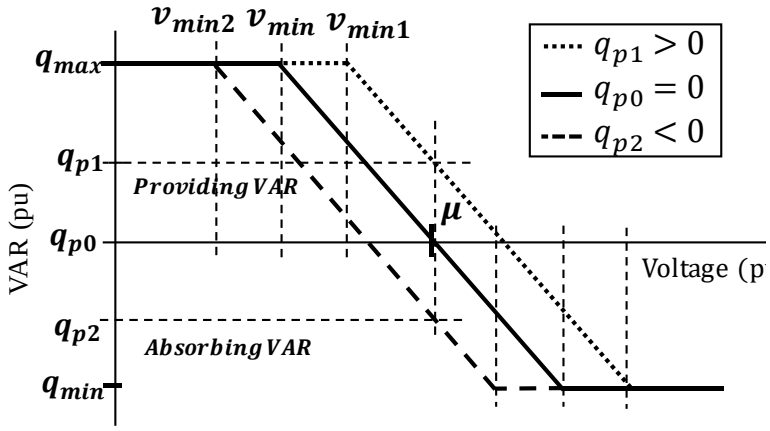

Figure 3.5 Adaptive VVC with different error adaptive parameter q_p

on a higher value than the set point, a negative term is added in q_i^p to facilitate more var absorption to lower the voltage. Similarly, a positive term is added in q_i^p to provide more var when voltage settles lower than the set point. A constant $k_i^d > 0$ is a correction factor which can be decided once from the off-line studies. A higher k_i^d brings SSE_{avg} within the desired range faster and vice versa. Figure3.5 depicts the adaptive control $f_i^p(V_{i,t}, cp_i)$ with different q_i^p values. Note that the solid curve with $q_i^p = 0$ is same as the conventional droop control $f_i(V_{i,t})$ in (2). Figure3.5 brings out an important feature of the proposed control that it can be seen as "shifted and adaptive" droop VVC which makes it compatible with the integration standards.

Nonetheless, it should be noted that the proposed approach may take more than one iterations to achieve near-zero SSE, unlike the analytical solution. However, it is compensated by the advantage that it requires only local bus information, making it more feasible. Nevertheless, the update strategy can always be made faster and more accurate using (3.22), if the information at other nodes is also available in the future.

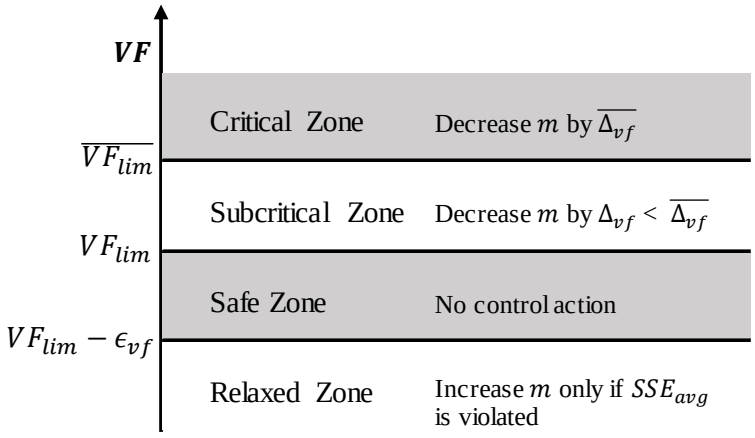

Figure 3.6 Control action region for adaptive outer loop control strategy II for flicker mitigation

3.3.2 Adaptive Slope Control: Strategy II

The objectives of the strategy II are to ensure stability as well as to keep voltage fluctuations within the IEEE 141 standard limit (19) by adapting parameter m_i. Therefore, voltage flicker (VF) is used as the control criteria which is defined as the voltage fluctuations in loads which cause irritation to user eyes (19). Based on (19), we define the short-term flicker calculation for each inverter bus at the beginning of each outer loop as

$$VF(t_o) = \sum_{t_i=1}^{T} \frac{(V_{t_o t_i} - V_{t_o t_i - 1})/V_{t_0 t_i}}{T} \times 100 \tag{3.25}$$

As seen in (15), voltage fluctuations are proportional to slope and can be reduced by decreasing m_i. For this purpose, the voltage flicker range is divided into four control regions as shown in Figure3.6. The IEEE standard 141 flicker curve provides the maximum fluctuation limit ($\overline{VF_{lim}}$) beyond which we define as *critical flicker zone*. The same standard also gives a borderline flicker limit (VF_{lim}). The region between ($\overline{VF_{lim}}$) and VF_{lim} is termed as the *subcritical flicker zone*. Further we define a tolerance ($VF_{lim} - \epsilon_{vf}$) and the tolerance band is termed as the *safe flicker zone*. The region below safe flicker zone is defined as the *relaxed flicker zone*. In critical zone, we update the parameters by a larger amount ($\overline{\Delta_{vf}}$) to avoid control instability and to return to subcritical zone faster. In subcritical zone,

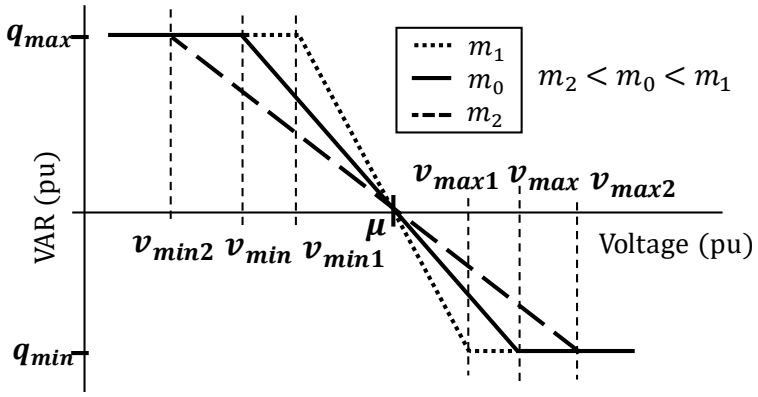

Figure 3.7 Adaptive strategy II: changing slope of droop curve by changing v_{min} and v_{max} parameters to keep flicker in the limit

the slope is decreased in a smaller step (Δ_{vf}) to avoid over-correction which might impact SSE_{avg} negatively. As soon as we reach the safe zone, no control action is taken. This is the desired range of control parameters. Though rarely required, in the relaxed zone, slope is increased to improve SSE only if SSE is out of range. Correction factors (Δ_{vf}) are estimated offline in this work, though they can always be made responsive to the online control performance, if required.

It is worth noting here that the the main feature of the proposed control lies in the decoupling of the two functionalities i.e. SSE and slope. since SSE is catered by q_i^p, the slope can always be in the conservative range (safe or relaxed zones) to ensure control stability. In this work, we use the earlier derived condition (3.9) to choose initial slopes. It is estimated using off-line studies for the base case, however, to keep safe margin it can be further reduced by a certain factor. Figure3.7 depicts the control strategy II with adaptive m_i.

3.3.3 Overall Adaptive Algorithm

Update strategy of error adaptive parameter and slope have been discussed above, however, there are few more control parameters which need to be updated i.e.$q^p_{max}, q^p_{min}, v^p_{min,i}$ and $v^p_{max,i}$.

Updating q^p_{max}, q^p_{min}: While it is possible to defer real power solar generation, in this work the consumer value is maximized by limiting var output to leftover capacity and not curtailing real power generation. To utilize the inverter capacity entirely, q^p_{max} and q^p_{min} are also updated in every outer loop as

$$q^p_{max}(t_o) = \sqrt{s^2 - p^2_{pv}(t_o)} \tag{3.26}$$

$$q^p_{min}(t_o) = -\sqrt{s^2 - p^2_{pv}(t_o)} \tag{3.27}$$

where, s is inverter rating and $p_{pv}(t_o)$ is the average solar PV real power generation in the last outer loop time interval.

Updating v^p_{max}, v^p_{min}: Thus, we get the new parameters $q^p_i(t_o)$, $q^p_{min,i}(t_o)$, $q^p_{max,i}(t_o)$ from strategy I and $m^p_i(t_o)$ from strategy II.

Finally, $v^p_{min,i}(t_o)$ and $v^p_{max,i}(t_o)$ parameters are calculated using (3.20) and dispatched to be used in the inner loop.

$$v^p_{min,i}(t_o) = \mu - \frac{q^p_{max,i}(t_o) - q^p_i(t_o)}{m^p_i(t_o)} \tag{3.28}$$

$$v^p_{max,i}(t_o) = \mu - \frac{q^p_{min,i}(t_o) - q^p_i(t_o)}{m^p_i(t_o)} \tag{3.29}$$

Overall detailed algorithm of the adaptive control strategy is shown below.

Algorithm 1: Adaptive control scheme

1. Real-time measurement and control criterion calculation
   - 1.1. Collect $V_{t=t_o.t_{in}} \forall t_{in} = 1, 2, \ldots, n$
   - 1.2. Calculate $SSE_{avg}(t_o)$ and $VF(t_o)$
2. Go to adaptive strategy I: error adaptive
   - 2.1. If $|SSE_{avg}(t_o)| > \mu + \epsilon_{sse}$
     $$q_p(t_o) = q_p(t_o - 1) - k_d.SSE_{avg}(t_o)$$
   - 2.2. Else,
     $$q_p(t_o) = q_p(t_o - 1)$$
   - 2.3. update $q_{max}(t_0)$ and $q_{min}(t_0)$: equation (3.27,3.26)
3. Go to adaptive strategy II: slope adaptive
   $$m^p(t_0) = m^p(t_0 - 1) + \Delta_m$$
   - 3.1. If $VF(t_o) > \overline{VF_{lim}}$ $\quad \Delta_m = -\overline{\Delta_{vf}}$
   - 3.2. Else if $VF(t_0) > VF_{lim}$ $\quad \Delta_m = -\Delta_{vf}$
   - 3.3. Else if $VF(t_0) > (VF_{lim} - \epsilon_{vf})$ $\quad \Delta_m = 0$
   - 3.4. Else, check if $|SSE_{avg}| > \mu + \epsilon_{sse}$ $\quad \Delta_m = \Delta_{vf}$
4. Update final parameters v_{min} and v_{max}: equation (3.28,3.29)
5. $t_o = t_o + 1$, go to step 1

3.4 Convergence of the Proposed Local Adaptive Control Algorithm

The convergence properties and conditions of the proposed adaptive control (3.19) will be investigated in this section. Since it's a two-layer control, we need to study the convergence of both the control loops. If we assume the time horizon T is sufficient for faster control to reach its steady state, the inner loop control equation within the time T can be written as

$$Q_{i,t_{in}+1} = q_i^p - m_i^p(V_{i,t_{in}} - \mu_i) \tag{3.30}$$

Where adaptive parameters q_i^p and m_i^p are constant for the time horizon T. Using the stability analysis performed in Section II, a sufficient convergence criteria for (3.30) can be derived which is same as given by condition (3.9) and remark 1, i.e. $m_i^p < m_i^c$. Therefore, the inner local control will always converge if the chosen slopes are below critical slope values. Adaptive control strategy II helps to maintain this condition by keeping slope in conservative range as discussed earlier.

3.4.1 Outer Loop Control Convergence

To derive the analytical expression for the outer loop convergence criteria, lets assume the system is currently at outer loop iteration t_o for which inner control has already reached its steady state ($\overline{V_{t_o}}$,$\overline{Q_{t_o}}$). This can be represented as

$$[\overline{Q}]_{t_o} = [q^p]_{t_o} - [M^p][S]_{t_o} \tag{3.31}$$

Where, let's represent the SSE_{t_0} vector with a shorter notation $S_{t_o} = [\overline{V}_{t_o} - \mu]$. Now the q^p parameter is locally updated for outer loop iteration $(t_o + 1)$ based on the update formula given in (3.24) i.e. $q^p_{i,t_o+1} = q^p_{i,t_o} - k_i^d.S_{i,(t_o)}$. Now a new updated inner loop steady state ($\overline{V}_{t_o+1}$,$\overline{Q}_{t_o+1}$) is reached for the outer loop iteration $(t_o + 1)$ which can be written in vector form as

$$[\overline{Q}]_{t_o+1} = [q^p]_{t_o} - [K^d][S]_{t_o} - [M^p][S]_{t_o+1} \tag{3.32}$$

Where K^d is a diagonal matrix with the correction factor k_i^d at each bus as its diagonal entries. Since the objective is to minimize SSE, we can replace all other state variable with S_{t_o} by subtracting (3.32) from (3.31) and using (3.6) i.e. $\Delta V = A\Delta Q$ as following:

$$[S]_{t_o} - [S]_{t_o+1} = A\Big[K^d.S_{t_o} - M^p(S_{t_o} - S_{t_o+1})\Big] \tag{3.33}$$

After manipulating (3.33), the outer loop control can be written as a discrete feedback dynamical system with SSE as the only state variable as following.

$$[S]_{t_o+1} = B[S]_{t_o} \tag{3.34}$$

Where $B = I - [I + AM^p]^{-1} AK^d$ is a constant matrix which defines the convergence behavior of the outer loop control. We know that any linear discrete system $x[k+1] = Bx[k]$ is asymptotically stable if and only if all eigenvalues of B have magnitude less than 1 (90). Consequently, the convergence condition for the outer loop control can be written as

$$\rho(B) < 1 \tag{3.35}$$

Where ρ is spectral radius of a matrix. Therefore, the convergence of the outer loop is ensured as long as the selection of K^d matrix does not violate the condition (3.35). In such cases, the outer loop control system (3.34) will always converge to zero SSE for any amount of initial SSE i.e. $\lim_{t_o \to \infty} S_{t_o} = 0$ for any $S_{t_o=0}$.

Remark 3: It is interesting to observe here if we choose a non-diagonal $K^d = A^{-1} + M^p$, B turns out to be zero and the SSE can be converged to zero in just one iteration. However, in that case, the q^p update ($q^p_{t_0+1} = q^p_{t_0} - K^d.S_{t_o}$) does not remain local i.e. to update q^p_i at i^{th} node, non-diagonal entries k^d_{ij} need to be multiplied with SSE at all other j^{th} nodes. Therefore, we compromise with the convergence speed to take advantage of the local feature of the control.

For a better understanding of this analysis, let's consider a simple example system described in Figure3.1. Note that this example system can be seen as an equivalent two-bus system as there is only one load bus (bus 3) when switch is open. In that case, $B = b$ and $K = k$ will be a scalars, $b = 1 - k/(a^{-1} + m)$. The sensitivity matrix $A = a_{33} = 0.2857$ var pu/volt pu is calculated offline for the base case. Using $m^c_i = (\sum_j |a_{ij}|)^{-1}$, derived from condition (3.9), the critical slope for this system turns out to be $m^c = 1/a_{33} = 3.5$. In order to be in conservative range, $m = 1$ is chosen as initial slope. This system converges to zero only if $|b < 1|$ i.e. $0 < k < 2(a^{-1} + m)$. Further, within this stable region, three special cases can be analyzed i.e. $k < (a^{-1} + m), k = (a^{-1} + m)$ and $(a^{-1} + m) < k < 2(a^{-1} + m)$. Figure3.8 demonstrates the SSE response of the example system under these three stable cases and one unstable case. In the first case of $k^d < 4.5$, the system converges to zero without oscillations (overdamped response). In the second case of $k^d = 4.5$, system reaches

zero SSE in just one iteration and in the third case of $k^d > 4.5$, it converges with decaying oscillations (underdamped response). For $k^d > 9$, the SSE starts diverging with non-decaying oscillations.

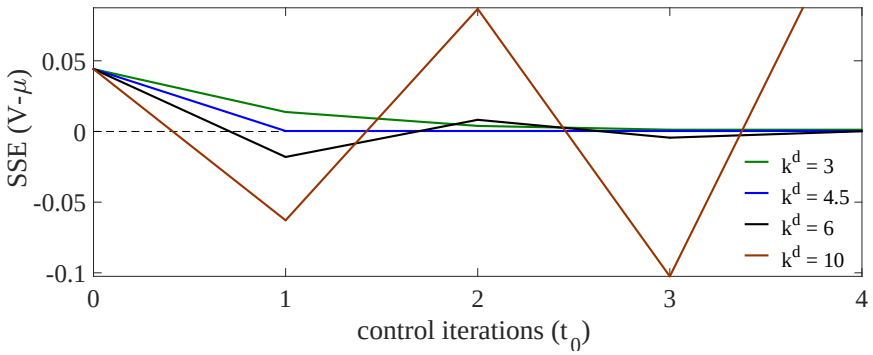

Figure 3.8 SSE convergence profile of the proposed adaptive outer loop control under different values of k^d

3.5 Case Study

3.5.1 4 Bus System Illustration

The proposed adaptive VVC performance is compared with delayed control for the example system described in the Section 3.2.3 in Figure3.9. Since it is a small system, outer loop time horizon of 10 seconds is adequate to demonstrate adaptive nature of the control. Other system setup details and parameters selections are same as described earlier. At $t = 60$, when the voltage profile gets a surge due change in substation voltage from 1.03 to 1.05, the adaptive control starts adapting itself to re-track the set-point in 2 steps. Whereas, the delayed VVC leads to voltage violation due to high SSE and non-adaptive nature. Similarly under non-conservative settings, in (b) and (c), adaptive control is able to maintain the control stability under the impact of sudden cloud cover and topology changes, unlike the delayed control.

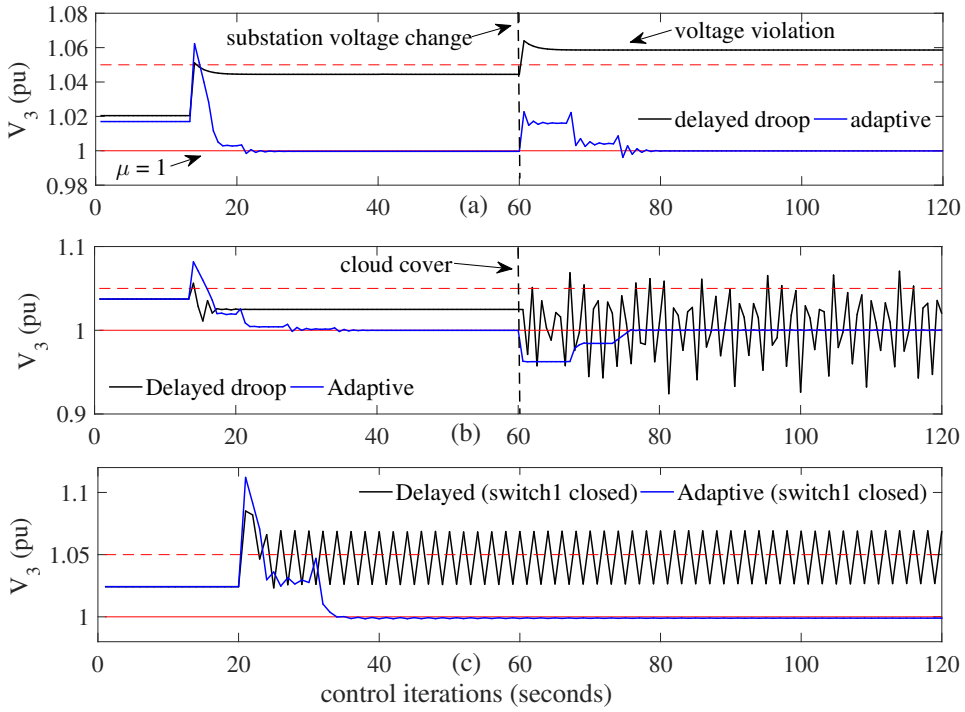

Figure 3.9 Adaptive VVC performance comparison with delayed VVC under impact of : a) substation voltage change; b) sudden cloud cover and; c) topology change

3.5.2 Large Test Case Modeling

The proposed adaptive control is tested on IEEE123 bus test system which is an unbalanced three-phase feeder (91). To create a more realistic simulation, the test system is further expanded with detailed secondary side house-load modeling at 120 volts resulting in 1500 nodes as shown in Figure3.10 using GridLAB-D platform; GridLAB-D is an open-source agent-based simulation framework for smart grids developed by Pacific Northwest National Lab (92). Each residential load is modeled in detail with ZIP loads and temperature dependent HVAC load (93)(94). Diversity and distribution of parameters within the residential loads is discussed in (95). The feeder is populated with 1280 residential houses with approximately 6 MW peak load. Inverter ratings are considered 1.1 times the panel ratings. Uniformly distributed solar PVs throughout the feeder create lesser problems than the PV units distributed in one area of the feeder. Therefore, to demonstrate the effectiveness of the control in more severe case, PV units are distributed randomly at 500 houses only in right half of the feeder. Temperature and solar irradiance data for January 2, 2011, is obtained from publicly available NREL data for Hawaii (96). Load and solar profiles for the day have been shown in Figure3.11.

3.5.3 Performance Metrics

We will be using three performance metrics to evaluate the proposed control approach.

1. *Mean Steady State Error (MSSE)*

   First metric is mean steady state error ($MSSE$) which evaluates control set-point tracking performance. It is absolute average percentage of voltage set-point deviation at all the houses with solar PV, throughout the day or over the concerned time period. It is calculated as

$$MSSE = \sum_{i=1}^{n} \sum_{t=1}^{h} \frac{|V_{t,i} - \mu|}{h} . \frac{1}{n} \times 100 \tag{3.36}$$

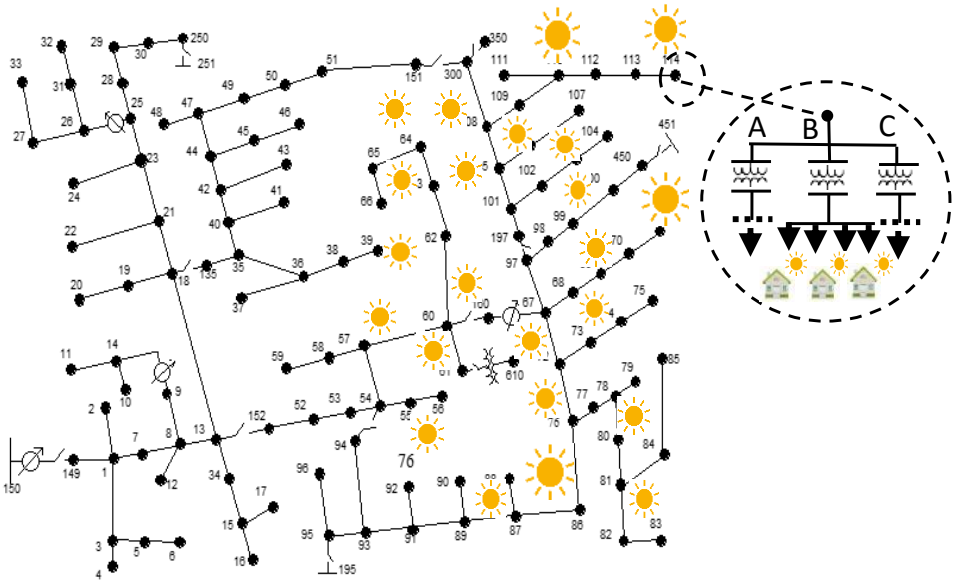

Figure 3.10 IEEE 123 bus test system with detailed secondary side modeling

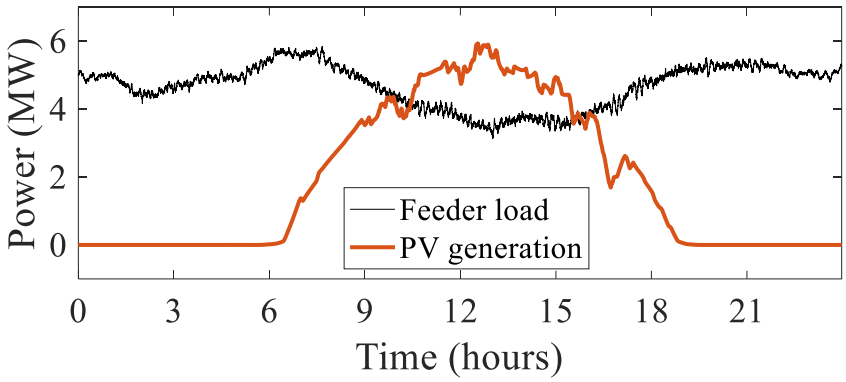

Figure 3.11 Total feeder load and solar PV profile for 24 hours

Where n is the total number of solar PV units and h is total time duration. A lower value of MSSE can be interpreted as better set point tracking performance of the control.

2. *Flicker Count (FC)*

   Second metric is flicker count (FC) where one flicker violation at one house is considered when VF value, as defined in (3.25), exceeds VF_{lim}. The total number of such flicker violations at all of the houses is termed as FC. A higher value of this metric is an indication of lesser power quality and an oscillatory voltage profile that in turn indicates the possibility of unstable control.

3. *Voltage Violation Index (VVI)*

   The third metric is voltage violation index (VVI) which is the total number of voltage violations at all of the buses during the concerned time period. Based on ANSI standards (15), both instantaneous (type A) and continuous (type B) violation limits are considered to calculate voltage violations. a voltage violation is counted if the voltage at a bus violates either 1) 1.06-0.9 pu band instantaneously (range A) or 2) 1.05-0.95 pu band continuously for 5 minutes (range B).

3.5.4 Results

In this section, we will demonstrate the effectiveness of the proposed control scheme in a wide range of external disturbances and operating conditions. The adaptive control performance (blue) will be compared with no control (green) and existing droop controllers i.e. conventional (orange) and delayed droop (black). Voltage profiles and parameters dispatched are shown at a randomly chosen solar PV unit at bus 92 whereas the performance metrics are calculated for the whole system. Dashed and solid red lines denote the voltage

violation limits and voltage set-point respectively. Outer loop horizon T is taken as 1 minute.

3.5.4.1 Control Performance on Static Load Condition

In order to evaluate how well the proposed control can track a given set-point, a sudden set-point change is applied at the static load conditions in Figure3.12. Load and solar conditions at 11 AM are used for this purpose. Figure3.12(a) compares the set point tracking performance of the adaptive control with no control, conventional droop control and delayed droop control cases. Set point μ is changed from 1 to 0.96 pu at the middle of the simulation for all the inverters. As expected, the voltage profile in the no control case is steady. The conventional control lowers the voltage on set point change but fails to track it accurately and settles down with high SSE value. It is interesting to observe that the delayed control has exactly same steady state performance as conventional control. We analyzed the same conclusion in earlier section as well through SSE derivation. The adaptive control scheme, however, is able to track the set-point accurately by adapting q_p parameter. It verifies the adaptability of the control to the changing set-points. Inverter var and q_p parameter dispatch in the adaptive control is shown in Figure3.12 (b).

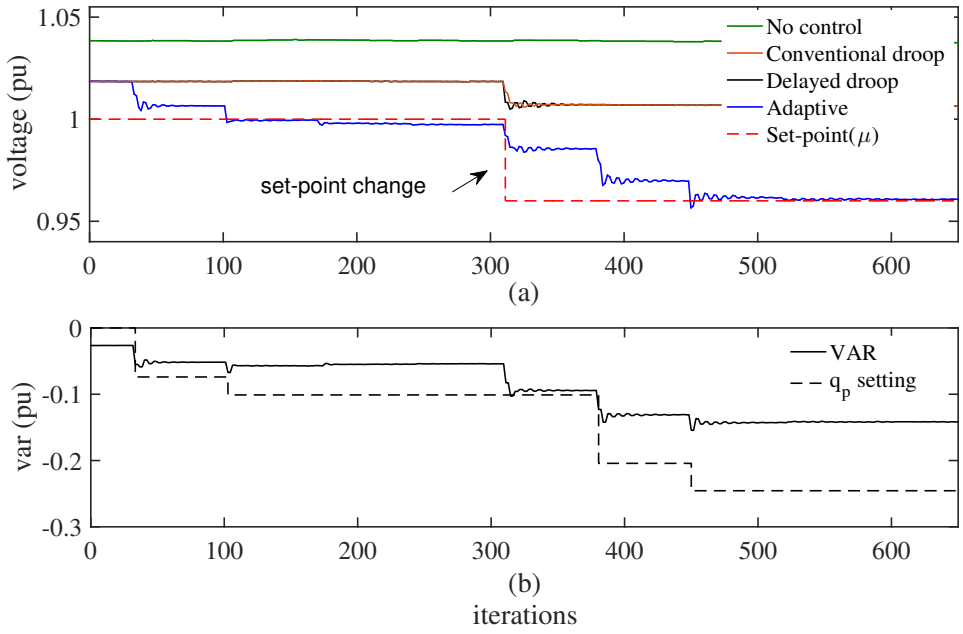

Figure 3.12 (a) inverter voltage profile to compare set-point tracking performance of adaptive control;(b) inverter var and q_p parameter dispatch in adaptive control scheme at bus 92

3.5.4.2 Dynamic Tests with Daily Load and Solar Variation

A day-long load and solar profile can be seen as continuous external disturbances in the system. Figure3.13(a) shows that during the daytime, non-adaptive droop controls are not able to track the set point voltage which might lead to voltage violations e.g. around 12 noon when the solar generation is at peak. $\mu = 0.97$ and homogeneous conservative settings ($m = 3$) are used for conventional and delayed control. Whereas the adaptive control adapts its parameters at each bus differently to keep a flat voltage profile throughout the day; note, this may not be entirely desirable for the utility, or the owners, due to increased var flows, but rather indicates the flexibility of the system for applications such as conservative voltage reduction, loss minimization etc. Figure3.13(b) shows the dynamic dispatch of adaptive error parameter q^p at bus 92. The performance metrics for the whole system are compared in 3.1. In this case, high MSSE in delayed control is because of selecting a conservative slope setting which can be improved by choosing higher slope, however, it will

make the control highly vulnerable to sudden external disturbances as demonstrated in the next results. Whereas due to its decoupled functionality, the proposed control is capable of achieving near-zero MSSE even at conservative settings, thus not making system prone to instability or voltage flicker.

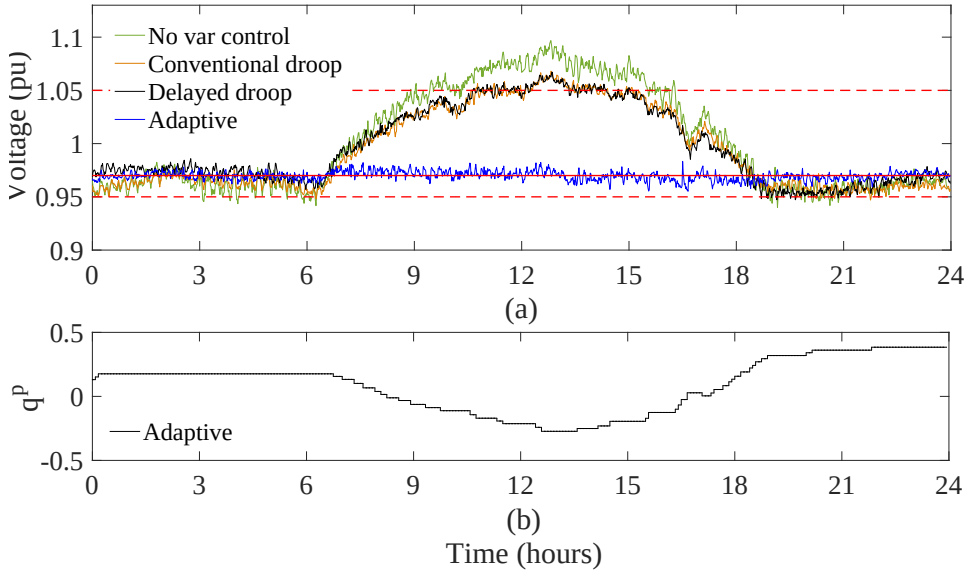

Figure 3.13 Comparison of adaptive control performance throughout the day: a) voltage profile; b) dispatch of error adaptive parameter (q^p)

Table 3.1 Performance Metrics Comparison for 24-hour profile

Metrics	No control	Conventional droop	Delayed droop	Adaptive control
MSSE	5.2%	4.3%	4.3%	0.3%
VVI	5×10^5	21853	16137	0
FC	0	0	0	0

3.5.4.3 Dynamic Tests with Sudden External Disturbances

Reliable performance under external disturbances is a unique feature of the proposed control. To demonstrate this, the control performance is tested with sudden external disturbances. A smaller window of 1-2 hours is considered when solar is at its peak to observe the most severe impact of disturbances.

A) Cloud Intermittency: Usually cloud covers cause two types of disturbances in PV generation i.e. intermittency and sudden drop in the generation as shown in Figure3.14 and Figure3.16 respectively. In this section, we will consider the impact of intermittent cloud behavior on voltage profile and the performanc of adaptive control. Cloud intermittency data of 30 seconds scale is considered. $\mu = 1$ and $m = 5$ are used for non-adaptive controls. Figure3.15 shows how cloud intermittency causes high voltage fluctuations in conventional control which leads to violations. Delayed control reduces the flicker significantly compared to conventional (from 6919 to 107), however, still results in a good number of violations due to high SSE as shown in Table 3.2. Though, the effect of intermittency is also visible in adaptive control voltage profile (Figure3.15 (b)), it manages to achieve zero indices of flicker and violations. It demonstrates the effectiveness of control in faster disturbances.

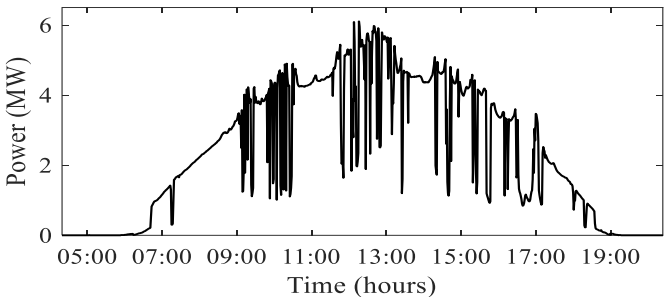

Figure 3.14 Solar profile with cloud intermittency

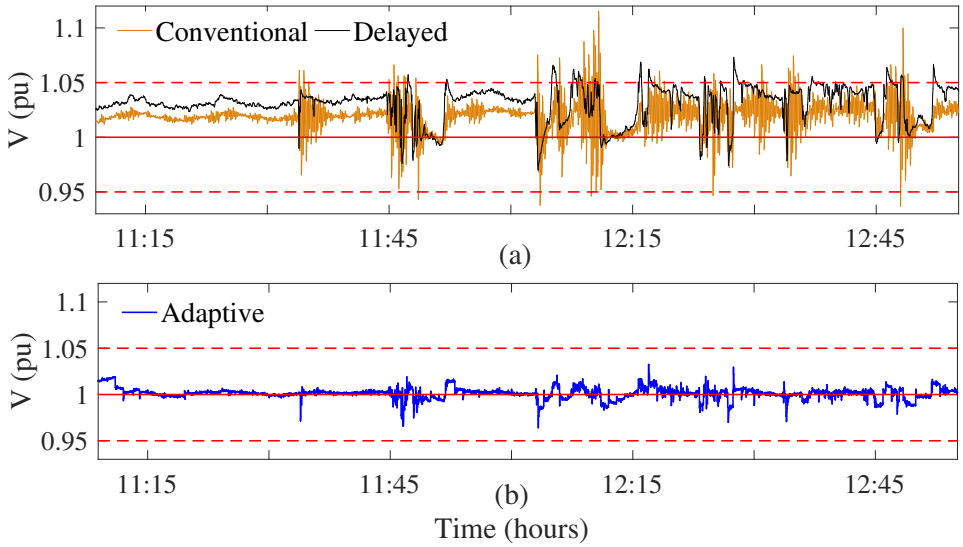

Figure 3.15 Control performance comparison under cloud intermittency

Table 3.2 Performance Metrics Comparison For Intermittent Solar-Profile For A Two-Hour Window

Metrics	No control	Conventional	Delayed	Adaptive
MSSE	3.5%	2.00%	2.00%	0.40%
VVI	5×10^5	21853	16137	0
FC	122	6919	107	0

B) Sudden Cloud Cover: On the other hand, using non-conservative settings ($m = 10$)to decrease violations can cause stability issues with sudden cloud cover as shown in Figure3.17. At 11.30 AM, a cloud cover results in a sudden drop in real power generation (Figure3.16) which frees the inverter capacity. Since conventional and delayed controls utilize all the free capacity immediately without monitoring, it increases the slope by a significant amount and results in voltage oscillations as shown in Figure3.17(a). Whereas, the adaptive control dynamically regulates the settings in real-time to ensure stable voltage profile as well as quick restore of the set-point tracking as visible in Figure3.17(b).

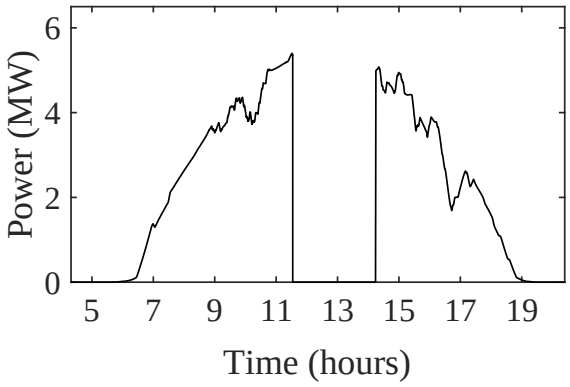

Figure 3.16 Solar profile with sudden cloud cover

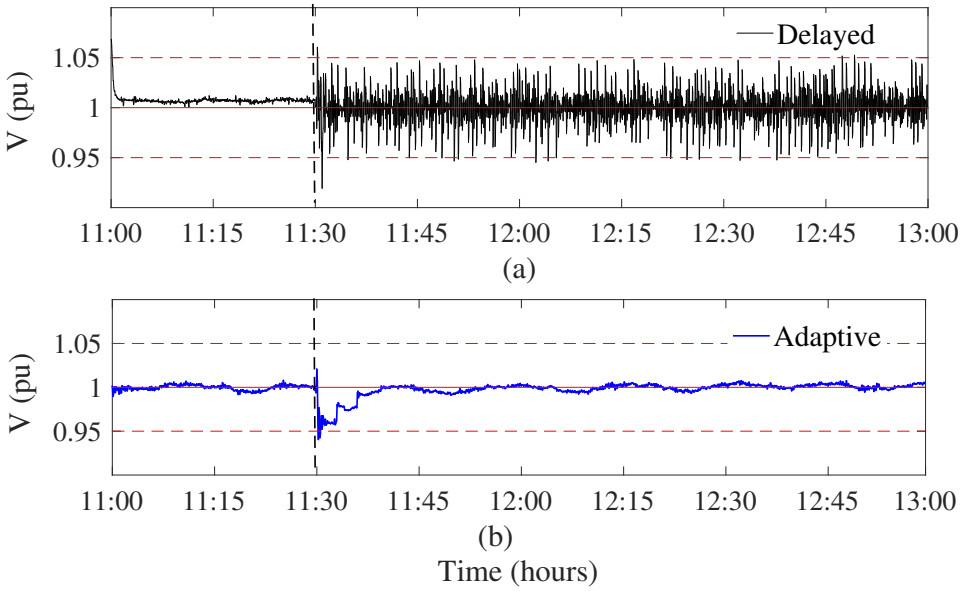

Figure 3.17 Control performance comparison under sudden cloud cover

C) Change in Substation Voltage: The primary side of substation voltage keeps changing due to changes in the transmission systems. conservative setting ($m = 5$) is used here for non-adaptive controls. In Figure3.18, at 12 noon, the feeder experiences a surge in primary substation voltage from 1 to 1.07 pu. Conventional control experiences high voltage oscillations. Delayed control does not experience voltage flicker but since it cannot reduce the SSE on its own, it waits for substation tap changer to operate to bring voltage within the limit again. Whereas adaptive control suffers from few instantaneous violations but immediately starts re-tracking the set-point, thus avoiding violations for long time period. Figure3.19shows how the tap changers behave after substation voltage change. It can be seen that it takes around 20 minutes for tap changers to settle down which is enough time to cause violations.

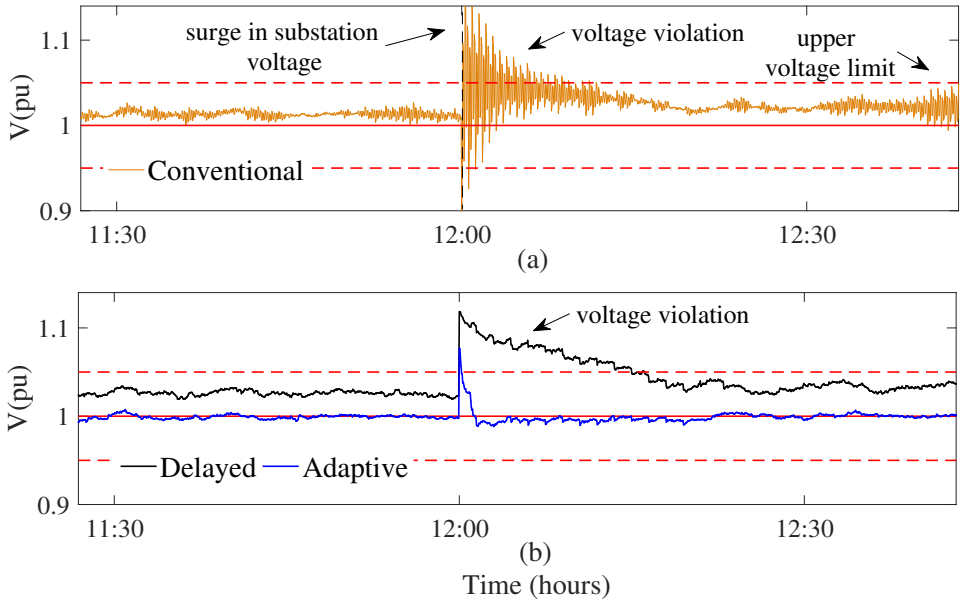

Figure 3.18 Impact of change in substation voltage on control performances

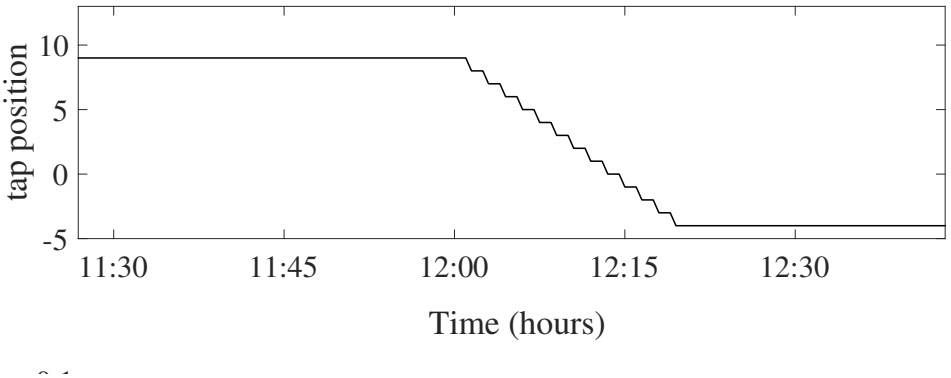

Figure 3.19 Impact of change in substation voltage on tap changers

D) Sudden Load Decrease: A sudden 40% load reduction is applied at 12:00 to test the robustness of the proposed control as shown in Figure3.20. The conservative parameter ($m = 5$), which provided stable voltage performance under normal conditions is causing instability on a sudden load disturbance as shown in Figure3.20(b). Delayed control improves the stability but the voltage is vulnerable to overvoltage violations. Whereas, the adaptive control adapts itself to the disturbance and maintains a stable and flat voltage profile without set point deviation.

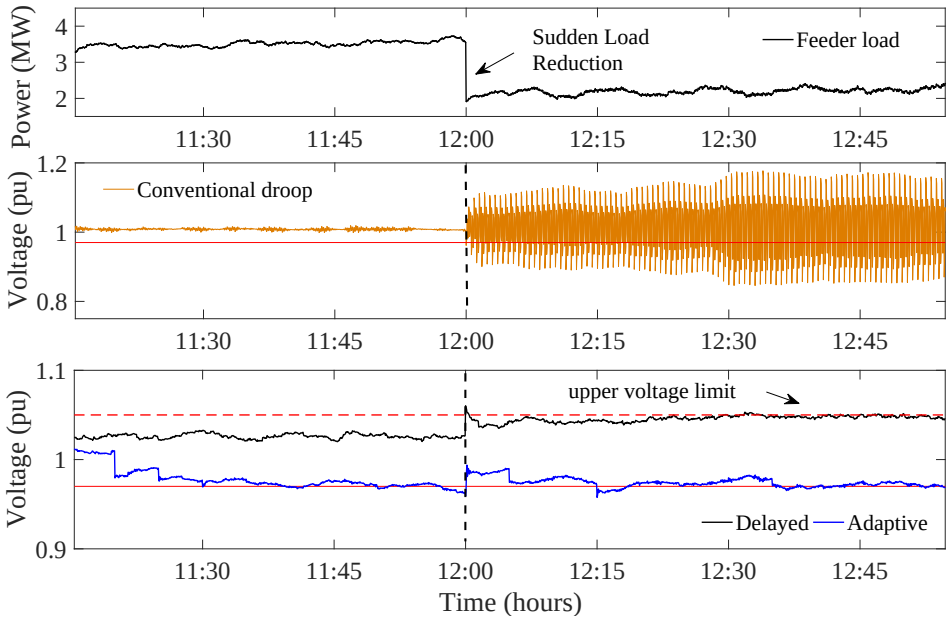

Figure 3.20 Impact of sudden load change on controls: a) sudden load reduction applied; b) voltage with conventional control; c) voltage with adaptive control

3.5.4.4 Adaptive to the error in feeder topology information

Usually in a large real-world system, fully reliable feeder topology info is not available or there are a lot of changes in the feeder which might not be communicated. This leads to change in feeder topology and sensitivity matrix A, thus old control settings might create issues. The proposed control is also adaptive to such errors or changes in feeder information. To simulate this, 25 new solar PV houses were added at the end of the original test system and the old non-conservative settings ($m = 10$) were used for delayed control. Figure3.21 compares the voltage profile before and after feeder change for delayed and adaptive controls. It can be seen that the voltage profile changes from smooth (FC=0, VVI=0) to highly fluctuating (FC=4047, VVI=1615) in the slightly expanded feeder with the delayed control. Whereas, the adaptive control provides a better performance with zero flicker and violations.

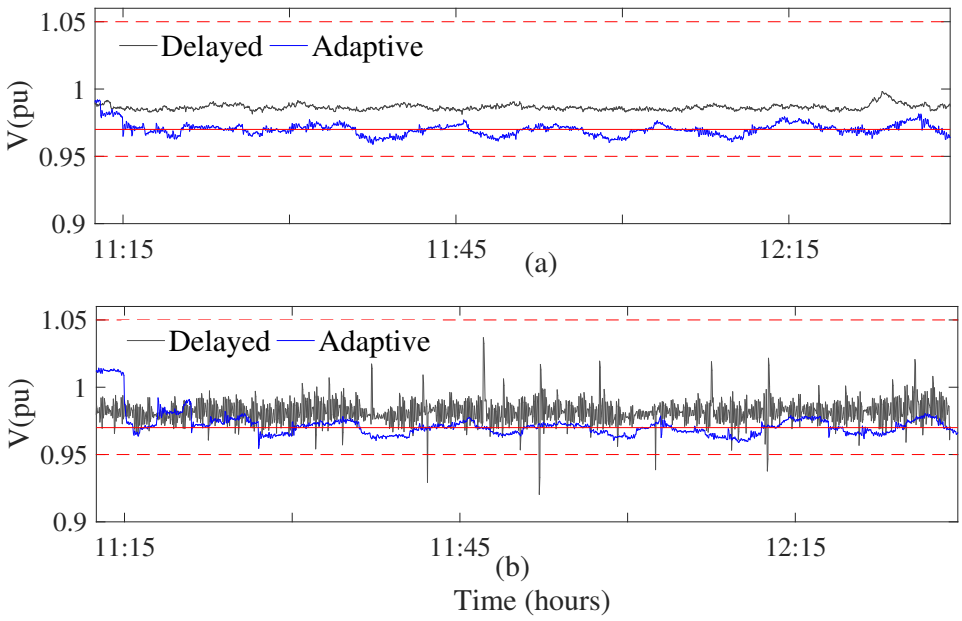

Figure 3.21 Control performance comparison before and after feeder growth

3.6 Conclusion

In this study, a real-time adaptive and local VVC scheme is proposed to mitigate voltage challenges associated with high PV penetration under external disturbances. In specific, the proposed approach addresses two major issues of slope sensitive droop VVC methods. First, the proposed framework (shifted and adaptive droop) enables VVC to achieve high set-point tracking accuracy (low SSE) and control stability (low voltage flicker) simultaneously without compromising either, by decoupling the two functionalities. Second, the adaptive algorithm enables dynamic self-adaption of control parameters in real-time which eliminates another major challenge of selecting appropriate control settings under wide range of operating conditions/external disturbances such as fast cloud transients, substation voltage change etc. All this is achieved while keeping the control purely local with no need of centralized topology information and ensuring that the developed control framework is compatible with the integration standards (IEEE1547) and utility practices (Rule 21). These features make the proposed VVC feasible and implementation friendly. The satis-

factory performance is demonstrated by comparing with existing droop methods in several cases.

It is worth mentioning that the proposed local VVC framework is easily extendable to centralized approaches. In fact, due to its tight voltage regulation feature and adaptive nature under external disturbances, it facilitates the use of PV inverters for other system-wide volt/var applications such as CVR, loss minimization, increasing PV penetration capacity etc. The integration with supervisory control and the impact of the VVC on transmission system will be explored in future studies.

CHAPTER 4. A FRAMEWORK TO AGGREGATE DERs' VOLT/VAR CAPABILITY TO SUPPORT TRANSMISSION GRID

4.1 Introduction

In the last chapter, we have seen how the distribution system performance can be improved by utilizing local var support DER smart inverters. Consequently, It is prudent to discuss the vital role var balance plays in maintaining transmission grid resiliency. Availability of sufficient var capability is often considered an indicator of voltage security in transmission systems (29; 30). The var related ancillary services have been mainly achieved by large synchronous generators and other strategically deployed var devices such as STATCOM and SVC. However, a growing footprint of distributed energy resources (DERs) is replacing fossil fuel based generation that may result in shortage of regional var availability (31; 32). It has initiated a discussion on utilizing DERs as alternative sources in the future grid, along with bulk generation plants, to provide essential ancillary services to the grid such as ramping requirements, ensuring adequate inertia, and maintaining var reserves (8; 9). This chapter concerns to the latter topic with DER as focus. Much of the extant literature focuses on utilizing the var control potential of DERs to improve the distribution system performance as discussed in 2. However, utilization of DERs' var potential for the benefit of the transmission grid has not been adequately explored.

In this light, we present a hypothesis that thousands of DER devices with var control capability can be seen as the geographically distributed var resources (*'mini- SVCs'*) from grid perspective that can provide enhanced flexibility options to the TSOs, if coordinated properly. We call the DER coordinating entity as distribution system operator (DSO). our

assertion is founded on strong reasonings from the literature and the utility practices which are listed and discussed in 2.2.1.

Thus, in this new environment of DERs, a consensus emerge from literature that motivates TSOs to consider DERs var flexibility in their optimization. Based on this premise, the main goal of this work is to adequately investigate the aggregation of var capabilities of multiple DER units in form of a net *P-Q capability curve* that can offer useful insight to TSO regarding the available var flexibility from distribution systems. Note that the DER inverter var control also affect the distribution network voltage profiles. therefore, we propose an optimal power flow based innovative methodology that systematically estimates the aggregated DER var flexibility region as function of DER real power curtailment without violating distribution system operational limits, and further enable readers to assess the impact of various dynamic factors on the flexibility region.

4.2 Envisioned Conceptual VAR Support Framework

Figure 4.1 depicts the overall framework of providing DERs' var support to the grid in an integrated T-D system, proposed in this work. Consider a transmission grid which is connected to multiple distribution feeders with high penetration of inverter-based DERs. In this study, only distributed solar photovoltaic (PV) are considered as DERs. The whole physical system can be seen in three parts i.e. transmission grid, boundary buses (substation) and the distribution buses with DERs. In this framework, we envision a distribution aggregator entity called distribution system operator (DSO) at substation level which exchange information with the transmission system operator (TSO) and DER devices at the customer level. As shown in the Figure 4.1, the framework consists of two major functions performed by the DSO. However, in this paper we only focus on the first function that is to dynamically aggregate the *net var capability curve* of the distribution system at the substation level in every 10-15 minutes time scale based on short-term forecast and send it to the TSO to include it in their planning and operational activities. Here we assume

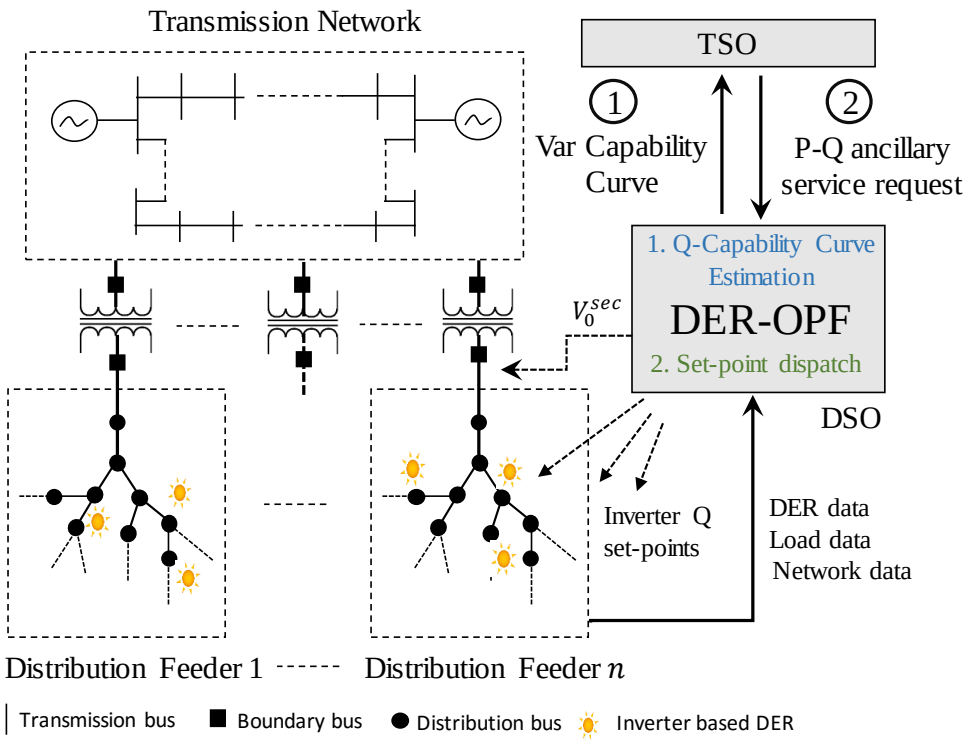

Figure 4.1 The proposed DER var support framework for an integrated T-D system which has two major functionalities for DSO. Functionality 1, providing 'Var Capability Curve' to TSO is the focus of this paper.

that the TSO has its own planning and control methods to request var support from the DSO in case of emergency. The second function of DSO is to dispatch optimal inverter var set-points to individual DER devices in order to meet the var support requested by the grid, however, in this work we do not provide details of this functionality and scope of this paper is to focus on developing a general framework to aggregate DER var capability. Other functions of the framework will be explored in the future studies.

4.3 Capability Curve Characterization

A typical distribution feeder connected to a transmission substation bus with solar PV penetration is shown in Figure 4.2. Load and PV generation at i^{th} node are denoted by $p_i^l + jq_i^l$ and $p_i^g + jq_i^g$ respectively, where p and q denote real and reactive power component respectively. The distribution loads and DERs can be aggregated separately as p_{sub}^{net} and q_{sub}^{net} at the substation as shown in the Figure 4.2. Consequently, the whole distribution network can further be aggregated as the net power demand or load at substation which includes actual loads, DERs and losses as shown in the same Figure 4.2. In this section, we will systematically build the characterization of aggregated var capability curve.

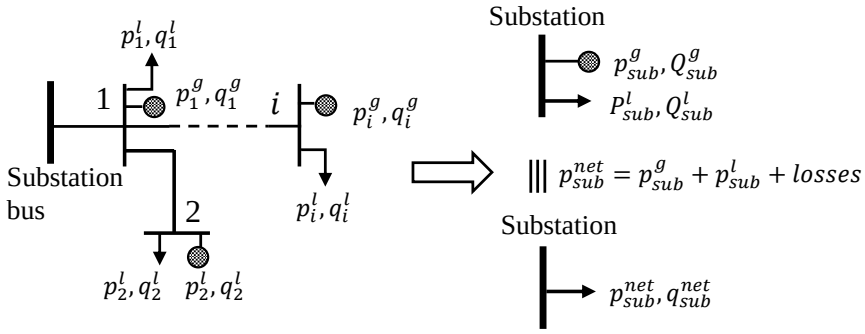

Figure 4.2 One line diagram of a typical distribution feeder with DER and its aggregated representation

4.3.1 Var Capability of Individual Solar PV

For each individual PV inverter, the *device flexibility domain* $\mathcal{C}_i$ can be characterize as following:

$$\mathcal{C}_i = \left\{ (p_i^g, q_i^g) \;\middle|\; \begin{array}{l} {p_i^g}^2 + {q_i^g}^2 \leq {S_i^g}^2 \\ p_i^g \leq 0 \\ |p_i^g| \leq \overline{p}_i^g \leq p_{i,rated}^g \end{array} \right\} \tag{4.1}$$

where, S_i^g and $p_{i,rated}^g$ are the hardware capacity of the inverter and solar panel respectively, whereas $\overline{p}_i^g$ is the solar generation at given point of time without any curtailment. $\mathcal{C}_i$ represents the available flexibility in var generation or absorption by the inverter for all possible amounts of real power generation. We consider the following sign convention: positive value represents the consumption/absorption and negative value represents generation/injection of real/reactive powers. A typical flexibility domain of a solar PV inverter can be graphically drawn as shown in Figure 4.3. The outer envelop of the domain $\mathcal{C}_i$ can be defined as a function $q_i^{g,cap} = f(p_i^g)$ which is usually termed as *device Q-capability curve*. This curve is a collection of maximum reactive power values that an individual DER inverter can inject or absorb for a given real power generation. The domain $\mathcal{C}_i$ shrinks or increases as the operating point $\overline{p}_i^g$ moves along the horizontal axis throughout the day.

4.3.2 DER Aggregation without Network

Before developing the net capability of the whole network, lets understand the aggregation of DERs. An *aggregated DER flexibility domain*, $\mathcal{C}_{sub}$, can be defined as the total flexibility provided by all the DERs combined at the substation as following:

$$\mathcal{C}_{sub} = \left\{ (p_{sub}^g, q_{sub}^g) \;\middle|\; \begin{array}{l} p_{sub}^g = \sum_{i=1}^N p_i^g \\ q_{sub}^g = \sum_{i=1}^N q_i^g \\ (p_i^g, q_i^g) \in \mathcal{C}_i \end{array} \right\} \tag{4.2}$$

where p_{sub}^g and q_{sub}^g are the total real power and var generation from DERs. The outer envelop of the domain $\mathcal{C}_{sub}$ can be defined as a function $q_{sub}^{cap} = f(p_{sub}^g)$ that we call as

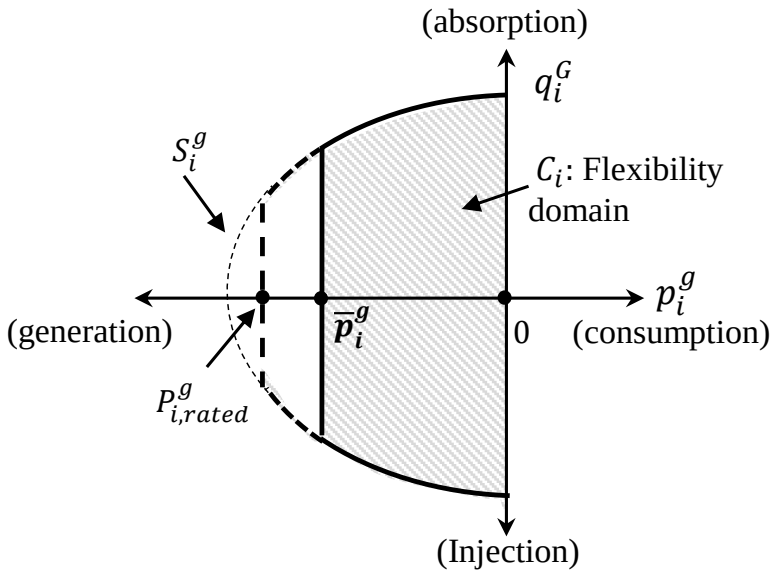

Figure 4.3 Capability curve of a solar PV inverter device

aggregated DER capability curve as shown in Figure 4.4. The horizontal axis can also be seen as variation of total curtailment where point A and origin denote zero and 100% DER curtailment. A point $H(p_{sub}^{g*}, q_{sub}^{g*})$ on the curve implies that for a given value of p_{sub}^g, the maximum possible var absorption is q_{sub}^{g*}. Note that a given p_{sub}^g can be achieved by multiple combinations of individual PV generations p_i^g via curtailment. In other words, H also denotes the operating point to achieve q_{sub}^{g*} var absorption with minimum solar curtailment. All other possibilities of achieving q_{sub}^{g*} which fall inside the domain incur higher real power curtailment of DER than necessary. The estimation of lower part of q_{sub}^{cap} can be formulated as the following convex optimization problem.

$$\text{minimize} \quad q_{sub}^g = \sum_{i=1}^{N} q_i^g \tag{4.3a}$$

$$\text{subject to} \quad p_{sub}^g = \sum_{i=1}^{N} p_i^g, \tag{4.3b}$$

$$p_i^{g^2} + q_i^{g^2} \leq S_i^{g^2}, \qquad \forall i, \tag{4.3c}$$

$$p_i^g < 0, |p_i^g| < p_{i,rated}^g, \quad \forall i \tag{4.3d}$$

Where p_{sub}^g is a given value. Similarly, the upper part of q_{sub}^{cap} can be estimated by

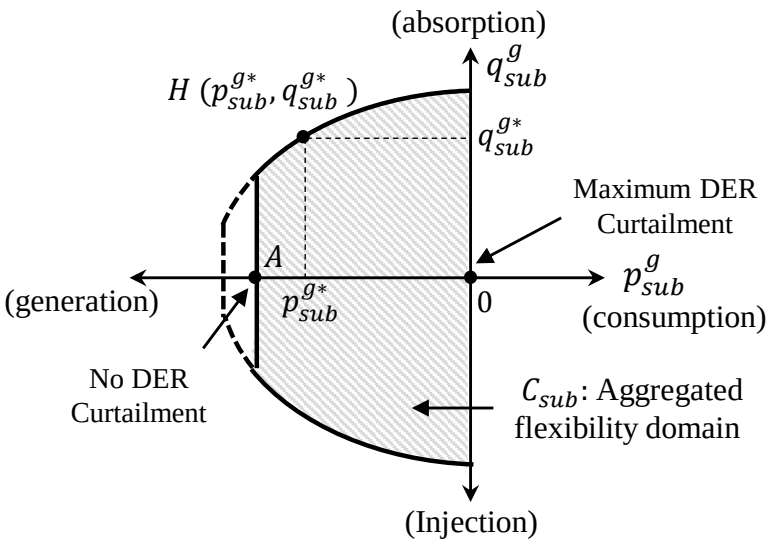

Figure 4.4 Aggregated DER Capability curve at Substation

maximizing the same objective function. The optimization (4.3) is particularly interesting as it has an analytical solution that can be derived using KKT conditions (97). For a given p^{g*}_{sub}, the optimal var absorption/injection occurs when the total real power generation is divided among all inverters in ratio of their ratings i.e.

$$p^{g*}_i = \frac{S^g_i}{\sum S^g_i} \times p^{g*}_{sub}$$

provided $p^{g*}_i \leq p^g_{i,rated}$. In such case, the expression for capability curve $q^{cap}_{sub} = f(p^g_{sub})$ can be derived as following:

$$q^{cap}_{sub} = f(p^g_{sub}) = \sqrt{(\sum S_i)^2 - (p^g_{sub})^2}$$

4.3.3 Net Aggregation with Network

In the last section, DER inverter devices were aggregated, however, the more useful information for TSO is the net available var at the substation which includes aggregated load, DER as well as network losses. Therefore, we define the *aggregated net var capability curve* that provides the information of maximum net var injection/absorption possible at the substation which is seen by the transmission system as net var demand. Henceforth, we

will simply refer it as aggregated capability curve for brevity. We have seen in Figure 4.4 that DER curtailment provides real power flexibility that can further enhance the var flexibility region. Therefore, we define aggregated capability curve as function of total DER curtailment, $p_{sub}^{g,cur}$, i.e. $q_{net}^{cap} = f(p_{sub}^{g,cur})$. A conceptual curve at a given operating condition is shown in Figure 4.5 that depicts the capacitive and inductive var flexibility domain. Another important point to consider is that the inverter var injection or absorption affects the voltage profile of the distribution system and consideration of voltage limits may shrink the flexibility domain in certain operating conditions as visible in the Figure 4.5. The p_{sub}^{g} and total curtailment $p_{sub}^{g,cur}$ can be written as

$$p_{sub}^{g} = \overline{p}_{sub}^{g}.(1 - p_{sub}^{g,cur})$$

Where $\overline{p}_{sub}^{g} = \sum_i \overline{p}_i^g$ is the total solar generation without any curtailment. Similarly, for each DER, we can write,

$$p_i^g = \overline{p}_i^g.(1 - p_i^{g,cur})$$

Finally, $p_{sub}^{g,cur}$ can be written in form of p_i^g and $p_i^{g,cur}$ as

$$p_{sub}^{g,cur} = (\sum_{i=1}^{N} \overline{p}_i^g.p_i^{g,cur}) / \sum_i \overline{p}_i^g$$

Although DER real power generation curtailment is not advisable in normal situations, this option of curtailment exhibits the higher flexibility of the system and provide more options to TSO to handle var related grid events. Nonetheless, utilizing this flexibility involves a greater discussion on policy, customer comfort, and related cost-benefit analysis.

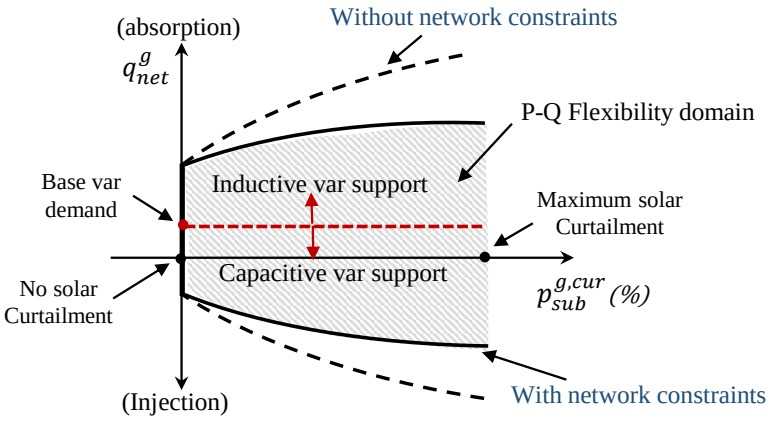

Figure 4.5 Feeder Net Capability curve at Substation

4.4 Process of Capability Estimation

4.4.1 System Modeling

In this section, we will utilize the 'LinDist Flow' equations for an unbalanced three-phase distribution system by (98) to develop a graph-representation model (50). Consider a radial distribution network with $N+1$ nodes represented by a tree graph $\mathcal{T} = (\mathcal{N}, \mathcal{E})$, where $\mathcal{N} := \{0, 1, \cdots, N\}$ is a set of distribution nodes, indexed by i and j. For simplicity, let's assume each $i \in \mathcal{N}$ has all three phases a, b and c. The set $\mathcal{E} := \{(i, j)\}$ contains all line segments with i as the upstream and j as the downstream node. Each line element $(i, j) \in \mathcal{E}$ will also have three phases. The subset $\mathcal{N}_j$ is a collection of all immediate downstream neighboring buses of node j. The secondary side of the substation is denoted by node 0. A typical network example is shown in Fig. . Let M be an $3N \times 3N$ graph incidence matrix of $\mathcal{T}$. The l^{th} column of matrix M corresponds to line segment $(i, j) \in \mathcal{E}$ with entries $M(i, k) = e$ and $M(j, k) = -e$, where e is a 3×3 identity matrix. All other entries of M are zero. Now, according to *LinDist3Flow* model, the voltages at node i and j can be written as

$$\mathbb{V}_i \mathbb{V}_i^* = \mathbb{V}_j \mathbb{V}_j^* - \mathbb{Z}_{ij}^p \mathbb{P}_j - \mathbb{Z}_{ij}^q \mathbb{Q}_j \tag{4.4}$$

where, $\mathbb{V}_j = [V_a V_b V_c]_j^T$ represent the vector of voltage phasors at node j. Similarly, $\mathbb{P}_j = [P_a\ P_b\ P_c]_j^T$ and $\mathbb{Q}_j = [Q_a\ Q_b\ Q_c]_j^T$ denote the real and reactive power entering at node j. $\mathbb{Z}_{ij}^q$ and $\mathbb{Z}_{ij}^p$ are the constant three phase impedance matrices for line segment (i, j) as given in (98). Now, let's define the vector of squared of voltage magnitude as a new variable $\mathbb{Y}_j = \mathbb{V}_j \mathbb{V}_j^* = [y_a\ y_b\ y_c]_j$ for $j \in \mathcal{N} \backslash \{0\}$. Assuming the reference node 0 voltage as $\mathbb{Y}_0$, the voltages at each node can be written in compact form as following:

$$[M_0\ M^T][\mathbb{Y}_0^T\ \mathbb{Y}^T]^T = M_0 \mathbb{Y}_0 + M^T \mathbb{Y} = -\mathbb{Z}_D^p \mathbb{P} - \mathbb{Z}_D^q \mathbb{Q} \tag{4.5}$$

Where, M_0 is a matrix of size $3N \times 3$ with first entry as e and rest as zero. $\mathbb{Z}_D^p$ and $\mathbb{Z}_D^q$ are diagonal matrices of size N where l^{th} entries are $\mathbb{Z}_{ij}^p$ and $\mathbb{Z}_{ij}^q$ respectively which correspond to l^{th} line segment (i, j).

The line flows $\mathbb{S}_j = \mathbb{P}_j + j\mathbb{Q}_j$ can be written in form of net injections as following:

$$\mathbb{S}_j \approx -s_j + \sum_{k \in \mathcal{N}_j} \mathbb{S}_k + L_j \tag{4.6}$$

Where $s_j = p_j + q_j$ is the vector of net injection at node j at all phases denoted by $s_{\phi,j}$ where, $\phi \in a, b, c$. Usually, in LinDistFlow model, line losses are neglected which introduce a relatively small error in the modeling as indicated by (54). However, to increase accuracy, we consider a constant loss term L_j in (4.6). The loss term L_j denotes the losses incurred in line ending at node j and can be estimated based on the offline study of the base operating point as indicated in (50). Equation (4.6) can be re-written in compact form as

$$-M\mathbb{P} = -p + L_p \tag{4.7}$$

$$-M\mathbb{Q} = -q + L_q \tag{4.8}$$

Where L_p and L_q are vectors of real and reactive loss factors. Using (4.5), (4.7) and (4.8), voltages in form of net injections can be written as following:

$$\mathbb{Y} = R^{eq} p + X^{eq} q - M^{-T} M_0 \mathbb{Y}_0 + L_c \tag{4.9}$$

Where $R^{eq} = -M^{-T}\mathbb{Z}_D^p M^{-1}$, $X^{eq} = -M^{-T}\mathbb{Z}_D^q M^{-1}$ and $L_c = R^{eq}L_p - X^{eq}L_q$ are constants. Lets assume that the substation voltage is balanced and has same magnitude in all phases denoted by a a scalar v_0. Further, due to radial structure of network, $M^{-T}M_0\mathbb{Y}_0$ is same as -$v_0^2\mathbb{I}$, where $\mathbb{I}$ is a column vector of size $3N$ with all entries as 1.

Substation secondary voltage v_0 can be controlled via an on-load tap changer (OLTC) within a range as $v_0 = v^{tm}.r$, where v^{tm} is primary side transmission voltage and r is tap ratio of OLTC. Usually each tap provides ± 0.0063 pu voltage regulation with maximum ± 16 taps. Therefore the maximum possible values of r are 1 ± 0.1.

Let's assume the DERs are located at the nodes collected in a subset $\mathcal{G} \subseteq \mathcal{N}$. In this case, only inverter based DERs are considered such as solar PV. The net power injection of real and reactive power at each node $j \in \mathcal{G}$ is denoted by $p_{\phi,j} = -p^g_{\phi,j} - p^l_{\phi,j}$ and $q_{\phi,j} = -q^g_{\phi,j} - q^l_{\phi,j}$ respectively. Superscript g and l denote DER and loads. For all other $j \in \mathcal{N} - \mathcal{G}$, $p^g_{\phi,j}$ and $q^g_{\phi,j}$ are considered zero. In our convention, the positive $q^g_{\phi,j}$ denotes var consumed and negative denotes the var injected by the inverter. For rest of the nodes $k \in \mathcal{N} \setminus \mathcal{G}$, $p_{\phi,j} = -p^l_{\phi,j}$ and $q_{\phi,j} = -q^l_{\phi,j}$ are considered. Only constant power loads are taken here and the capacitors are modeled as reactive power loads.

Net Power Flows at Substation: The net reactive power demand at the substation, q^{net}_{sub} is sum of var flow of all three phases in the first line coming out from node 0 i.e. sum of first three entries of vector $\mathbb{Q}$ from (4.8). However, in order to account for losses, a more accurate q^{net}_{sub} can be written as

$$q^{net}_{sub}(q^g_j, y^q_j) = \sum_{\phi\in\{a,b,c\}} \Big(\sum_{j\in\mathcal{G}} q^g_{\phi,j} - \sum_{j\in\mathcal{N}} q^l_{\phi,j} + \sum_{j\in\mathcal{N}} \mathcal{L}(y_{\phi,j}) \Big) \tag{4.10}$$

Equation (4.10) is sum of the net injection of var at each node due to load, capacitors and DER inverter and reactive power losses incurred at each line across all three phases. The loss term, $\mathcal{L}(y_{\phi,j})$ is the reactive power losses in line j of the distribution network. In a balanced LinDist Flow model, the losses in line j can be written as $(P_j^2 + Q_j^2)/V_j^2.x_j$ (99). However, it is not straightforward in an unbalanced system due to interaction of all

three phases. To simplify it, an approximation is considered that assumes the influence of non-diagonal entries of $\mathbb{Z}$ negligible compared to the influence of diagonal entries while estimating the losses. Based on this assumption, $\mathcal{L}(y_{\phi,j})$ can be written as:

$$\mathcal{L}(y_{\phi,j}) = \frac{(P_{\phi,j}^2 + Q_{\phi,j}^2)}{y_{\phi,j}} x_{\phi\phi,j} \tag{4.11}$$

Where, $y_{\phi,j} = V_{\phi,j}^2$. Henceforth, we drop the subscript ϕ for the convenience of the notations.

4.4.2 DER-OPF Formulation

Our objective here is to construct the net capability curve $q_{net}^{cap} = f(p_{sub}^{g,cur})$ as shown in Figure 4.5. To achieve it, we need to estimate both the capacitive ($\underline{q}_{net}^{cap}$) and inductive ($\overline{q}_{net}^{cap}$) var capabilities of the network which is same as minimizing and maximizing the net var flow at the substation. Based on the already defined preliminaries, following DER-OPF can be written to estimate $\underline{q}_{net}^{cap}$:

$$\underset{p_j^{g,cur},\, q_j^g,\, v_0}{\text{minimize}} \quad q_{sub}^{net}(y_j, q_j^g) \tag{4.12a}$$

subject to

$$\mathbb{Y} = R^{eq}p + X^{eq}q + (v_0)^2\mathbb{I} + L_c, \tag{4.12b}$$

$$p_j = \overline{p}_j^g.(1 - p_j^{g,cur}) - p_j^l, \qquad \forall j \in \mathcal{N}, \tag{4.12c}$$

$$q_j = q_j^g - q_j^l, \qquad \forall j \in \mathcal{N}, \tag{4.12d}$$

$$\underline{y} \leq y_j \leq \overline{y}, \qquad \forall j \in \mathcal{N}, \tag{4.12e}$$

$$|q_j^g| \leq \sqrt{S_j^{g^2} - \overline{p}_j^{g^2}(1 - p_j^{g,cur})^2} \quad \forall j \in \mathcal{G}, \tag{4.12f}$$

$$0 \leq p_j^{g,cur} \leq 1, \qquad \forall j \in \mathcal{G}, \tag{4.12g}$$

$$\sum_{j \in \mathcal{G}} \overline{p}_j^g.p_j^{g,cur} = p_{sub}^{g,cur}.\sum_{j \in \mathcal{G}} \overline{p}_j^g \quad , \tag{4.12h}$$

$$v_{tm}\underline{r} \leq v_0 \leq v_{tm}\overline{r}, \tag{4.12i}$$

$\overline{p}_j^g$ is the solar generation at given operating point without any curtailment and $p_{sub}^{g,cur}$ is the given total DER curtailment which is ensured by (4.12h). Constraint (4.12e) ensures the voltages are within the ANSI limits (15). $\overline{y}$ and $\underline{y}$ are upper and lower allowable voltage limits, and are usually taken as 1.05^2 and 0.95^2, respectively. Constraint (4.12f) manifest the hardware capacity limit of an inverter. To avoid integer programming, r is taken as a continuous variable. Upper and lower saturation limits on OLTC tap ratios are denoted by $\overline{r}$ and $\underline{r}$ respectively. In an integrated T-D network, v_{tm} is affected by the changes in the net power flow through substation, however, for this section, we set a nominal value, $v_{tm} = 1$ and defer this discussion for the next section. The solution of the optimization (4.12) provides the optimal var set dispatch (q_j^{g*}) and real power curtailment ($p_j^{g,cur*}$) for each DER and optimal secondary side voltage set-point (v_0^*).

Similar to (4.12), upper part of the net capability curve ($\overline{q}_{net}^{cap}$) can be estimated by maximizing the net var demand at substation which is same as following,

$$\underset{p_j^{g,cur}, q_j^g, v_0}{\text{minimize}} \quad -q_{sub}^{net}(y_j, q_j^g) \tag{4.13a}$$

$$\text{subject to}$$

$$(4.12b) - (4.12i) \tag{4.13b}$$

Unfortunately, the objective function in (4.13) is not convex due to losses term $\mathcal{L}(y_j)$ in (4.10) being quadratic as shown in (4.11). However, it can be converted to a convex expression by removing the $\mathcal{L}(y_j)$ term as following:

$$\underset{p_j^{g,cur}, q_j^g, v_0}{\text{minimize}} \quad -\Big(\sum_{j\in\mathcal{G}} q_{\phi,j}^{inv} - \sum_{j\in\mathcal{N}} q_{\phi,j}^{L}\Big) \tag{4.14a}$$

$$\text{subject to}$$

$$(4.12b) - (4.12i) \tag{4.14b}$$

Usually, the var losses is a much smaller component of q_{sub}^{net} compared to combined var consumption by the loads and the inverters, therefore, it doesn't affect the optimal point

significantly. In fact, in most cases, the optimal point of (4.14) is also optimal for (4.13) except when lower voltage boundary constraints of (4.12e) at all nodes are not active. In those cases, (4.13) tries to further reduce voltage to its minimum in order to increase losses which adds a negligible error in optimal net var flow q_{sub}^{net} calculated by (4.14). Therefore, $\overline{q}_{cap}^{net}$ is estimated via (4.10) using optimal q_j^{g*} resulting from (4.14).

4.4.3 Coupling of Capability Curve with TN

It is pertinent to discuss that the grid side voltage v_{tm} is a function of the p_{sub}^{net} and q_{sub}^{net} at all the substations of a transmission network. This means there is an inherent coupling between the DER watt/var dispatches and the v_{tm} that evolves based on the operating condition. Fortunately OLTC tap ratio provides a limited decoupling between primary and secondary side of the substation within the range of r. Due to this, the desired optimal secondary voltage v_0^* can be achieved by adjusting tap ratio for any value of v_{tm} which lies in the decoupling range $\mathcal{D}$ defined as,

$$\mathcal{D} = [\, v_0^*/\overline{r},\ v_0^*/\underline{r}\,] \tag{4.15}$$

This decoupling is lost when $v_{tm} \notin \mathcal{D}$ i.e. the OLTC tap gets saturated. Note that the v_{tm} is the voltage that is expected as result of var capability dispatch and needs to be predicted by TSO before requesting var capability from the DSO. To address this concern, DSO estimates the var capability $q_{net}^{cap} = [\underline{q}_{net}^{cap},\ \ \overline{q}_{net}^{cap}]$ and $\mathcal{D}$ for nominal value of $v_{tm} = 1$ and send this information to TSO to be included in their optimizations. Although, it is unlikely that the v_{tm} will lie outside the decoupling range $\mathcal{D}$ even after var support from DSO, because the purpose of aggregating var capability is to improve the transmission side voltage and keep it close to the nominal operating point.

Flow chart of the overall process of the var capability curve estimation for a given operating condition is shown in Figure 4.6.

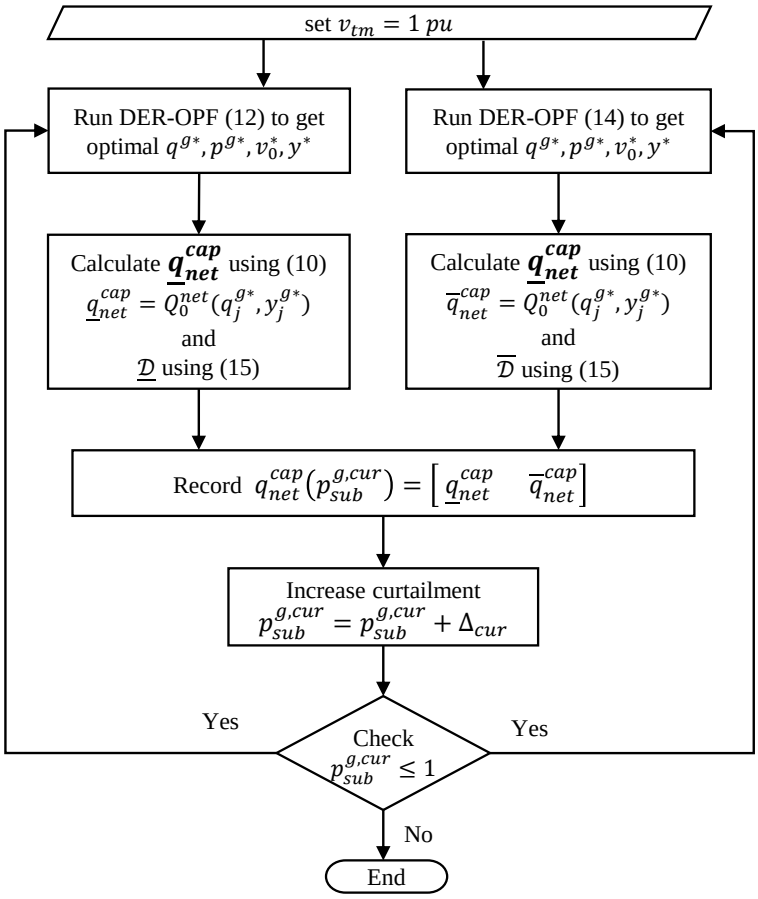

Figure 4.6 Flow chart of the process of estimating var capability curve as function of DER real power curtailment

4.5 Test Case Study

4.5.1 Reactive Power Flexibility Region (RPFR)

In order to numerically evaluate the var flexibility provided by DER, we define reactive power flexibility region (RPFR) as the range $[a,\ b]$ at any give operating condition,

$$a = \frac{\underline{q}_{net}^{cap} - q_{net}^{base}}{q_{net}^{base}}; \quad b = \frac{\overline{q}_{net}^{cap} - q_{net}^{base}}{q_{net}^{base}}$$

where q_{net}^{base} is the net var demand at the substation when all DER inverters are operating in unity power factor mode. The a and b denote the maximum available capacitive and inductive var support in MVar, respectively. A higher magnitudes of both a and b with negative and positive signs respectively represent a larger flexibility region. A zero value of both a and b denotes no available var flexibility.

4.5.2 Test System Description

An unbalanced 3-phase IEEE distribution 37 bus test system is considered with 2 MW as peak load and around 90% solar PV penetration as shown in Figure . Here, we define the penetration level is a ratio of peak solar generation to peak load demand. Around 100 Single phase DER (solar PV) units are equally distributed throughout the distribution feeder nodes in all three phases. Inverter ratings are considered 1.1 times the peak solar generation. Maximum and minimum values of v_{tm} are considered as 0.9 and 1.1.

4.5.3 Aggregated Net Capability Curves

Let's consider two cases with different loading conditions to compare the aggregated net capability curves i.e. high loading case 1 with peak load and low loading case 2 with half of the peak load. The nominal ($v_{tm} = 1$) capability curve for case 1 is shown in Figure 4.8 as function of DER curtailment with black solid lines. The blue shaded region is P-Q flexibility or capability domain and the dashed back line is base var demand (2000 kvar) with no var dispatch by DERs. The region above and below base var demand line

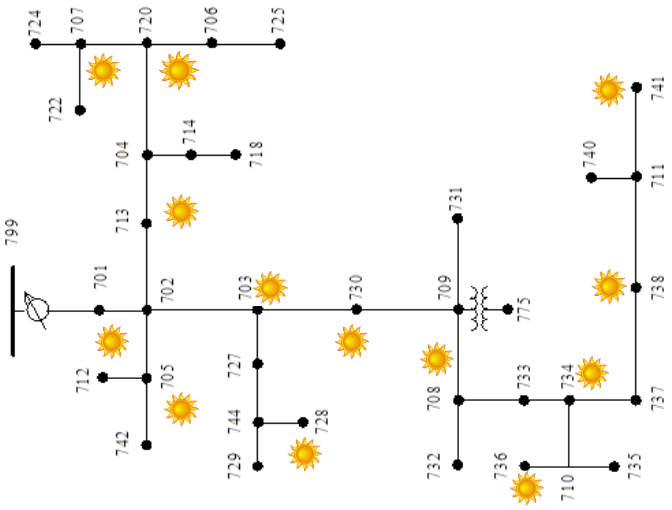

Figure 4.7 IEEE 37 bus distribution test system

can be seen as inductive and capacitive var support region respectively. Essentially, any point in the flexibility domain area can be achieved by appropriately curtailing the real power and dispatching the reactive power of DER units. It can be seen that the capacitive support region (magnitude of a) increases with increasing curtailment for both case 1 and 2 as increasing real power curtailment frees the inverter capacity as well as it reduces the voltages due to increase in net load. This provides more scope for DERs to supply var leading to higher magnitude of a. However, the inductive var support region (magnitude of b) first increases with curtailment but starts decreasing towards the end for case 1 while for case 2, it continuously increases. This is because both the increasing curtailment and inductive var support cause low voltages and after a certain curtailment level, the voltage of at least one node reaches to its minimum limit. Whereas, in case 2, the voltages do not reach to the minimum limit due to low load condition as shown in Figure 4.9.

4.5.4 Day-ahead Capability Curve

In the last section, capability curve were shown for a given operating condition which are utilized for real-time operations. However, the day-ahead capability curves can also be

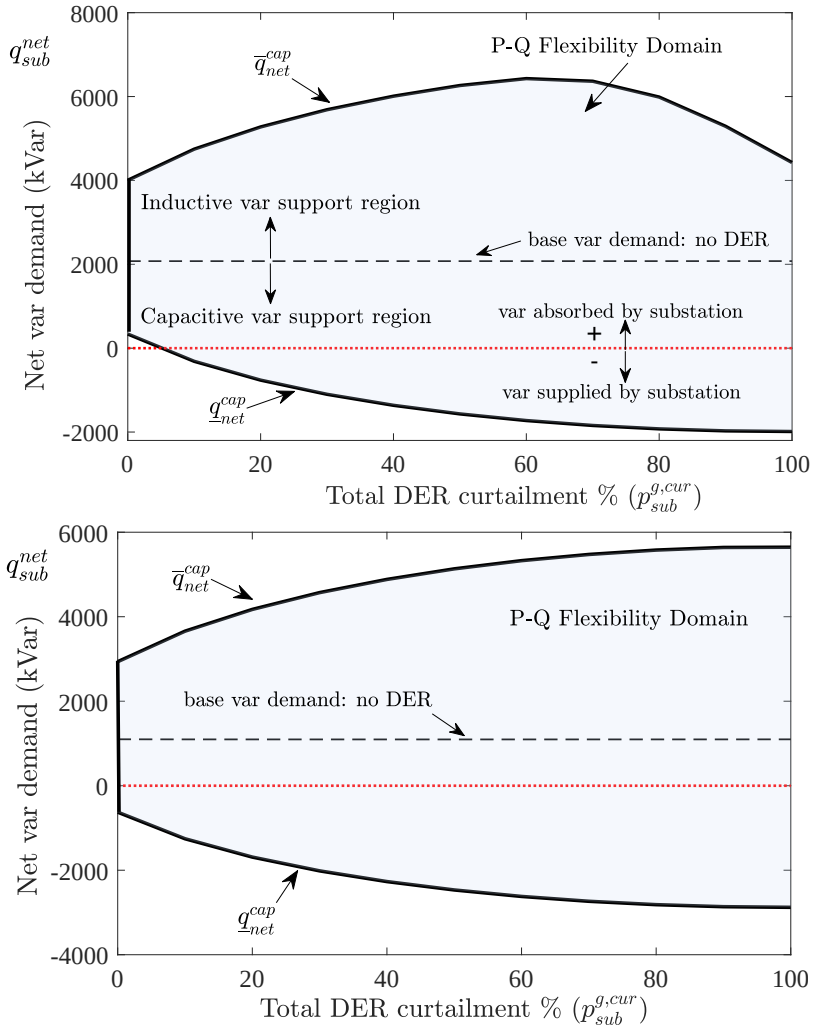

Figure 4.8 The aggregated net capability curve of a distribution system with high DER penetration as function of DER curtailment for (a) case 1: peak load, (b) case 2: low load

Table 4.1 % RPFR at different DER curtailment level for Case 1 (peak load) and Case 2 (low load)

DER	0%	40%	60%	80%
Case 1	[-0.84, 0.89]	[-1.64, 1.84]	[-1.81, 2.04]	[-1.90, 1.83]
Case 2	[-1.57, 1.67]	[-3.06, 3.44]	[-3.38, 3.85]	[-3.56, 4.07]

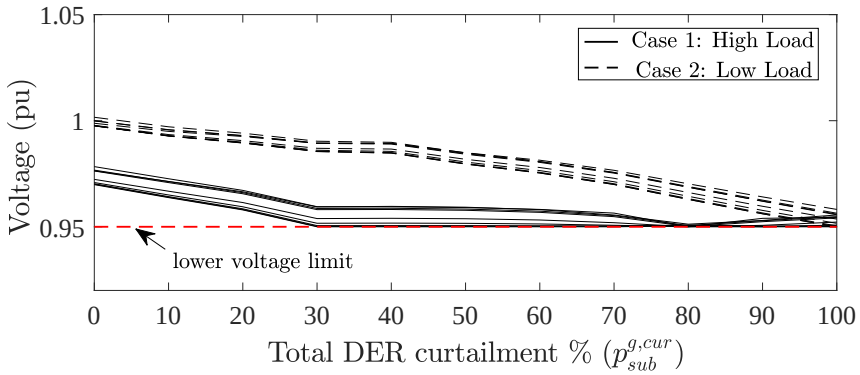

Figure 4.9 Voltage at all nodes downstream of node 733 in IEEE 37 bus system for case 1 and case 2 while estimating inductive capability curve ($\overline{q}_{net}^{cap}$)

estimated to be utilized by TSO for day-ahead planning. It can be obtained by repeating the capability estimation procedure for each operating point. A normalized daily load curve and solar PV generation profile is applied to each load and PV unit respectively as shown in Figure 4.10. Figure 4.11 shows a capability curves (black solid lines) and var support region (grey shaded area) of the test system at hourly operating points with no curtailment . The day-ahead curve gives more visual information of how the aggregated capability varies with changing operating condition throughout the day. It can be seen that the flexibility range is minimum at noon when least inverter capacity is available for var support, however, a 40% curtailment free the inverter capacity and expands the flexibility area by adding an extra blue shaded portion during peak solar hours as shown in Figure 4.11.

Remark: While plotting the capability curve here, we assumed that the substation transformer is lossless since we did not include the transformer impedance. However, it can easily be included in the model and the resulting capability curves should shrink by small percentage i.e. 2 3 % as the substation transformers of 1 MVA rating typically have 97 99 % efficiency.

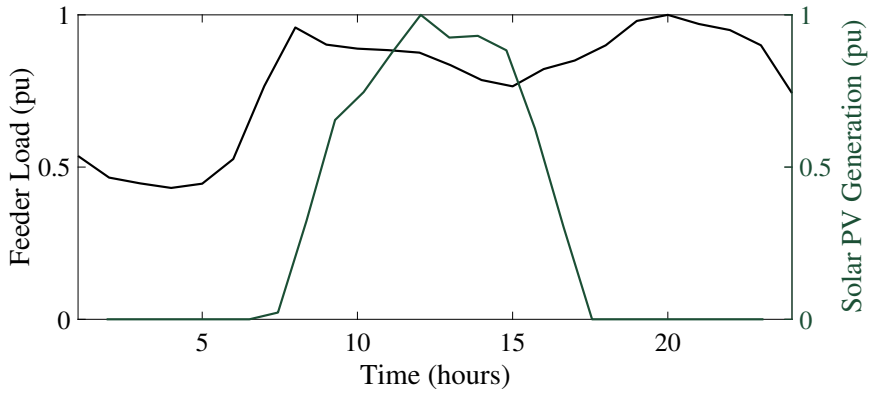

Figure 4.10 Normalized Daily load profile and solar PV generation profile for 24 hours with maximum value as 1 pu

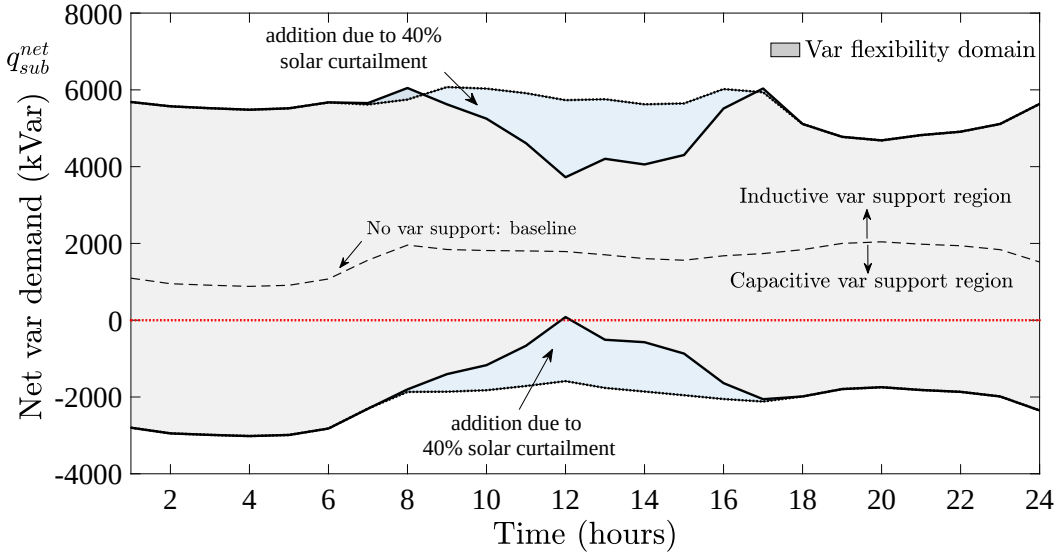

Figure 4.11 Day-ahead aggregated flexibility region of a distribution system with and without real power curtailment

Table 4.2 % RPFR for different DER penetration at zero curtailment

DER penetration →	20%	40%	60%	80%	100%
[a,	[-0.19,	[-0.38,	[-0.59,	[-0.78,	[-0.98,
b]	0.17]	0.39]	0.61]	0.83]	1.05]

Table 4.3 % Reactive power flexibility range (RPFR) for different inverter sizing at zero curtailment

Inverter oversize →	0%	10%	20%
No DER curtailment	[0, 0]	[-0.84 0.89]	[-1.20, 1.30]
40% DER curtailment	[-1.44, 1.58]	[-1.64, 1.84]	[-1.84, 2.08]

4.5.5 Factors Affecting Capability Curve

4.5.5.1 Impact of DER penetration levels

Table 4.2 shows the $RPFR$ values for increasing DER penetration level at no DER curtailment level for the high load condition. As expected, both capacitive and induction flexibility region increase with higher DER penetration.

4.5.5.2 Impact of Inverter size

Inverter size plays a crucial role in available DER capability. Table 4.3 compare the $RPFR$ for different inverter sizes during peak solar generation. Inverters with no oversize and with no curtailment results in zero flexibility region, however, the flexibility can be increased by real power curtailment as shown in the Table 4.3 (row 2). It shows the trade-off between oversizing and curtailment to achieve desired flexibility during peak solar as both options have economic cost associated. This trade-off is also relevant while complying to the integration standard 1547-2018 as discussed in the next section.

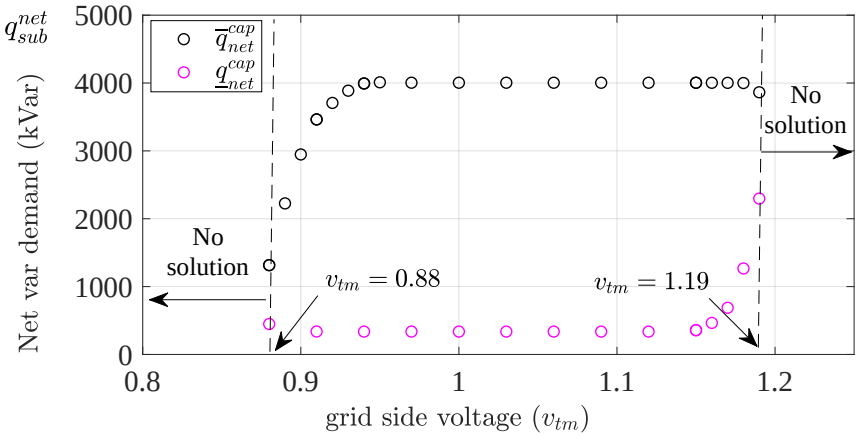

Figure 4.12 Impact of grid side voltage on the capability region

4.5.5.3 Impact of grid side voltages

From transmission side, the primary substation voltage is a crucial factor that can affect the capability domain significantly. Though, usually we expect the v_{tm} to be around 1, in case of contingencies and other events, it can significantly deviate from nominal value. Figure 4.12 shows how the capability region varies with change in v_{tm} at no curtailment. Note that the flexibility region shrinks as v_{tm} moves away from nominal 1 pu on either side beyond the decoupling range $\mathcal{D}$. It can be seen that the DER-OPF becomes infeasible for v_{tm} greater than 1.19 pu and less than 0.88 pu that means no flexibility is available without violating the voltage limits.

4.5.6 Integration Standard IEEE1547 Compliance

The recently revised DER integration standard IEEE1547-2018 has made it compulsory for each inverter-based DER unit to provide var capability of 44% of its kW rating at all operating conditions. In order to comply with it, there are two possible options i.e. either oversize the inverter by 1.113 times the kW rating (11.3% oversize) with no DER curtailment or 10.2% DER curtailment during peak hours with no inverter oversize. Here, we have compared the impact of IEEE1547 compliance on the aggregated RPFR by choosing both the options in form of two cases as shown in Figure 4.13. Case 1 is shown by black

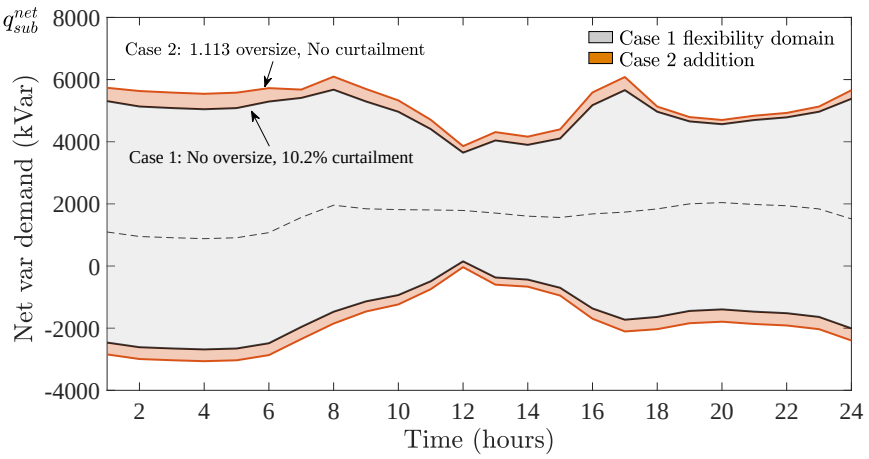

Figure 4.13 Two different day-ahead aggregated capability curves and domains due to compliance to IEEE1547 var capability requirements

solid lines where 10.2% curtailment is applied to each DER with no oversized inverters and case 2 is shown by orange solid lines where each inverter is oversize by 1.113 times. Note that both the cases comply to IEEE1547 standard, however the case 2 has broader aggregated RPFR compare to case 1 e.g. [-1.02 1.16] and [-0.91 1.04] respectively at 12 noon. The case 1 might be more beneficial for the customers as the curtailment will be only required in rare cases when the var is needed by TSO and inverter oversize cost will be saved. However, it depends on many other factors such as policy, incentive structure, ancillary service market etc. and further cost-benefit analysis is needed of specific cases to arrive at any decision.

4.5.7 Community Solar v/s Distributed Solar

Utilities have recently started community solar projects in which a large amount of concentrated solar PV is installed at one location rather than distributed throughout the network. We have considered one distributed solar case where solar is equally distributed throughout the system. We create three more cases for community solar where:

- Solar is installed at the beginning of the feeder only (near substation) (node 701,702,713).
- Solar is installed at the end of the feeder only (node 711, 740, 741).

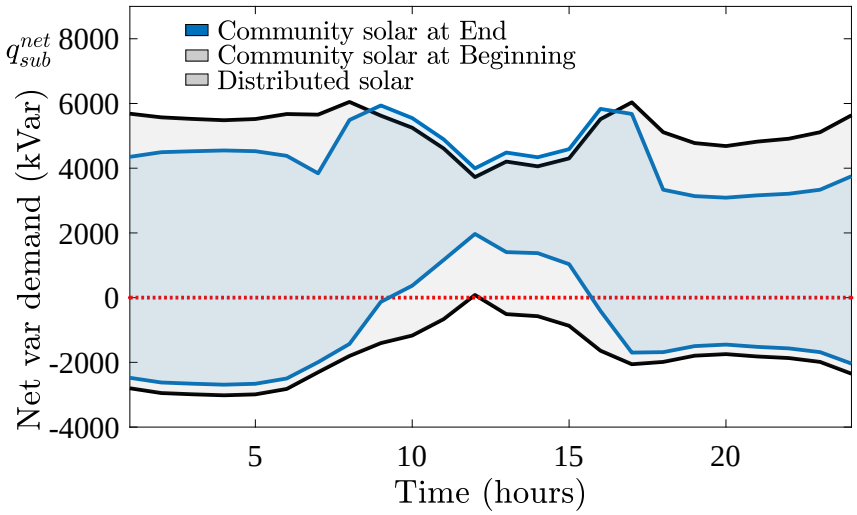

Figure 4.14 Impact of distributed and community solar locations on the capability regions

- Solar is installed in three chunks at beginning, middle and end of the feeder

The day ahead flexibility domain for 90% DER penetration is compared in Figure 4.14. It can be seen that the flexibility region at noon reduces in case of community solar at the feeder end. The capacitive RPFR values are compared in the Table 4.4 (row 1). This reduction is caused by the constrained voltage profile that can be seen in Figure 4.15. Voltage profile in the case of community solar at the end is constrained at both upper and lower end that leaves less scope for flexibility. However, this problem does not arise when DER penetration is lower such as 30% as can be seen in the Figure 4.16. Note that the flexibility region remain almost same for distributed solar and community solar near substation as the voltage profile is not constraining. Overall, based on the observation, we can comment that though distributed solar provides better voltage control leading to probably higher flexibility, the utility control on those solar inverter is limited. On the contrary, community solar facilitates better utility control, however may lead to voltage constraint issues.

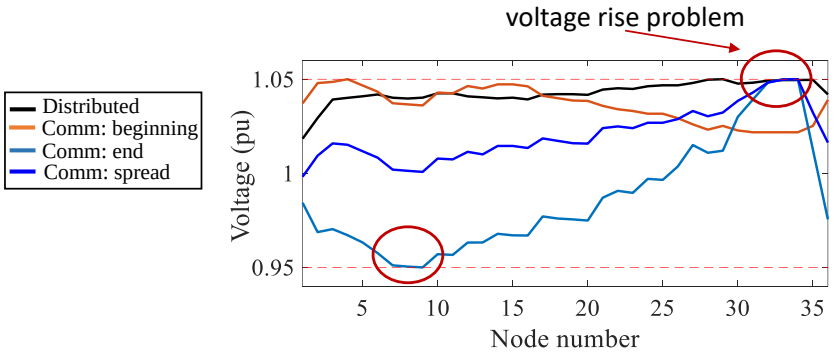

Figure 4.15 Voltage profiles comparison with distributed and community solar at 90% DER penetration

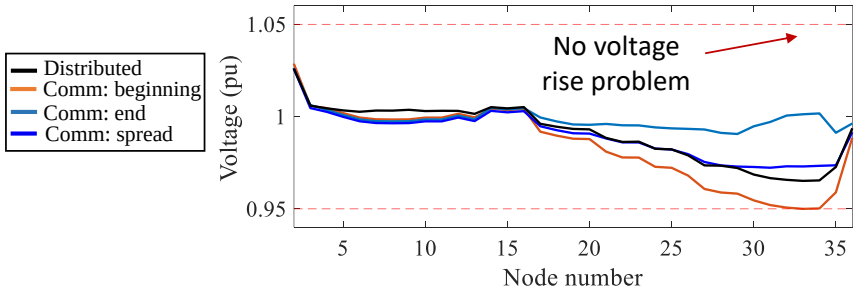

Figure 4.16 Voltage profiles comparison with distributed and community solar at 30% DER penetration

Table 4.4 % RPFR comparison of distributed and community solar locations at zero curtailment

DER Penetration	Distributed solar	Community solar		
		Beginning	End	Spread out
90%	-0.84	-0.82	0	-0.83
30%	-0.38	-0.36	-0.38	-0.38

4.6 Impact of Aggregated DER Var Support on the Transmission Grid

The proposed framework estimates the aggregated var capability curve for the transmission grid. However, the grid might not want the maximum var support all the time; rather it can ask for the var support in specific needs e.g. in case of voltage dips due to line contingencies. In this section, we will demonstrate how the proposed aggregated var capability can potentially enhance the options for TSO on an integrated transmission-distribution test system. A T-D co-simulation platform is developed to accurately asses the impact (84). An integrated T-D test system is constructed by replacing aggregated loads at all three load buses (T5,T7,T9) of the IEEE 9 bus transmission test system by multiple IEEE 37 bus distribution feeders as shown in Figure 4.17.

Let's consider a operating point with peak solar generation to demonstrate the impact of minimum available var flexibility. We will compare the impact of DER var support under line T5-6 contingency for following cases: a) No DER var support provided by any DSO; b) DSO at bus T9 provide just enough DER var support to comply with integration standard 1547; c) DSO at both bus T9 and T5 provide just enough DER var support to comply with integration standard 1547; d) DSO at bus T9 provide more DER var support than case (b) by 20% curtailment. Figure 4.18 shows the var support provided by DSO at $t = 10$ after line T5-6 contingency in all 4 cases. Figure 4.19 compare the voltages at transmission buses for all cases. At $t = 5$, line 5-6 is removed that leads to dip in voltages and bus T5 and T9 suffer under voltage violation. In case (b), the support by only T9 is not enough to recover voltages above 0.95. In such cases, TSO either can request var flexibility from both T9 and T5 as recommended by 1547 standard i.e. case (c) or it can request extra support from T9 that can be provided by some curtailment i.e. case (d). It can be seen that both case (c) and (d) recover voltages above the limit, however, the amount of voltage boost at T9 and T5 differ based on the cases. Figure 4.20 show the distribution buses voltage profile that remains within the limit while providing var support to the grid. Note that the estimation of optimal var support request profile depends on the various factor such as objective of

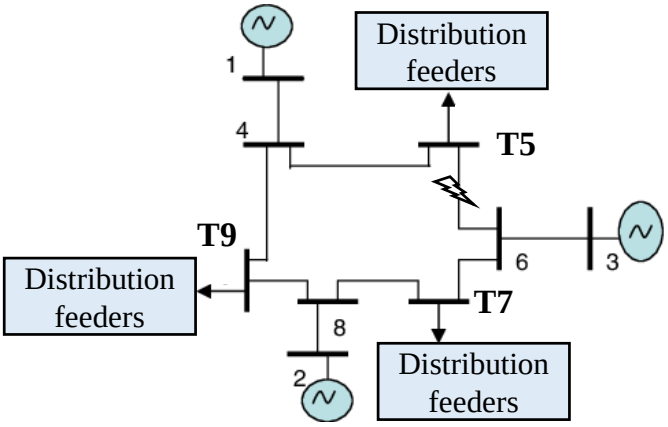

Figure 4.17 Integrated T-D test system with coupled IEEE 9 bus transmission and IEEE 37 bus distribution test systems

TSO, availability of DER flexibility, economic compensation policies etc and needs to be achieved via an optimization process which is beyond the scope of this paper. The 4 cases here demonstrate the potential of the proposed framework that provides higher flexibility to TSO in utilizing DER var capability as ancillary service for the benefit of the grid.

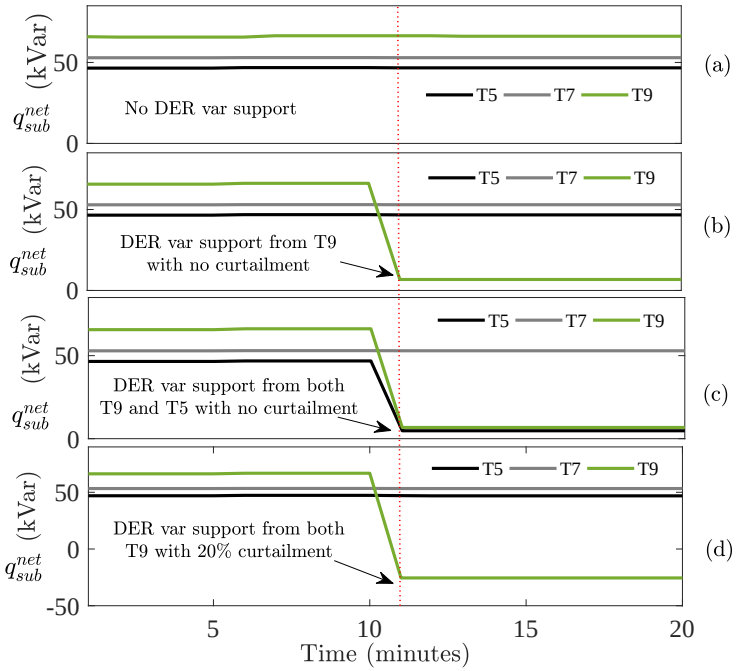

Figure 4.18 The var provision by DSO at substation T5 and T9 of the grid after transmission line 5-6 contingency in various cases: a) no support from DER; b) DER var support from bus T9; c) DER var support from both bus T9 and T5; d) DER var support from bus T9 with 20% curtailment

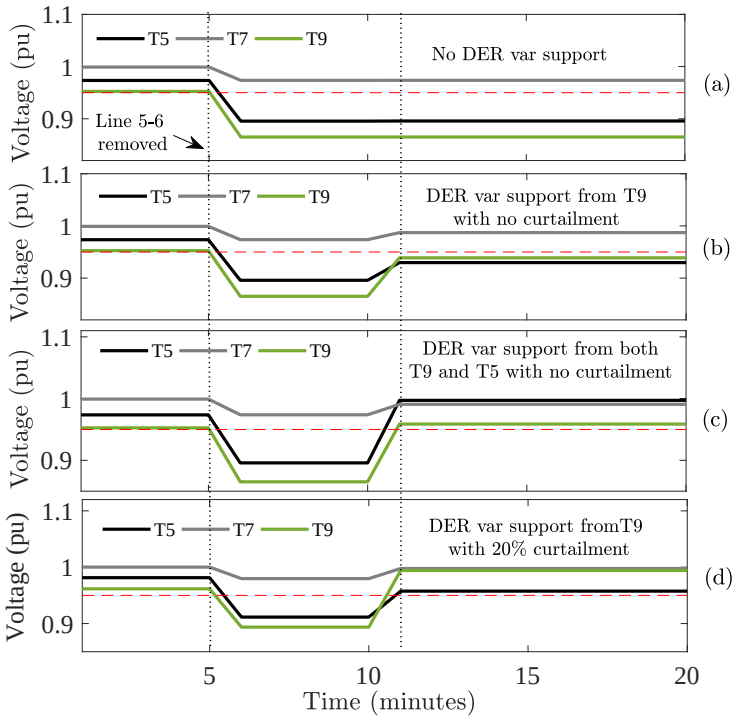

Figure 4.19 Impact of Aggregated DER var support on grid voltages after transmission line 5-6 contingency in various cases

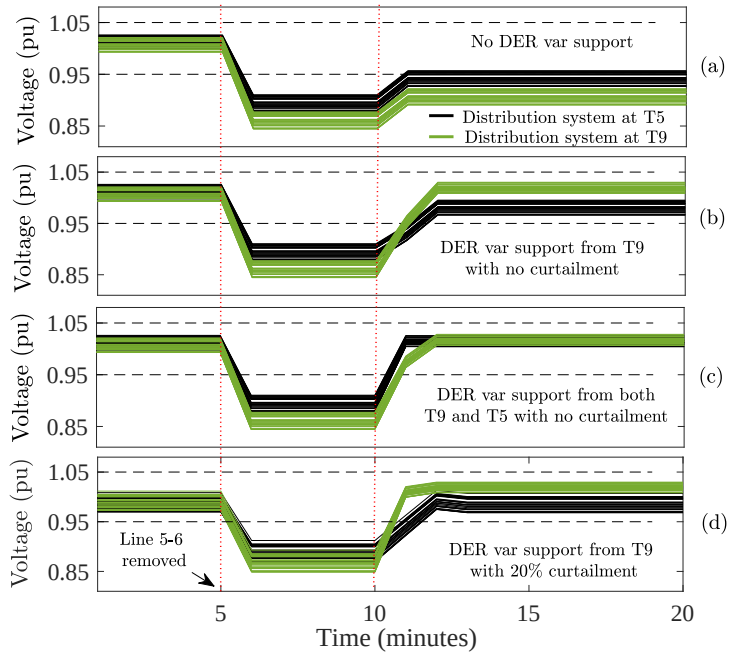

Figure 4.20 Impact of Aggregated DER var support on distribution system voltages after transmission line 5-6 contingency in various cases

4.7 Conclusion

This work is one component of the overall pursuit to utilize a vast amount of expected DER penetration for the benefit of the future grid, driven by the proposition that multitude of geographically distributed DERs with var control capability can be seen as flexible var resources (mini SVCs) for the grid. To facilitate this vision, a systematic OPF based methodology is proposed to construct an *aggregated net var capability curve* and flexibility region of a distribution network with high DER penetration, analogous to a conventional bulk generator. The proposed capability curve also accounts for DER curtailment that enables TSO to utilize both P and Q flexibilities provided by DERs into their planning and operational activities. The results on an unbalanced 37 bus test system confirms the availability of significant flexibility by DERs in most of the conditions. Further, the impact of distribution voltage constraints, inverter sizing and, T-D coupling on the flexibility region is discussed. In order to comply with new grid codes such as IEEE1547, either curtailment or inverter oversize might be necessary. It is observed that a large chunk of DERs concentrate at the end of the feeder shrinks the flexibility region significantly due to voltage constraints. Finally, the potential impact of such var provision on the transmission system performance is verified on an integrated T-D test system in cosimulation environment.

Certainly, the formulation and details of inclusion of the proposed flexibility in grid planning and operations remain an exciting challenge for future studies that also require a larger discussion on policy, payment structure etc. Nonetheless, the results are encouraging and indicate that the proposed aggregated capability indeed has potential to improve grid optimality by providing enhanced flexibility services to TSO.

CHAPTER 5. IMPACT OF DSITRIBUTION SYSTEM WITH DER ON LONG-TERM VOLTAGE STABILITY OF THE GRID

5.1 Introduction

Long-term voltage stability assessment (VSA) of independent transmission (T-VSA) and distribution (D-VSA) systems have been studied since long to estimate load margins. However, their impacts on each other have been neglected due to simplified assumptions i.e. in transmission systems, loads are assumed to be aggregated, and in distribution systems, substation bus voltage is assumed to be constant. In reality, both transmission and distribution systems are coupled physically and affect each other. Especially, at high load operating condition near the point of collapse (PoC), the substation voltage is significantly lower than the assumed constant value, thus leading to considerable exaggeration in load margin estimation of distribution feeders. Similarly, it is hard to represent distribution network losses, its power transfer limit and DERs voltage supporting capability in T-VSA. Therefore, it is essential to consider an integrated transmission-distribution (TD) system and conduct TD-VSA studies for accurate estimation of load margin of the overall system. Further, in order to assess the true impact of DERs var provision capability, it becomes all the more important to investigate the VSA of an integrated transmission-distribution (TD-VSA) system rather than relying on T-VSA.

In this chapter, we have following objectives: a) To analyze integrated TD-VSA by superimposing transmission system PV curve and distribution system hypersurface. This approach point out the possibility of system voltage collapse being caused by the distribution

system rather than the transmission system; b) To investigate the impact of DERs' var support on the load margin of the integrated T-D system.

5.2 Independent Systems Analysis

In this section, we will analyze VSA of independent transmission (T-VSA) and independent distribution systems (D-VSA) to further develop an integrated T-D system analysis (TD-VSA) in the next section.

5.2.1 Transmission System VSA (T-VSA)

To analyze VSA of a transmission system, parameterized transmission power flow (TPF) equations can be written by introducing the loading parameter λ as follows:

$$G_T(x_T, \lambda) = S_T(\lambda) - S_{TT}(x_T) = 0 \tag{5.1}$$

Where, S_T is a vector of net complex power injections (generation-load) at all transmission system buses; S_{TT} is a vector of total complex power flowing out of each bus. Loading parameter is denoted by λ and voltage magnitude and angle variables are denoted by $x_T = [v_T, \theta_T]$.Using CPF [3], PV curve for a transmission system can be traced to assess loadability limit at $\lambda = \lambda_T^{max}$ and consequently load margin from the operating point. A typical transmission system and PV curve are shown in Figure 5.1.

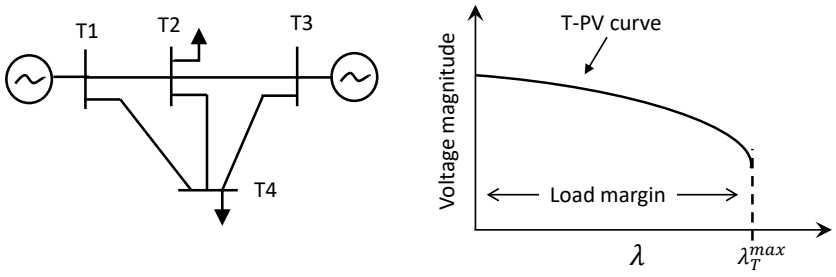

Figure 5.1 A typical transmission system and PV curve

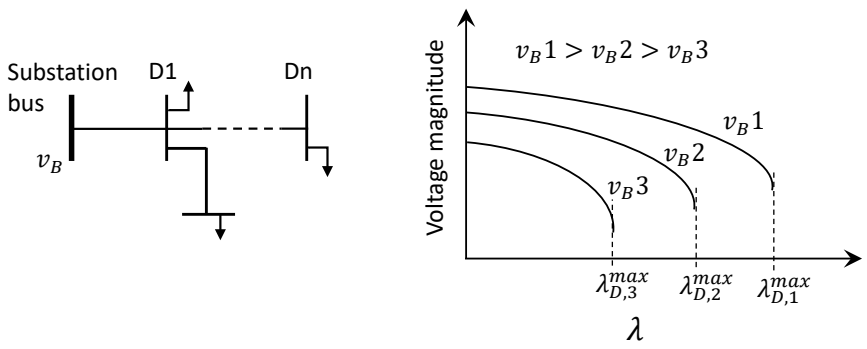

Figure 5.2 A typical distribution system and PV curve on various substation voltage values

5.2.2 Distribution System VSA (D-VSA)

A typical distribution system is shown in Figure 5.2. Similar to (5.1), parameterized distribution power flow (DPF) equations can be written as follows:

$$G_D(x_D, v_B, \lambda) = S_D(\lambda) - S_{DD}(x_D, v_B) = 0 \tag{5.2}$$

Notations are similar to TPF in (5.1) where subscript D denotes the distribution system buses. It is crucial to note there are two independent parameters in DPF equation (5.2) i.e. loading parameter (λ) and substation bus voltage (v_B). For distribution system analysis, substation bus is considered a slack bus and v_B is treated as a fixed parameter instead of a variable. But in real-world integrated T-D system, v_B is not fixed and decided by the transmission power flow solution. Therefore, to observe the impact of v_B on D-VSA, PV curve for a distribution system can be traced for different v_B values as shown in Figure 5.2. Higher value of substation voltage leads to higher loadability limit (λ_D^{max}) and consequently higher load margin. In other words, the distribution system has two parameters where critical value of loading parameter (λ_D^{max}) is a function of another parameter v_B. In a multi-parameter space, we can construct a hypersurface H which is a boundary of the feasible region of operation at stable equilibrium [14]. Surface H is a set of substation voltage magnitude and corresponding critical loading. A typical H surface is shown in Figure 5.3. Horizontal axis is loading parameter and the vertical axis is substation voltage

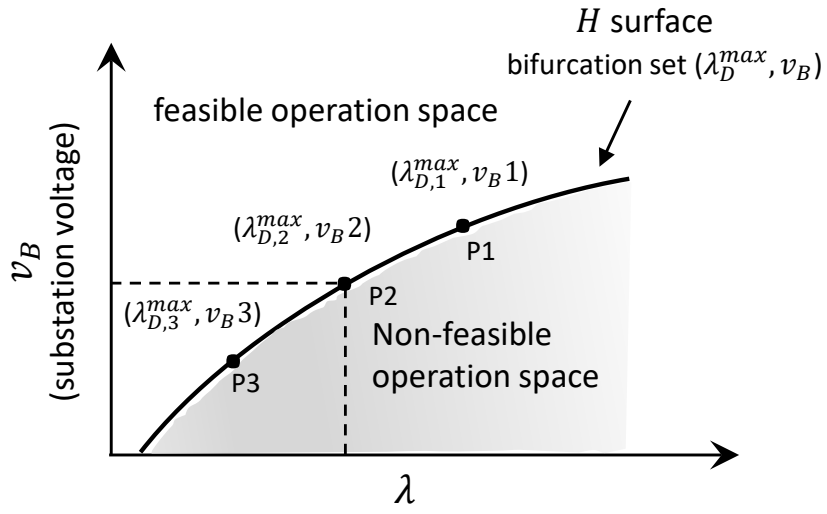

Figure 5.3 An example of a hypersurface H of a distribution system

magnitude. A point P2 on the surface indicates that if substation voltage is maintained at $v_B 2$, the load on distribution system can only be increased till $\lambda = \lambda_{D,2}^{max}$. To increase the loadability limit to $\lambda_{D,1}^{max}$, substation voltage must be increased to $v_B = v_B 1$. The space above the H surface is a feasible solution region. As we approach towards the surface, we move closer to the collapse point. On the surface, we reach to nose points where a slight increase in load or decrease in v_B may result in voltage collapse. The impact of decreasing substation voltage can easily be understood by plotting H surface. We will analyze how H surface affects integrated T-D VSA in the next section.

5.3 Integrated T-D System Analysis

5.3.1 Integrated TD-VSA Formulation

To understand the role of both the transmission and distribution systems, a parameterized integrated T-D system can be modeled through master-slave splitting method [15]. In this method, the integrated T-D system is split into three subsystems as shown in a representative example in Figure 5.4 i.e. master (M), boundary (B) and slave (S). M and S

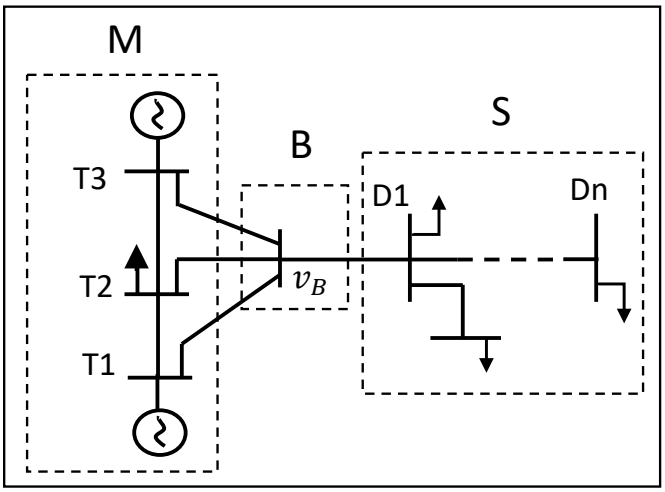

Figure 5.4 AA representative example of an integrated T-D system with master (M), boundary (B) and slave (S) subsystems

subsystems include all transmission and distribution systems buses, respectively excluding T-D boundary buses which are included in subsystem B. A set of parameterized power flow equations for such system can be written as follows:

$$G_{TD}(x_M, x_B, x_S, \lambda) = \begin{cases} G_M(x_M, x_B, \lambda) = 0 \\ G_B(x_M, x_B, x_S, \lambda) = 0 \\ G_S(x_B, x_S, \lambda) = 0 \end{cases} \tag{5.3}$$

G_M, G_B, G_S are power flow equations and x_M, x_B, x_S are voltage magnitude and angle variables for the master, boundary and slave subsystems respectively. To see the impact of independent T-VSA and D-VSA on integrated VSA, we can explicitly write G_M, G_B, G_S as follows:

$$\begin{aligned} G_M &= S_M(\lambda) - S_{MM}(x_M) - S_{MB}(x_M, x_B) \\ G_B &= -S_{BB}(x_B) - S_{BM}(x_B, x_M) - S_{BS}(x_B, x_S) \end{aligned} \tag{5.4}$$

$$G_S = S_S(\lambda) - S_{SS}(x_S) - S_{SB}(x_S, x_B) \tag{5.5}$$

S_X denotes a vector of net complex power injection of buses of system X; and S_{XY} denotes the complex power flow from buses of system X to system Y. In (4), we can see the components of T-VSA and D-VSA in (5.4) and (5.5) respectively. Equation (5.4) is similar to T-VSA (5.1) except an additional term $S_{BS}(x_B, x_S)$ which denotes the net power transfer from substation (boundary) to distribution system (slave). In T-VSA (5.1), this power transfer was part of $S_T(\lambda)$ in form of fixed aggregated loads. In (5.4), however, S_{BS} is not an aggregated load but a separate variable being decided by (5.5) . S_{BS} contains information of the physical distribution network which can not be captured accurately by an aggregated load modeling such as real and reactive power losses, power transfer limitation of distribution lines etc. This leads to error in estimation by T-VSA. Similarly, (5.5) is same as D-VSA (5.2) except the fact that the substation voltage v_B is not an independent parameter but a variable being decided by (5.4) . Change in v_B significantly affects the loadability limit of distribution lines which is hard to capture with the assumption of constant v_B in D-VSA. This leads to error in D-VSA estimation. Thus, in an integrated T-D system, the D-VSA and T-VSA are coupled through two variables at boundary bus i.e. voltage magnitude and net power transfer from distribution system to boundary bus. A realistic capture of these two variables leads to a true estimation of load margin in TD-VSA compare to T-VSA and D-VSA. By using CPF on (4), we can trace the PV curve for T-D system and estimate loadability limit at $\lambda = \lambda_{TD}^{max}$.

5.3.2 PV Curve Superimposition Analysis

Since, in an integrated system, voltage at the boundary bus v_B is a coupling factor and loading parameter λ is the same for both T and D system buses, we can superimpose H surface of the distribution system as shown in Figure 5.3 with T-PV curve of transmission system as shown in Figure 5.1. Please note that the y-axis in T-PV curve is voltage at the same boundary bus v_B. The superimposition of the two curves reveals some useful

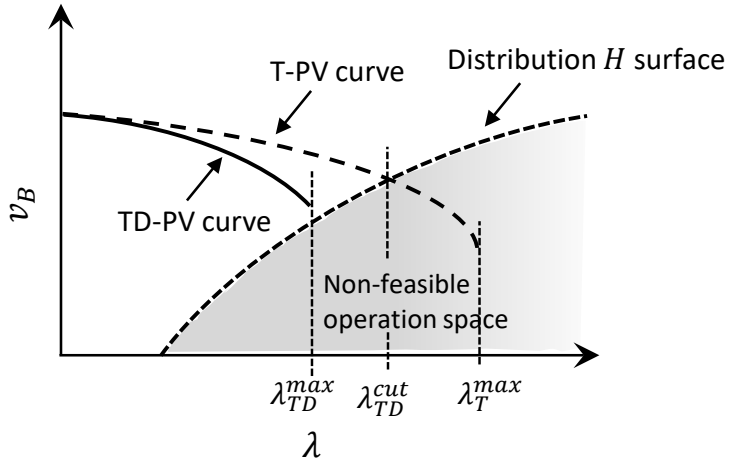

Figure 5.5 Case A: distribution hypersurface intersects T-PV curve i.e. distribution loadability is limiting factor

inferences regarding T-D VSA. Superimposition provides possibility of the two cases which are explained in detail below:

5.3.2.1 Case A: Constrained by Distribution System

This is the case where distribution H surface intersects T-PV curve at $\lambda_{TD}^{cut} < \lambda_{T}^{max}$ on superimposition as shown in Figure 5.5. Independent transmission system (T-PV curve) can go till λ_{T}^{max} but since the coupled TD system can not cross the H surface and enter into infeasible grey region, it has to stop before the intersection λ_{TD}^{cut}. Physically, the voltage at the boundary bus goes lower than the minimum substation voltage distribution feeder can handle at that particular load level and thus the distribution loadability limit arrives before the transmission system loadability limit. So, this is the case where overall system voltage collapse is being caused by the distribution systems. It should be noted since the S_{BS} includes distribution feeder losses in TD-VSA, the TD-PV curve does not exactly follow the T-PV curve. As load increase, losses increase and TD-PV curve moves away from the T-PV curve more. The analysis indicates the actual loadability limit will be less than λ_{TD}^{cut}

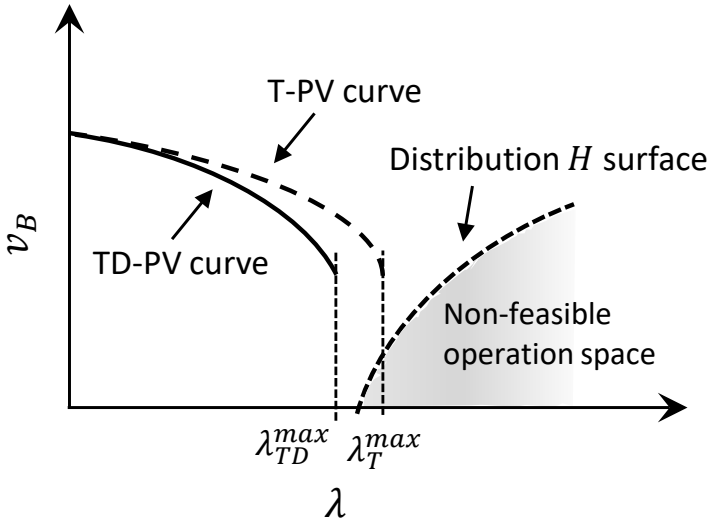

Figure 5.6 Case B: distribution hypersurface doesnt intersect T-PV curve i.e. transmission loadability is limiting factor

i.e. $\lambda_{TD}^{max} \leq \lambda_{TD}^{cut}$. If losses in distribution system are to be considered zero or negligible, then $\lambda_{TD}^{max} \approx \lambda_{TD}^{cut}$.

5.3.2.2 Case B: Constrained by Transmission System

This is the case when the distribution H surface does not intersect the T-PV curve as shown in Figure 5.6. It indicates that the transmission system hits the loadability limit before the distribution system. It infers that the distribution feeder is not being the limiting factor in maximum loadability of the coupled system. Since, the loadability limit is caused mainly by the transmission system, λ_{TD}^{max} is very close to λ_T^{max} but not exactly same because of distribution losses taken into account. Generally, $\lambda_{TD}^{max} \leq \lambda_T^{max}$ but if losses can be neglected, then $\lambda_{TD}^{max} \approx \lambda_T^{max}$. Though the exact λ_{TD}^{max} can be estimated by solving equations (5.4-5.5), this analysis provides additional information that which system is constraining the overall coupled system so that the appropriate actions can be taken.

5.3.3 Impact of DERs on the Integrated System VSA

DERs directly impact the net real power and reactive power transfer of distribution feeder to the transmission system. Though some of these impacts can be modeled while assessing independent T-VSA such as reduction in net load due to generation but other impacts are very difficult to consider, that is, significant impact on losses in the feeder, substation voltage support from their volt/var capability. It can exaggerate or underestimate the load margins. Therefore, integrated TD-VSA becomes essential and provides more accurate assessment. Especially, in cases where loadability is limited by distribution systems, integrated analysis can evaluate how the DERs affect H surface of feeders in order to identify or relieve the most critical feeders. The impact of DERs depends on whether they are operating in unity power factor (PF) mode or in var support mode (volt/var control).

5.3.3.1 DERs with Unity PF Mode:

DERs at unity PF mode have two major effect on the load margin. First, they decrease the net real power demand of the system which shifts the operating point backwards in terms of loading. This should increase the load margin by the same amount. Second, they also reduce the net PF of the substation as they only decrease real power demand while not altering the var demand. And as we know, PV curves shifts downwards and maximum loadability limit decreases as PF decreases. This leads to decrease in load margin. Thus the net effect of DERs at unity PF could be anything as a combination of the two opposite factors. So, the load margin may increase but it would be less than the decrease in the net load.

5.3.3.2 DERs with Var Support Mode

: The impact of DERs in var support mode is much more than the unity PF mode as it has potential to decrease net var demand of the substation. However, if the DERs are being utilized to maintain voltage at lower level by absorbing var, they might be detrimental to

the load margin in certain situations such as sudden contingency in low load conditions or applying CVR at peak load etc. So, the impact can vary based on the voltage set-point of the DER inverters and operating conditions. Nonetheless, the DERs with var support has high capability to improve load margin and can definitely be exploited in emergency conditions.

In either case, DERs' impact is more visible in the cases where the distribution feeder is constraining the overall loadability of the system. DERs improve the H surface of the critical feeders by increasing their λ_{TD}^{cut}. Therefore, from the load margin perspective, DERs located at the most critical feeder bring the most benefit to the system

5.4 Co-Simulation Approach to Solve Integrated T-D System

A T-D co-simulation platform is developed to simulate the T-D interaction and validate the numerical results on test cases. The master-slave splitting (MSS) method based power flow algorithm has been used in developing this platform (84). We extend the MSS method to develop co-simulation for widely accepted full-scale open-source solvers. A python based power flow solver Pypower is utilized to model the transmission network. Similarly, GridlabD [12] is used to model and solve the unbalanced three-phase distribution systems. Both the solvers communicate and exchange the variables at the interface which is developed using a software "Framework for Network Co-Simulation (FNCS)" [13]. All three software are open-source, and GridlabD and FNCS are developed by Pacific Northwest National Laboratory (PNNL). Aggregated loads at the transmission buses are replaced by the several distribution feeders and interchange the variables as shown in Figure 5.7. For a particular operating point (loading condition), distribution feeders solve the power flow and send the net substation power information to the transmission solver via FNCS. Transmission solver runs power flow for the received loading and sends the resultant voltage to the distribution solver s via FNCS. This interchange of variables occurs until convergence is reached. More details about the co-simulation method can be found in [14][15].

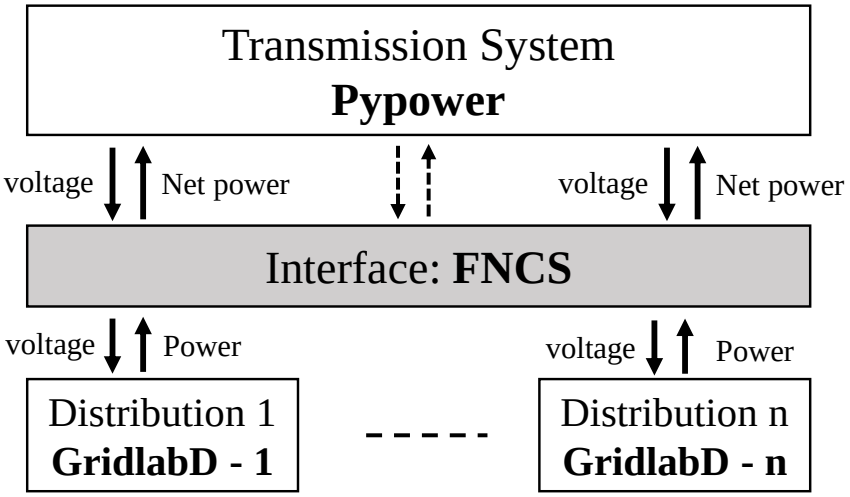

Figure 5.7 A co-simulation framework to solve integrated transmission-distribution system with their detailed modeling

5.5 Case Study and Results

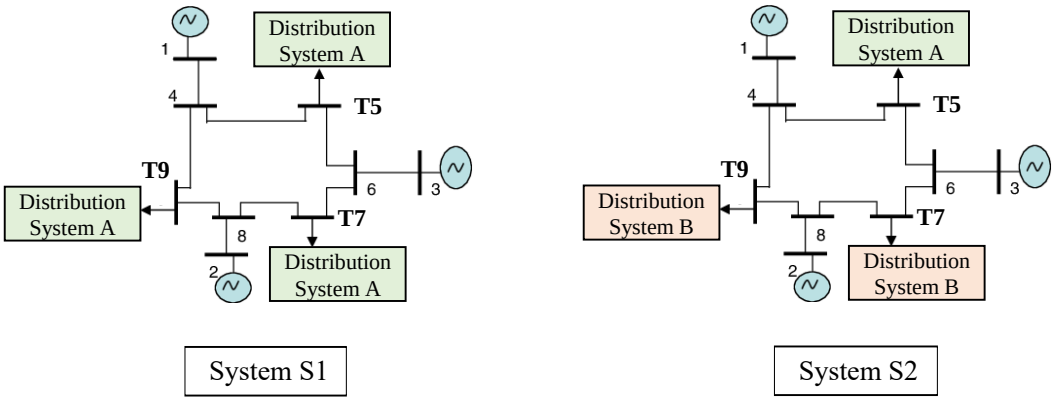

Figure 5.8 Two Integrated T-D test systems; Integrated System S1: all 3 load buses of IEEE 9 bus transmission test system are coupled with unablanced distribution feeder A ; Integrated System S2: same as system S1 with distribution feeders A are replaced by feeder B on T7 and T9 transmission buses

5.5.1 Integrated Test System Description

IEEE 9 bus test system is used as transmission network and the loads at all three load buses T5, T7 and T9 are replaced with the unbalanced distribution test systems A and B as shown in Figure 5.8. Several identical feeders are attached at each transmission bus to match the base load (90, 100 and 125 MW respectively). Distribution systems A is same as unbalanced IEEE 37 distribution test system while system B is a modified version of it. The line impedances of system B are reduced by scaling factor of 0.5. The variation in the impedances is comparable to the various line configurations present in the IEEE distribution test systems [10]. We create 2 cases as following:

- Integrated system S1: distribution network A is attached to all three load buses i.e. T5, T7, T9.
- Integrated system S2: distribution network A is replaced by network B at T7 and T9.

For the load increase scenario, the loads at all the distribution buses and generation at all transmission buses are increased with the same scaling factor λ. Maximum loading condition is considered when either transmission or distribution power flow stops converging. Load margin is MW difference between base load and maximum possible loading.

5.5.2 Comparison between T-VSA and TD-VSA

Table 5.1 compare the load margin estimated from T-VSA and TD-VSA for both the system S1 and S2. Note that the T-VSA is same (454 MW) for both systems because it can not capture the impact of distribution systems, leading to inaccurate results. Further, TD-VSA results in 140 and 184 MW load margins which is significantly lesser compared to T-VSA. It indicates that in both of these cases, distribution systems are being the critical factors. System S2 has higher load margin than S1 that can be interpreted as improved distribution system loadability in S2. This makes sense as System S2 has distribution feeders type B which are less constraining than feeder A due to reduced impedances. Note

that the feeder A is the original IEEE test feeder representing real world feeders. These results indicate that distribution system play a crucial role in estimating load margin even without DER penetration.

Table 5.1 Comparison of load margin (MW) from T-VSA and TD-VSA for system S1 and S2

Load margin (MW) from	System S1	System S2
T-VSA	454	454
TD-VSA	140	184

5.5.3 Impact of DER on VSA

All distribution feeders at all three transmission buses are augmented to have with 50% solar PV penetration in both the systems S1 and S2. Table 5.2 presents the load margin comparison for various cases with DER for both the systems S1 and S2. First, compare the load margins estimated by T-VSA and TD-VSA with DER without var support i.e. unity PF (column 2). As expected, T-VSA significantly over-estimates the margin for both S1 and S2.

Now, let's observe the impact of DER var support. We create three cases where feeder attached to substation bus T5, T7 and T9 provide DER var support, one at a time. The amount of var support is same as mandated by integration standard IEEE1547-2018 as minimum var support. Note that in system S1, the improvement in load margin is maximum (from 193 MW to 240 MW) when DER var support is provided by T9 implying that the feeders attached at bus T9 make it critical load bus. Figure 5.9 shows the PV curves for system S1 with DER penetration in different cases. It can be seen that the nose point is farthest when var support is at bus T9. However, in system S2, the maximum improvement happens when DER var support is provided by feeders attached at bus T5. It is because in

system S2, T7 and T9 feeders are replaced with type B which is less constraining than type A as discussed in the last section. This relieves the T9 bus and, in turn, makes the T5 the critical substation. It should also be noted that the var support at non-critical load buses does not improve the load margin significantly. It signifies the importance of considering distribution system in long-term stability assessment.

Table 5.2 Impact of 50% DER penetration on load margin (MW) with and without volt/-var control mode for Case A and Case B

Load margin (MW) from	DER with unity PF	DER with var support at		
		T5	T7	T9
T-VSA	471	490	490	510
System S1: TD-VSA	193	211	213	240
System S2: TD-VSA	249	292	249	260

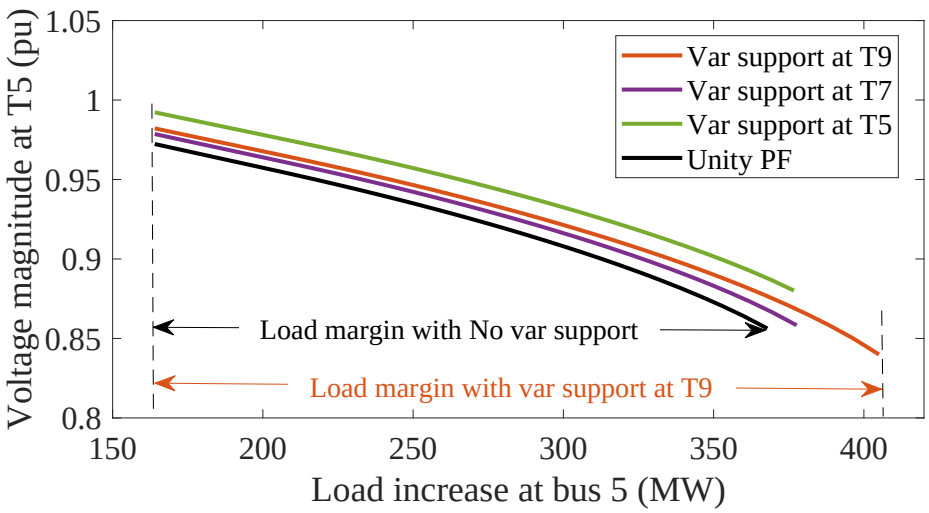

Figure 5.9 PV curves to observe the impact of DER on load margin of the System S1 under following cases: with unity PF mode (no var support), IEEE1547 required var support at transmission bus T5, T7 and T9 one at a time

5.6 Conclusion

The results discussed above lead to the following 3 conclusions:

1. The investigation reveals the possibility of distribution system being critical in causing long-term voltage collapse rather than the transmission system.

2. The investigation demonstrates the significant error in load margin assessment if distribution systems is ignored; thus draw attention to the need of TD-VSA and cosimulation platform.

3. The DERs var support improves the load margin of the system, given the support is from the substation which has critical distribution system connected.

CHAPTER 6. FINAL CONCLUSION

6.1 Concluding Remarks

With increasing solar PV penetration, the need to address the voltage challenges in distribution system has increased. Simultaneously, the volt/var capability of numerous solar PV devices (DER, in general) also presents an opportunity for the transmission system. In this work, we attempt to address the challenges for distribution systems as well as to explore opportunities for the bulk grid due to high DER penetration. Specific novel research contributions have been discussed in chapter 1 (1.3). The summary of overall contributions and significance of the work is presented as follows.

First, we proposed a fully local real-time adaptive volt/var control strategy with high solar PV integration to mitigate over-voltage that addresses two main issues with the existing local droop VVC: a) it ensures both the control stability and high set-point tracking performance by proposing a modification which decouples these two objectives; b) it addresses the parameter selection problem by making parameters self-adaptive to fast external disturbances such as cloud intermittency, load changes, substation voltage changes etc. The satisfactory performance is successfully demonstrated on an IEEE 123 bus test system (˜1500 nodes) with detailed house-level load modeling by comparing with the existing droop control methods in several cases. The proposed approach enables operators to utilize PV inverters beyond over-voltage mitigation, that is, for other volt/var related applications in distribution systems (e.g. CVR, loss minimization) as well as in transmission systems (e.g. aggregated var support) by virtue of a) real-time adaptive nature, b) tight voltage control

with low SSE and, c) compatibility with the integration standards and utility practices (IEEE1547, Rule 21 (CA)).

Second, we explore the possibility of utilizing DERs volt/var capability for the grid benefits. We present a proposition that multitude of geographically distributed DERs with var control capability can be seen as flexible var resources (mini SVCs) for the grid. To facilitate this vision, a systematic OPF based methodology is proposed to construct an *aggregated net var capability curve* and flexibility region of a distribution network with high DER penetration, analogous to a conventional bulk generator. The proposed capability curve also accounts for DER curtailment that enables TSO to utilize both P and Q flexibilities provided by DERs into their planning and operational activities. The results on an unbalanced 37 bus test system confirms the availability of significant flexibility by DERs in most of the conditions. Further, the impact of distribution voltage constraints, inverter sizing and, T-D coupling on the flexibility region is discussed. In order to comply with new grid codes such as IEEE1547, either curtailment or inverter oversize might be necessary. It is observed that a large chunk of DERs concentrate at the end of the feeder shrinks the flexibility region significantly due to voltage constraints. Finally, the potential impact of such var provision on the transmission system performance is verified on an integrated T-D test system in cosimulation environment.

Third, we explore the impact of DERs on the long-term voltage stability assessment (VSA) of an integrated T-D system. We analyze the TD-VSA using PV curve superimposition analysis. Further, we develop a T-D cosimulation platform using open-source established solvers to verify the results on an integrated T-D system. A IEEE 9 bus test system coupled with IEEE 37 bus distribution test system is considered as test case. The investigation indicates that the distribution system may also be a critical cause of voltage collapse which can not be captured in tradition T-VSA analysis. As a result, T-VSA may significantly overestimate the load margin of the overall system compared to the actual margin (TD-VSA). Further, it is found that DER in general improves the load margin by

reducing the net load, however DER with var support mode improves the voltage stability margin more compared to unity PF case. We also observed that in an integrated T-D system, DER var support from those substations give the most improvement with whom the critical distribution systems are connected. Overall, we demonstrated the importance of co-simulation to capture the true impact of DER on the voltage stability assessment.

6.2 Possible Future Extensions

- Due to its high set-point tracking accuracy and self-adaptive nature to local disturbances, the proposed local adaptive VVC approach can be extended to utilize PV inverter capability to improve/assist other volt/var dependent applications in modern distribution systems such as loss minimization, conservative voltage reduction (CVR) etc.

- The formulation and details of inclusion of the proposed flexibility in grid planning and operations remain an exciting challenge for future studies. The proposed aggregated capability curve can be modeled as constraints in transmission optimization problems such as economic dispatch.

- The proposed DER utilization can be extended to combine with demand response control and other inverter based DER technologies such as electric vehicle and storage; thus combined real power and reactive power control can be implemented to provide watt and var support to the transmission system as well as enhancing the benefits to the customers at the distribution level.

BIBLIOGRAPHY

[1] R. Fu, D. Feldman, R. Margolis, M. Woodhouse, and K. Ardani, "U.S. Solar Photovoltaic System Cost Benchmark: Q1 2017," Technical Report NREL/TP-6A20-68925, National Renewable Energy Laboratory, Sept. 2017.

[2] S. Sayeef, S. Heslop, D. Cornforth, and T. Moore, "Solar intermittency: Australias clean energy challenge," tech. rep., CSIRO, June 2012.

[3] B. Owens, "The Rise of Distributed Power," tech. rep., GE, 2014.

[4] "SEIA ANNUAL REPORT 2016," tech. rep., SOLAR ENERGY INDUSTRIES ASSOCIATION, 2016.

[5] "SunShot Vision Study," tech. rep., US Department of Energy.

[6] P. Gagnon, R. Margolis, J. Melius, C. Phillips, and R. Elmore, "Rooftop Solar Photovoltaic Technical Potential in the United States: A Detailed Assessment," tech. rep., NREL, Jan. 2016.

[7] J. Bank, B. Mather, J. Keller, and M. Coddington, "High Penetration Photovoltaic Case Study Report," Tech. Rep. NREL/TP-5500-54742, National Renewable Energy Laboratory, Jan. 2013.

[8] A. Keane, L. F. Ochoa, C. L. T. Borges, G. W. Ault, A. D. Alarcon-Rodriguez, R. A. F. Currie, F. Pilo, C. Dent, and G. P. Harrison, "State-of-the-Art Techniques and Challenges Ahead for Distributed Generation Planning and Optimization," *IEEE Transactions on Power Systems*, vol. 28, pp. 1493–1502, May 2013.

[9] I. J. Perez-Arriaga, "The Transmission of the Future: The Impact of Distributed Energy Resources on the Network," *IEEE Power and Energy Magazine*, vol. 14, pp. 41–53, July 2016.

[10] E. J. Coster, J. M. A. Myrzik, B. Kruimer, and W. L. Kling, "Integration Issues of Distributed Generation in Distribution Grids," *Proceedings of the IEEE*, vol. 99, pp. 28–39, Jan. 2011.

[11] b. Mather, R. Seguin, J. Woyak, D. Costyk, and J. Hambrick, "High-Penetration PV Integration Handbook for Distribution Engineers," tech. Rep., National Renewable Energy Laboratory (NREL), Jan. 2016.

[12] P. P. Barker and R. W. D. Mello, "Determining the impact of distributed generation on power systems. I. Radial distribution systems," in *2000 Power Engineering Society Summer Meeting (Cat. No.00CH37134)*, vol. 3, pp. 1645–1656 vol. 3, 2000.

[13] E. M. Stewart, T. P. Aukai, S. D. J. MacPherson, B. P. Quach, D. Nakafuji, and R. Davis, "A realistic irradiance-based voltage flicker analysis of PV applied to Hawaii distribution feeders," in *2012 IEEE Power and Energy Society General Meeting*, pp. 1–7, July 2012.

[14] K. Rahimi, R. Broadwater, S. Omran, and M. Dilek, "Quasi-Steady-State computation of voltage flicker with cloud motion simulator," in *2017 IEEE Power and Energy Conference at Illinois (PECI)*, pp. 1–8, Feb. 2017.

[15] *ANSI C84.1: American National Standard for Electric Power Systems and Equipment-Voltage Ratings (60 Hertz)*. NEMA, Oct. 2016.

[16] M. E. Baran and F. F. Wu, "Optimal capacitor placement on radial distribution systems," *IEEE Transactions on Power Delivery*, vol. 4, pp. 725–734, Jan. 1989.

[17] C. L. Masters, "Voltage rise: the big issue when connecting embedded generation to long 11 kV overhead lines," *Power Engineering Journal*, vol. 16, pp. 5–12, Feb. 2002.

[18] H. E. Farag and E. F. El-Saadany, "Voltage regulation in distribution feeders with high DG penetration: From traditional to smart," in *2011 IEEE Power and Energy Society General Meeting*, pp. 1–8, July 2011.

[19] "IEEE Recommended Practice for Electric Power Distribution for Industrial Plants," *IEEE Std 141-1993*, pp. 1–768, Apr. 1994.

[20] W. H. Kersting, *Distribution System Modeling and Analysis, Fourth Edition*. CRC Press, Aug. 2017. Google-Books-ID: IhUwDwAAQBAJ.

[21] H. G. Yeh, D. F. Gayme, and S. H. Low, "Adaptive VAR Control for Distribution Circuits With Photovoltaic Generators," *IEEE Transactions on Power Systems*, vol. 27, pp. 1656–1663, Aug. 2012.

[22] B. A. Robbins, C. N. Hadjicostis, and A. D. Domnguez-Garca, "A Two-Stage Distributed Architecture for Voltage Control in Power Distribution Systems," *IEEE Transactions on Power Systems*, vol. 28, pp. 1470–1482, May 2013.

[23] M. McGranaghan, D. Ortmeyer, D. Crudele, T. Key, Smith, and J. Baker, "Advanced grid planning and operation," tech. Rep., Sandia National Laboratories, 2008.

[24] M. H. J. Bollen and A. Sannino, "Voltage control with inverter-based distributed generation," *IEEE Transactions on Power Delivery*, vol. 20, pp. 519–520, Jan. 2005.

[25] P. M. S. Carvalho, P. F. Correia, and L. A. F. M. Ferreira, "Distributed Reactive Power Generation Control for Voltage Rise Mitigation in Distribution Networks," *IEEE Transactions on Power Systems*, vol. 23, pp. 766–772, May 2008.

[26] "IEEE Standard for Interconnection and Interoperability of Distributed Energy Resources with Associated Electric Power Systems Interfaces," *IEEE Std 1547-2018 (Revision of IEEE Std 1547-2003)*, pp. 1–138, Apr. 2018.

[27] "Impact of IEEE 1547 Standard on Smart Inverters," Technical Report PES-TR67, IEEE PES Industry Technical Support Task Force, May 2018.

[28] *Rule 21 Interconnection Standard, CA*.

[29] H. Song, B. Lee, S.-H. Kwon, and V. Ajjarapu, "Reactive reserve-based contingency constrained optimal power flow (RCCOPF) for enhancement of voltage stability margins," *IEEE Transactions on Power Systems*, vol. 18, pp. 1538–1546, Nov. 2003.

[30] L. Bao, Z. Huang, and W. Xu, "Online voltage stability monitoring using VAr reserves," *IEEE Transactions on Power Systems*, vol. 18, pp. 1461–1469, Nov. 2003.

[31] P. Goergens, F. Potratz, M. Gdde, and A. Schnettler, "Determination of the potential to provide reactive power from distribution grids to the transmission grid using optimal power flow," in *2015 50th International Universities Power Engineering Conference (UPEC)*, pp. 1–6, Sept. 2015.

[32] H. Barth, D. Hidalgo, A. Pohlemann, M. Braun, L. H. Hansen, and H. Knudsen, "Technical and economical assessment of reactive power provision from distributed generators: Case study area of East Denmark," in *2013 IEEE Grenoble Conference*, pp. 1–6, June 2013.

[33] F. Marten, K. Diwold, L. Lwer, L. M. Faiella, P. Hochloff, L. H. Hansen, and M. Braun, "Analysis of a reactive power exchange between distribution and transmission grids," in *2013 IEEE International Workshop on Inteligent Energy Systems (IWIES)*, pp. 52–57, Nov. 2013.

[34] F. Marten, L. Lwer, J. Tbermann, and M. Braun, "Optimizing the reactive power balance between a distribution and transmission grid through iteratively updated grid equivalents," in *2014 Power Systems Computation Conference*, pp. 1–7, Aug. 2014.

[35] D. S. Stock, A. Venzke, T. Hennig, and L. Hofmann, "Model predictive control for reactive power management in transmission connected distribution grids," in *2016 IEEE PES Asia-Pacific Power and Energy Engineering Conference (APPEEC)*, pp. 419–423, Oct. 2016.

[36] D. S. Stock, F. Sala, A. Berizzi, and L. Hofmann, "Optimal Control of Wind Farms for Coordinated TSO-DSO Reactive Power Management," *Energies*, vol. 11, p. 173, Jan. 2018.

[37] R. O'Gorman and M. A. Redfern, "Voltage control problems on modern distribution systems," in *IEEE Power Engineering Society General Meeting, 2004.*, pp. 662–667 Vol.1, June 2004.

[38] A. Keane, L. F. Ochoa, E. Vittal, C. J. Dent, and G. P. Harrison, "Enhanced Utilization of Voltage Control Resources With Distributed Generation," *IEEE Transactions on Power Systems*, vol. 26, pp. 252–260, Feb. 2011.

[39] T. Senjyu, Y. Miyazato, A. Yona, N. Urasaki, and T. Funabashi, "Optimal Distribution Voltage Control and Coordination With Distributed Generation," *IEEE Transactions on Power Delivery*, vol. 23, pp. 1236–1242, Apr. 2008.

[40] Y. Xu, Z. Y. Dong, R. Zhang, and D. J. Hill, "Multi-Timescale Coordinated Voltage/-Var Control of High Renewable-Penetrated Distribution Systems," *IEEE Transactions on Power Systems*, vol. 32, pp. 4398–4408, Nov. 2017.

[41] E. DallAnese, S. V. Dhople, and G. B. Giannakis, "Optimal Dispatch of Photovoltaic Inverters in Residential Distribution Systems," *IEEE Transactions on Sustainable Energy*, vol. 5, pp. 487–497, Apr. 2014.

[42] M. Farivar, R. Neal, C. Clarke, and S. Low, "Optimal inverter VAR control in distribution systems with high PV penetration," in *2012 IEEE Power and Energy Society General Meeting*, pp. 1–7, July 2012.

[43] W. Zheng, W. Wu, B. Zhang, H. Sun, and Y. Liu, "A Fully Distributed Reactive Power Optimization and Control Method for Active Distribution Networks," *IEEE Transactions on Smart Grid*, vol. 7, pp. 1021–1033, Mar. 2016.

[44] B. Zhang, A. Y. S. Lam, A. D. Domnguez-Garca, and D. Tse, "An Optimal and Distributed Method for Voltage Regulation in Power Distribution Systems," *IEEE Transactions on Power Systems*, vol. 30, pp. 1714–1726, July 2015.

[45] H. Chen, W. Zhang, J. Lian, and A. J. Conejo, "Robust distributed volt/var control of distribution systems," in *2017 IEEE 56th Annual Conference on Decision and Control (CDC)*, pp. 6321–6326, Dec. 2017.

[46] K. Turitsyn, P. ulc, S. Backhaus, and M. Chertkov, "Distributed control of reactive power flow in a radial distribution circuit with high photovoltaic penetration," in *IEEE PES General Meeting*, pp. 1–6, July 2010.

[47] E. DallAnese, S. V. Dhople, B. B. Johnson, and G. B. Giannakis, "Decentralized Optimal Dispatch of Photovoltaic Inverters in Residential Distribution Systems," *IEEE Transactions on Energy Conversion*, vol. 29, pp. 957–967, Dec. 2014.

[48] K. E. Antoniadou-Plytaria, I. N. Kouveliotis-Lysikatos, P. S. Georgilakis, and N. D. Hatziargyriou, "Distributed and Decentralized Voltage Control of Smart Distribution Networks: Models, Methods, and Future Research," *IEEE Transactions on Smart Grid*, vol. 8, pp. 2999–3008, Nov. 2017.

[49] D. K. Molzahn, F. Drfler, H. Sandberg, S. H. Low, S. Chakrabarti, R. Baldick, and J. Lavaei, "A Survey of Distributed Optimization and Control Algorithms for Electric Power Systems," *IEEE Transactions on Smart Grid*, vol. 8, pp. 2941–2962, Nov. 2017.

[50] H. Zhu and H. J. Liu, "Fast Local Voltage Control Under Limited Reactive Power: Optimality and Stability Analysis," *IEEE Transactions on Power Systems*, vol. 31, pp. 3794–3803, Sept. 2016.

[51] K. Turitsyn, P. Sulc, S. Backhaus, and M. Chertkov, "Options for Control of Reactive Power by Distributed Photovoltaic Generators," *Proceedings of the IEEE*, vol. 99, pp. 1063–1073, June 2011.

[52] B. Zhang, A. D. Domnguez-Garca, and D. Tse, "A local control approach to voltage regulation in distribution networks," in *2013 North American Power Symposium (NAPS)*, pp. 1–6, Sept. 2013.

[53] B. Seal and M. McGranaghan, "Standard Language Protocols for PV and Storage Grid Integration," tech. rep., EPRI, May 2010.

[54] M. Farivar, L. Chen, and S. Low, "Equilibrium and dynamics of local voltage control in distribution systems," in *52nd IEEE Conference on Decision and Control*, pp. 4329–4334, Dec. 2013.

[55] P. Jahangiri and D. C. Aliprantis, "Distributed Volt/VAr Control by PV Inverters," *IEEE Transactions on Power Systems*, vol. 28, pp. 3429–3439, Aug. 2013.

[56] M. Bello, D. Montenegro, B. York, and J. Smith, "Optimal Settings for Multiple Groups of Smart Inverters on Secondary Systems Using Autonomous Control," in *2017 IEEE Rural Electric Power Conference (REPC)*, pp. 89–94, Apr. 2017.

[57] H. Li, M. Rylander, and J. Smith, "Analysis to Inform CA Grid Integration: Methods and Default Settings to Effectively Use Advanced Inverter Functions in the Distribution System," Tech. Rep. 3002007139, EPRI, Dec. 2015.

[58] M. Rylander, H. Li, J. Smith, and W. Sunderman, "Default volt-var inverter settings to improve distribution system performance," in *2016 IEEE Power and Energy Society General Meeting (PESGM)*, pp. 1–5, July 2016.

[59] S. R. Abate, T. E. McDermott, M. Rylander, and J. Smith, "Smart inverter settings for improving distribution feeder performance," in *2015 IEEE Power Energy Society General Meeting*, pp. 1–5, July 2015.

[60] C. Zhang, Y. Xu, Z. Y. Dong, and J. Ravishankar, "Three-Stage Robust Inverter-Based Voltage/Var Control for Distribution Networks with High-Level PV," *IEEE Transactions on Smart Grid*, vol. PP, no. 99, pp. 1–1, 2017.

[61] A. R. Malekpour and A. Pahwa, "A Dynamic Operational Scheme for Residential PV Smart Inverters," *IEEE Transactions on Smart Grid*, vol. 8, pp. 2258–2267, Sept. 2017.

[62] N. Karthikeyan, B. R. Pokhrel, J. R. Pillai, and B. Bak-Jensen, "Coordinated voltage control of distributed PV inverters for voltage regulation in low voltage distribution networks," in *2017 IEEE PES Innovative Smart Grid Technologies Conference Europe (ISGT-Europe)*, pp. 1–6, Sept. 2017.

[63] D. Shah and M. L. Crow, "Online Volt-Var Control for Distribution Systems With Solid-State Transformers," *IEEE Transactions on Power Delivery*, vol. 31, pp. 343–350, Feb. 2016.

[64] A. Safavizadeh, G. R. Yousefi, and H. R. Karshenas, "Voltage Variation Mitigation using Reactive Power Management of Distributed Energy Resources in a Smart Distribution System," *IEEE Transactions on Smart Grid*, vol. PP, no. 99, pp. 1–1, 2017.

[65] E. DallAnese, S. Guggilam, A. Simonetto, Y. C. Chen, and S. V. Dhople, "Optimal Regulation of Virtual Power Plants," *IEEE Transactions on Power Systems*, vol. PP, no. 99, pp. 1–1, 2017.

[66] A. Singhal, V. Ajjarapu, J. C. Fuller, and J. Hansen, "Real-Time Local Volt/VAR Control Under External Disturbances with High PV Penetration," *IEEE Transactions on Smart Grid*, pp. 1–1, 2018.

[67] R. J. Konopinski, P. Vijayan, and V. Ajjarapu, "Extended Reactive Capability of DFIG Wind Parks for Enhanced System Performance," *IEEE Transactions on Power Systems*, vol. 24, pp. 1346–1355, Aug. 2009.

[68] P. Cuffe, P. Smith, and A. Keane, "Transmission System Impact of Wind Energy Harvesting Networks," *IEEE Transactions on Sustainable Energy*, vol. 3, pp. 643–651, Oct. 2012.

[69] J. Silva, J. Sumaili, R. J. Bessa, L. Seca, M. Matos, and V. Miranda, "The challenges of estimating the impact of distributed energy resources flexibility on the TSO/DSO boundary node operating points," *Computers & Operations Research*, vol. 96, pp. 294–304, Aug. 2018.

[70] S. Kundu, K. Kalsi, and S. Backhaus, "Approximating Flexibility in Distributed Energy Resources: A Geometric Approach," Mar. 2018.

[71] E. Kaempf, H. Abele, S. Stepanescu, and M. Braun, "Reactive power provision by distribution system operators Optimizing use of available flexibility," in *IEEE PES Innovative Smart Grid Technologies, Europe*, pp. 1–5, Oct. 2014.

[72] P. Cuffe, P. Smith, and A. Keane, "Capability Chart for Distributed Reactive Power Resources," *IEEE Transactions on Power Systems*, vol. 29, pp. 15–22, Jan. 2014.

[73] V. Ajjarapu and B. Lee, "Bibliography on voltage stability," *IEEE Transactions on Power Systems*, vol. 13, pp. 115–125, Feb. 1998.

[74] V. Ajjarapu and C. Christy, "The continuation power flow: a tool for steady state voltage stability analysis," *IEEE Transactions on Power Systems*, vol. 7, pp. 416–423, Feb. 1992.

[75] *Voltage Stability of Power Systems: Concepts, Analytical Tools, and Industry Experience*. IEEE, 1990. Google-Books-ID: lgspPQAACAAJ.

[76] R. B. Prada and L. J. Souza, "Voltage stability and thermal limit: constraints on the maximum loading of electrical energy distribution feeders," *Transmission and Distribution IEE Proceedings - Generation*, vol. 145, pp. 573–577, Sept. 1998.

[77] H. Sheng and H. D. Chiang, "CDFLOW: A Practical Tool for Tracing Stationary Behaviors of General Distribution Networks," *IEEE Transactions on Power Systems*, vol. 29, pp. 1365–1371, May 2014.

[78] P. C. Chen, V. Malbasa, and M. Kezunovic, "Analysis of voltage stability issues with distributed generation penetration in distribution networks," in *2013 North American Power Symposium (NAPS)*, pp. 1–6, Sept. 2013.

[79] J. Xu, B. Li, Y. Zou, C. Li, X. Mao, X. Mao, S. Pan, and N. Zhou, "Characteristics of static voltage stability for distributed generation integrated into power system and its impacts analysis," in *2013 IEEE PES Asia-Pacific Power and Energy Engineering Conference (APPEEC)*, pp. 1–6, Dec. 2013.

[80] J. Yaghoobi, N. Mithulananthan, T. K. Saha, and R. C. Bansal, "Investigating static voltage stability of distribution system with rooftop PV units," in *2013 Australasian Universities Power Engineering Conference (AUPEC)*, pp. 1–6, Sept. 2013.

[81] R. S. A. Abri, E. F. El-Saadany, and Y. M. Atwa, "Optimal Placement and Sizing Method to Improve the Voltage Stability Margin in a Distribution System Using Distributed Generation," *IEEE Transactions on Power Systems*, vol. 28, pp. 326–334, Feb. 2013.

[82] N. Hemdan and M. Kurrat, "Influence of distributed generation on different loadability aspects of electric distribution systems," in *CIRED 2009 - 20th International Conference and Exhibition on Electricity Distribution - Part 1*, pp. 1–4, June 2009.

[83] Z. Li, Q. Guo, H. Sun, and J. Wang, "Impact of Coupled Transmission-Distribution on Static Voltage Stability Assessment," *IEEE Transactions on Power Systems*, vol. PP, no. 99, pp. 1–1, 2016.

[84] H. Sun, Q. Guo, B. Zhang, Y. Guo, Z. Li, and J. Wang, "Master #x2013;Slave-Splitting Based Distributed Global Power Flow Method for Integrated Transmission and Distribution Analysis," *IEEE Transactions on Smart Grid*, vol. 6, pp. 1484–1492, May 2015.

[85] B. Palmintier, E. Hale, T. M. Hansen, W. Jones, D. Biagioni, H. Sorensen, H. Wu, and B. M. Hodge, "IGMS: An Integrated ISO-to-Appliance Scale Grid Modeling System," *IEEE Transactions on Smart Grid*, vol. 8, pp. 1525–1534, May 2017.

[86] T. M. Hansen, B. Palmintier, S. Suryanarayanan, A. A. Maciejewski, and H. J. Siegel, "Bus.py: A GridLAB-D communication interface for Smart distribution Grid simulations," in *2015 IEEE Power Energy Society General Meeting*, pp. 1–5, July 2015.

[87] T. M. Hansen, R. Kadavil, B. Palmintier, S. Suryanarayanan, A. A. Maciejewski, H. J. Siegel, E. K. P. Chong, and E. Hale, "Enabling Smart Grid Cosimulation Studies: Rapid Design and Development of the Technologies and Controls," *IEEE Electrification Magazine*, vol. 4, pp. 25–32, Mar. 2016.

[88] J. J. Grainger and W. D. Stevenson, *Power system analysis*. McGraw-Hill, Jan. 1994. Google-Books-ID: NBIoAQAAMAAJ.

[89] R. A. Horn and C. R. Johnson, *Matrix Analysis*. Cambridge University Press, Oct. 2012. Google-Books-ID: 5I5AYeeh0JUC.

[90] C.-T. Chen, *Linear System Theory and Design*. Oxford University Press, 2013. Google-Books-ID: UTNcNAEACAAJ.

[91] *IEEE 123 Bus Test System*.

[92] D. P. Chassin, J. C. Fuller, and N. Djilali, "GridLAB-D: An Agent-Based Simulation Framework for Smart Grids," *Journal of Applied Mathematics*, vol. 2014, p. e492320, June 2014.

[93] K. P. Schneider, J. C. Fuller, and D. P. Chassin, "Multi-State Load Models for Distribution System Analysis," *IEEE Transactions on Power Systems*, vol. 26, pp. 2425–2433, Nov. 2011.

[94] K. P. Schneider, E. Sortomme, S. S. Venkata, M. T. Miller, and L. Ponder, "Evaluating the magnitude and duration of cold load pick-up on residential distribution using multi-state load models," *IEEE Transactions on Power Systems*, vol. 31, pp. 3765–3774, Sept. 2016.

[95] J. Fuller and others, "Evaluation of Representative Smart Grid Investment Grant Project Technologies," tech. rep., PNNL, Feb. 2012.

[96] M. Sengupta and A. Andreas, "Oahu Solar Measurement Grid:1-Second Solar Irradiance; Oahu, Hawaii (Data)," tech. rep., NREL, 2010.

[97] S. Boyd and L. Vandenberghe, *Convex Optimization*. Cambridge University Press, Mar. 2004. Google-Books-ID: IUZdAAAAQBAJ.

[98] D. B. Arnold, M. Sankur, R. Dobbe, K. Brady, D. S. Callaway, and A. V. Meier, "Optimal dispatch of reactive power for voltage regulation and balancing in unbalanced distribution systems," in *2016 IEEE Power and Energy Society General Meeting (PESGM)*, pp. 1–5, July 2016.

[99] M. E. Baran and F. F. Wu, "Network reconfiguration in distribution systems for loss reduction and load balancing," *IEEE Transactions on Power Delivery*, vol. 4, pp. 1401–1407, Apr. 1989.

APPENDIX ADDITIONAL MATERIAL

Data for Real-Time Adaptive VVC (chapter 3)

Small 4-bus example system information: length of lines 1-2, 2-3 and 3-4 are 2000, 4500 and 4500 feet respectively. Transformer is step-down (12.47kV/4.16 kV).

In all cases $d = 0$ and $\tau = 0.1$ are considered. Note that in conventional and delayed droop control, all settings remain constant throughout the day except q_{min} and q_{max} which change with change in PV generation and cloud cover. For adaptive control, all of these settings are decided by the proposed algorithm.

Table A.1 Conventional and delayed droop VVC settings: 4 bus system

droop	q_{min}	q_{max}	v_{min}	v_{max}
conservative ($m = 2$)	-0.2	0.2	0.9	1.1
non-conservative ($m = 6$)	-0.2	0.2	0.967	1.033

Table A.2 Conventional and delayed droop VVC settings: 123 bus system

droop	q_{min}	q_{max}	v_{min}	v_{max}
conservative ($m = 3$)	-0.4	0.4	0.867	1.133
conservative ($m = 5$)	-0.4	0.4	0.92	1.08
non-conservative ($m = 10$)	-0.4	0.4	0.96	1.04

House Modeling for Test Case

IEEE 123 test bus feeder is converted to equivalent model with detailed secondary side house load. At each triplex node, the residential spot load was replaced with a number of residential house models, which under peak conditions approximately matched the original spot load. The number of house models replacing the original peak load depended upon a scaling factor unique to each taxonomy feeder model and was used to calibrate the populated feeder model to the peak load study. For example, if the original spot load was 10 kVA and the feeder scaling factor was determined to be 5 kVA / house, the spot load would be replaced with two house models.

Each house conatins ZIP load, multi-state HVAC load, and solar PV generation unit. All of these devices are modeled in the GridlabD software. Their modeling details can be found at (93) and (95) (pg. 133), however, we will list the input data required for these models.

Load Parameters

1. **Residential thermal integiry values**: Thermal resistance, R (units of °F.sf.h/BTU) values of following components of house.
    - Roof
    - Wall
    - Floor
    - Doors
    - Windows

2. **Temperature set-points**: Heating and cooling set-points range is selected based on the minimum, maximum and desired teperature with uniform distribution. Similarly a temperature deadband is also used for HVAC operations.

3. Few other parameters such as floor area, HVAC pf, ZIP fractions (0.2, 0.4, 0.4) are used.

Table A.3 shows the average thermal integrity properties of 7 different type of houses in different regions. Each of these parameters was then randomized, where appropriate, around the average value with a normal distribution to create a diversified population which approximately represents the average household characteristics in that region.

Solar Parameters

Rating of the solar unit is decided based on the floor area of the house. For example, a smaller house will have a smaller roof area, thus will have smaller PV installation capacity. Apart from that solar panel type, panel efficiency, tilt angle, panel orientations are also specified.

Dynamically changing input throughout the day

1. Outside weather file for a whole day with 3 seconds resolutio is used which includes following parameters:
    - Temperature
    - Humidity
    - Solar direct irradiance
    - Solar global irradiance
    - Solar diffuse irradiance

2. ZIP load schedule based on the season (winter, summer) and the day (weekend, weekday). This is used to create a daily load profile

3. HVAC smart thermostat set-point schedule: Additionally, 9 different 24 hour schedules of heatings are used for different customers to simulate smart thermostats.

Table A.3 Various house parameters used in the modeling of the test case

Parameters	type 1	type 2	type 3	type 4	type 5	type 6	type 7
Rroof_stdev	4	5	4	5	4	4	12
Rroof_mean	19	30	19	30	14	14	23
Rwall_stdev	3	3	3	3	2	2	9
Rwall_mean	11	19	11	19	6	6	13
Rfloor_stdev	1	3	1	3	1	1	7
Rfloor_mean	11	15	11	15	5	5	11
Rdoors_stdev	0	0	0	0	0	0	1
Rdoors_mean	3	5	3	5	3	3	4
Rwindows_stdev	0.5	0.5	0.5	0.5	0.5	0.5	0.75
Rwindows_mean	1.25	1.75	1.25	1.75	1.25	1.25	1.5
hvac_pf_stdev	0	0	0	0	0	0	0
hvac_pf_mean	0.97	0.97	0.97	0.97	0.97	0.97	0.97
floor_area_stdev	500	500	900	900	750	200	1800
floor_area_mean	1100	1100	3000	3000	750	500	2100
Tmin_mean	68	68	68	68	68	68	68
Tmin_stdev	2	2	2	2	2	2	2
Tmin_lower	66	66	66	66	66	66	66
Tmin_upper	70	70	70	70	70	70	70
Tmax_mean	78	78	78	78	78	78	78
Tmax_stdev	2	2	2	2	2	2	2
Tmax_lower	76	76	76	76	76	76	76
Tmax_upper	80	80	80	80	80	80	80
Tdesired_mean	72	72	72	72	72	72	72
Tdesired_stdev	3	3	3	3	3	3	3
Tdesired_lower	70	70	70	70	70	70	70
Tdesired_upper	75	75	75	75	75	75	75
halfband_stdev	0	0	0	0	0	0	0
halfband_mean	1	1	1	1	1	1	1